POLYELECTROLYTE COMPLEXES FOR FIRE PROTECTION OF MATERIALS

A Dissertation

by

THOMAS JOHN KOLIBABA

Submitted to the Office of Graduate and Professional Studies of
Texas A&M University
in partial fulfillment of the requirements for the degree of

DOCTOR OF PHILOSOPHY

Chair of Committee,	Jaime C. Grunlan
Committee Members,	Karen L. Wooley
	Sarbajit Banerjee
	Hong Liang
Head of Department,	Simon W. North

May 2021

Major Subject: Chemistry

ABSTRACT

Fire and flammability continue to plague society, causing tens of thousands of needless deaths and injuries per year, in addition to billions of dollars in property damage. Common materials such as wood exhibit dangerous flammability and are ubiquitous in home furnishing and construction. Additionally, flammability dramatically limits the applications of three-dimensionally (3D) printed parts, despite their great promise in a multitude of areas such as medicine and aerospace. Reducing the flammability and associated fire hazard of these materials is critical to the preservation of human life as flammable polymeric materials continue to proliferate society.

Layer-by-layer assembled flame retardants have risen to prominence as of late as a method of providing environmentally-friendlier approaches to fire protection. Unfortunately, wood and additive manufacturing filaments present unique challenges to this technique that render it impractical. This dissertation describes these challenges, and presents strategies to mitigate them through the use of electrostatically assembled polyelectrolyte complexes. These polyelectrolyte assemblies act as environmentally benign and extremely effective flame retardant coatings or additives to wood or 3D printing filaments, respectively.

DEDICATION

To my wife, Ciani, for your unending love and support, for always encouraging me to follow my passions, and for holding my best intentions in your heart. To my parents, Brian and Kate, for cheering me on every step of the way, for teaching me to work hard, and for reminding me to always be thankful.

ACKNOWLEDGEMENTS

I would like to thank Dr. Jaime Grunlan for touching base with me almost 6 years ago and suggesting that I consider Texas A&M for graduate school. I have been greatly blessed by my time here and by working for you, and I'm thankful for your wisdom and help throughout my graduate career. Thanks are also owed to Dr. Grunlan for letting me pursue many ideas that were 'off the beaten path' for our group's research, I appreciate the chances you gave me to pursue wild ideas (even when they didn't bear fruit). I'd like to also thank Dr. Karen Wooley, Dr. Sarbajit Banerjee, and Dr. Hong Liang for taking the time to serve as members of my committee.

I am indebted to both the past and present members of the Polymer Nanocomposites Laboratory for their ideas, time, and friendship throughout this process. A special thanks are owed to Dr. Ryan Smith and Dr. Simone Lazar, both of whom helped me formulate big ideas, pursue new projects, and expand the scope of my knowledge tremendously. I would like to also thank the undergraduates with whom I worked closely: Jacob Brehm, Troy Pangburn, and Annie Benson. Your careful work and enthusiastic attitude were always appreciated and I owe much of my productivity to your willingness to learn new things and help me out.

I would also like to thank the collaborators who helped me accomplish my projects. The 3D printing work in this dissertation would not have been possible without the help of Dr. Bruce Tai, whose group helped tremendously in developing and utilizing our specialty filaments. I am thankful for thought-provoking discussions with Dr. Alex Morgan from the University of Dayton Research Institute. Finally, I am indebted to Dr. David Truong from the Soft Matter Facility, who allowed me entrance to the facility months before it was officially due to open in order for me to utilize equipment necessary for my research.

CONTRIBUTORS AND FUNDING SOURCES

Contributors

The work herein was performed under the supervision of a committee comprised by: Professor Jaime C. Grunlan as chair and thesis advisor, Professor Karen L. Wooley from the Texas A&M Department of Chemistry, Professor Sarbajit Banerjee from the Texas A&M Department of Chemistry, and Professor Hong Liang from the Texas A&M Department of Mechanical Engineering.

The collaborative work discussed in Chapter V was carried out in partnership with Professor Bruce Tai of the Texas A&M University Department of Mechanical Engineering. The collaboration in Appendix I was carried out in collaboration with Professor Etienne Grau from the University of Bordeaux.

Funding Sources

The work presented in Chapters III and IV were supported by the United States Airforce Research Laboratory (Award Number FA9300-15-C0004). All work presented herein was infrastructurally and financially supported by the Texas A&M Engineering Experiment Station (TEES).

TABLE OF CONTENTS

Page

LIST OF FIGURES

Page

LIST OF TABLES

Page

CHAPTER I

INTRODUCTION

1.1 Background

Fire and flammability continue to plague society, causing tens of thousands of needless deaths and injuries per year, in addition to billions of dollars in property damage.[1] Common materials such as wood exhibit dangerous flammability and are ubiquitous in home furnishing and construction.[2] Recently, it has also been noted that outdoor wood structures like fences may contribute to the proliferation of wildfires.[3] Additionally, flammability dramatically limits the applications of three-dimensionally (3D) printed parts, despite their great promise in a multitude of areas such as medicine and aerospace.[4–6] Furthermore, 3D printer failures have led to an increased awareness of the fire hazard that they pose in both residential and professional settings.[7,8] Reducing the flammability and associated fire hazard of these materials is critical to the preservation of society as flammable polymeric materials continue to proliferate everyday life.

Flame retardants containing halogens, such as bromine and chlorine, have been utilized for decades as bulk additives to plastics. Unfortunately, they have been shown to have serious issues of bioaccumulation and toxicity.[9–12] These safety concerns have led to halogenated compounds being largely regulated out of the marketplace. In some cases, fire safety standards have been relaxed in order to facilitate the removal of these materials, which leads to a potential increase in fire hazard for consumers.[13] Importantly, bulk additives also harm the recyclability of plastics, due to interactions caused when they are heated and reprocessed.[14]

Surface treatments offer an appealing alternative to bulk additives because they avoid the issues described above. First, many surface treatments can utilize environmentally-benign materials and approaches to deposit flame retardant coatings.[15,16] Additionally, surface treatments

localize the flame retardant to the outermost portion of the material, which is where combustion processes occur. Some materials, such as wood, aren't amenable to approaches that utilize bulk additives and coating technologies are the only option. Other materials, such as additive manufacturing filaments, must have effective flame retardant solutions that avoid toxic chemistries, as 3D printing continues to infiltrate hobbyist and engineering applications. Polyelectrolyte-based materials are particularly attractive for both 3D printing filaments and wood because many of them are either of biological origin or are environmentally benign and can be deposited as surface coatings, or prepared as an additive with water-based processes.

1.2 Objective and Dissertation Outline

The work described herein aims to demonstrate processes to improve the fire safety of wood and additive manufacturing filaments without the use of toxic or environmentally harmful materials/processes. This is achieved chiefly through the use of polyelectrolyte complexes.

Chapter II introduces the field of flame retardants, with a discussion about the mechanism of combustion and common modes of flame retardant action. This section includes a brief review of layer-by-layer approaches to flame retardant coatings, along with a discussion of the more recent process of buffer-cured polyelectrolyte complex coatings.

Chapter III illustrates the use of a fully renewable, nanobrick wall coating for the fire protection of wood. The wood's surface chemistry is altered to facilitate better coating growth and performance.[15]

Chapter IV demonstrates the use of a buffer-cured polyelectrolyte complex to improve the fire resistance of wood. This coating deposits much more quickly than the nanobrick wall

coating and provides greater improvements to fire resistance, while simultaneously improving the mechanical strength of the wood.[16]

Chapter V demonstrates the use of a bulk polyelectrolyte complex mixed with polylactic acid to form a composite additive manufacturing filament. This filament enables the 3D printing of self-extinguishing parts.[17]

Chapter VI is a summary of this dissertation work and describes future work that can be undertaken to utilize polyelectrolyte complexes as flame retardants for other substrates. Of particular importance is the development of a polyelectrolyte complex that can be deposited in a single step, which improves the potential of this technology for commercialization. A proposed method of 3D printing bulk flame retardant polyelectrolyte complexes with controllable mechanical properties is also outlined.

CHAPTER II

LITERATURE REVIEW*

2.1 Hazards and Impacts of Fires

Damage and injuries from fire lead to enormous loss of life and property worldwide each year. Between 2012 and 2016, there were over 17.5 million fires reported worldwide, which led to 220,000 fatalities and nearly 350,000 injuries.[1] In 2017, the United States alone suffered $23 billion in property loss from fire damage. The dangers of fires to both lives and historical icons have been further underscored by the tragic Grenfell tower catastrophe in London in 2017 and the fire at Notre-Dame Cathedral in Paris in 2019.[18,19] As a result of such events, the development of safe and effective flame retardants has long been a goal for scientists and engineers. As polymers continue to proliferate everyday life and improve our standard of living, the inherent flammability of these materials necessitates research to improve safety and preserve lives.

Although a handful of inherently flame retardant materials exist, these materials are often expensive or do not have the appropriate properties for many applications. For this reason, polymeric materials have historically been made less flammable by incorporating small molecule flame retardants. Unfortunately, bulk incorporation of flame retardants often leads to the degradation of mechanical properties as well as difficulty in recycling of the polymer.[20] Furthermore, bulk flame retardants have the tendency to be released into the environment upon breakdown of the material, often with insidious health or bioaccumulation outcomes (especially in the case of halogenated flame retardants).[12,21] As a result, researchers are developing flame retardant surface treatments, which preserve the bulk properties of a material and localize the

*Parts of this chapter have been reprinted with permission from Lazar, S.; Kolibaba, T.J.; Grunlan, J.C., Flame-Retardant Surface Treatments, *Nature Reviews Materials* **2020**, *5(4)*, 259-275.

additive to the surface of a material where combustion occurs.

2.2 Mechanism of Combustion

An understanding of the mechanism of combustion is required to develop flame retardants. For many years, this complex process was simply understood as the fire triangle, but it has now been revised to a fire tetrahedron consisting of four key contributors: fuel, oxygen, heat, and a chain reaction (**Figure 2.1**). For example, the common house fire begins with pyrolysis, an endothermic process that results from a flammable material experiencing heat from an ignition source like a smoldering cigarette or a faulty electrical appliance. As the bulk material depolymerizes owing to thermal exposure, it releases unstable radicals and gaseous products. The volatile decomposition products act as fuel that, in the presence of an ignition source and enough oxygen from the air, ignite and lead to combustion.[22] This process means that the bulk material itself is not responsible for combustion, but rather the decomposition products that evolve. The temperature for combustion to take place must be above the ignition temperature (or flash point) of the polymer, allowing for the transition into an exothermic process that releases toxic gases and smoke, while generating copious amounts of heat for further pyrolysis.[23]

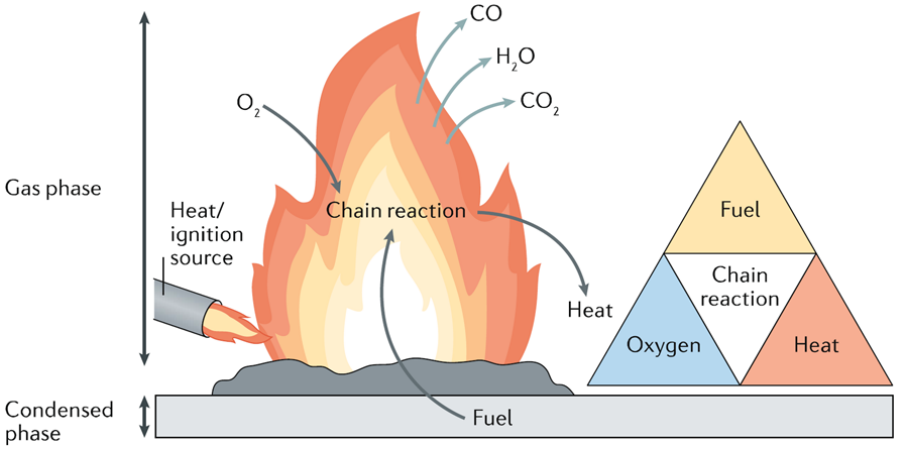

Figure 2.1. A schematic representation of the mechanism of combustion and the associated fire tetrahedron.[24]

This thermal feedback, whether it is conductive, convective, and/or radiative, continues to fuel the flame, resulting in a chain reaction that propagates the fire. It is for this reason that surface treatments hold so much promise for imparting flame retardancy. Each treatment localizes the active components where they will be most effective in disrupting this chain reaction. High surface area substrates (e.g. textiles and foams) require thinner coatings than low surface area materials (e.g. plastic film), because the active ingredient(s) conformally covers the 3D surface and fights fire at the point of ignition. Lower surface area materials are still amenable to surface treatments, but may require thicker coatings and potentially different chemistries, especially if the material releases large amounts of heat during combustion. For all materials, the chemistry and decomposition rate and decomposition mechanism of the substrate dictates which modes of flame retardant action are most effective.

2.3 Flame Retardant Mechanisms

Flame retardants prevent one or more of the fire tetrahedron components from taking part in combustion. As pyrolysis is inevitable in extreme heat situations, it is not always realistic for flame retardants to completely negate ignition. The primary objectives of flame retardants is to impede pyrolysis and time to ignition (TTI), prevent flame spread, and suppress the production of toxic smoke, which provides time for people to safely evacuate the premises.[22] These objectives can be achieved by chemical and/or physical means in the gas or condensed-phase, by cutting off the fuel that feeds the flame, dissipating the heat felt by the flammable material, limiting the oxygen consumed by the flame, or by inhibiting the chain reaction of the combustible decomposition products.

2.3.1 Gas-Phase Action

The small amounts of high energy $OH^{\cdot}$ and $H^{\cdot}$ radicals produced during an initial chemical reaction between oxygen and generated fuel are sufficient to ignite a polymeric material.[25] Ignition leads to a series of chemical chain-branching, chain-propagating, and chain-terminating reactions that help sustain the flame by, respectively, changing the amount, type, and mole ratio of radicals present in the gas phase.[26] Radicals of lower energy are required to scavenge the unstable $OH^{\cdot}$ and $H^{\cdot}$ radicals. Replacement of the unstable radicals with less reactive ones interrupts the combustion chain reaction and can lead to self-extinguishing behavior in a treated system (**Figure 2.2**). Improved fire performance can also be physically achieved in the gas phase by attenuating the combustible gases through an endothermic release of non-flammable gases such as N_2, H_2O, and CO_2.[27]

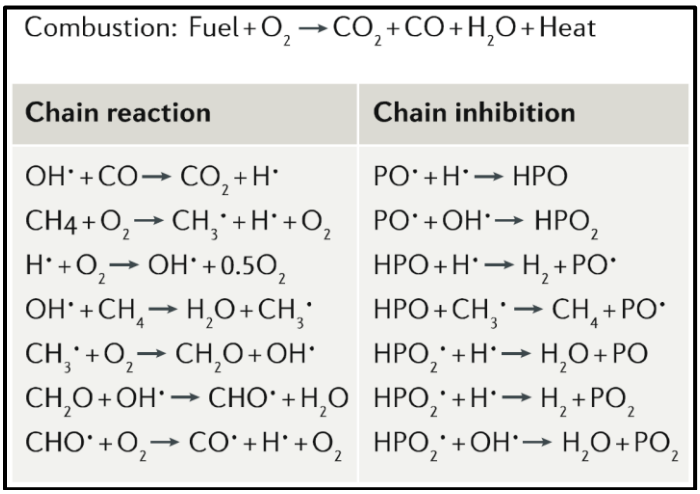

Figure 2.2. The overall chemical reaction for combustion that leads to a series of chain reactions and examples of phosphorus-based radicals that can scavenge unstable radicals in the gas phase.[27,28]

2.3.2 Condensed-Phase Action

Mass and heat transfer in the condensed phase continually feed the flammable decomposition products that cause a fire to spread.[23,29] A protective layer on the surface of a flammable material reduces the amount of thermal feedback that contributes to the propagation of

the fire. This protective layer is often an insulating, thermally-stable physical barrier applied on the surface, but it can also be chemically formed at the interface during pyrolysis of the material.[30] This condensed-phase action prevents the polymeric fuel from taking part in combustion, further justifying the application of flame retardant treatments at the interface where an ignition source meets a flammable material.

2.4 Flame Retardant Chemistries

Although a variety of chemical elements have proven to be effective as flame retardants, the elements able to reduce the inherent flammability of a given material is dictated by macromolecular make-up of the material. The specific chemistries required to act in either the gas or condensed phase generally depend on the pyrolysis behavior of the material. However, as a consequence of toxicity, pollution, and bioaccumulation concerns, many of the most effective halogen-based and antimony-based flame retardants have been limited or completely banned in much of the world. These concerns have triggered efforts to find more environmentally-friendly approaches to reduce the flammability of polymeric materials.[9] In addition to those listed below, many elements commonly found in minerals and ceramics (e.g. boron,[31] silicon,[32] aluminum, iron, and metal hydroxides[33]) all find use in flame retardant systems owing to their inherent lack of flammability. There are a variety of ways to incorporate these elements, but they usually must be paired with or incorporated into other materials as a consequence of their inherently difficult processing brought on by brittleness and/or lack of malleability.[34]

2.4.1 Phosphorus

Phosphorus-containing flame retardants often replace halogenated flame retardants, because these compounds can act in both the gas and condensed phases.[28,35] In general, phosphorus-based radicals ($PO^{\cdot}$, $PO_2^{\cdot}$, $HPO_2^{\cdot}$) act in the gas phase, similar to the way halogen radicals inhibit chain-branching reactions (**Figure 2.2**),[36] and phosphate and phosphonate-compounds act in the condensed-phase by promoting and stabilizing char residue.[37] Phosphorus chemistry has been studied for many years owing to its ability to reduce flammability.[38] Although most phosphorus research has been focused on bulk additives, the mechanisms of action are essentially the same when implemented in a surface treatment. Phosphorus flame retardants are extremely versatile, and can be tailored by adjusting the inorganic-organic content, phosphorus loading, and oxidation state. There are a variety of phosphorus-containing moieties that can be implemented in flame retardant surface treatments, including polyphosphates, phosphate esters, and other phosphate derivatives.

2.4.2 Nitrogen

Nitrogen-rich small molecules or polymers are able to provide synergistic flame retardant properties when combined with other flame retardant elements.[39] Although synergy is a quantitative measure based on calculations,[40] the combination of nitrogen with other flame retardant elements can often demonstrate qualitative improvements with regards to flame suppression. Melamine is a good example because it releases nitrogen gas and water (gases that are low in toxicity) when the material sublimes at ~350°C.[41] Synergistic effects arise when phosphorus-functionalized melamine derivatives are used. This combination of phosphorus, along with the high nitrogen content of melamine, is especially effective for flame-retarding polymers that drip and melt away when exposed to a flame (e.g. thermoplastics).

2.4.3 Intumescent Systems

Intumescent flame retardants comprise an acid source, a blowing agent, and a carbon source, that act in the condensed phase by forming a protective char layer on the surface of a substrate (**Figure 2.3**). The success of intumescent flame retardants to protect against fire is heavily dependent on the sequential and timely activation of the intumescent components by a series of chemical reactions.[42] The mechanism is initiated by the release of an inorganic acid at temperatures typically below 250°C. Most materials do not start to degrade until heated >250 °C, and, as a result, the flame retardant coating will typically begin to degrade prior to decomposition of the bulk material.[43] The acid released then reacts with the carbon source (polyols are most common) to form a carbonaceous layer on the surface via dehydration. As this layer is forming, the blowing agent (usually a spumific) begins to breakdown and release non-flammable gases such as nitrogen and ammonia. The breakdown of the blowing agent dilutes the combustible gases produced and causes the char layer to expand. This char layer is then solidified through crosslinking and condensation reactions, creating a stable, low thermal conductivity shell on the surface of the flammable polymer. One of the most commonly used chemicals in intumescent systems is ammonium polyphosphate owing to its widespread availability and effectiveness owing to the presence of both ammonia (a nitrogen source and thus a blowing agent) and phosphate (an acid source).

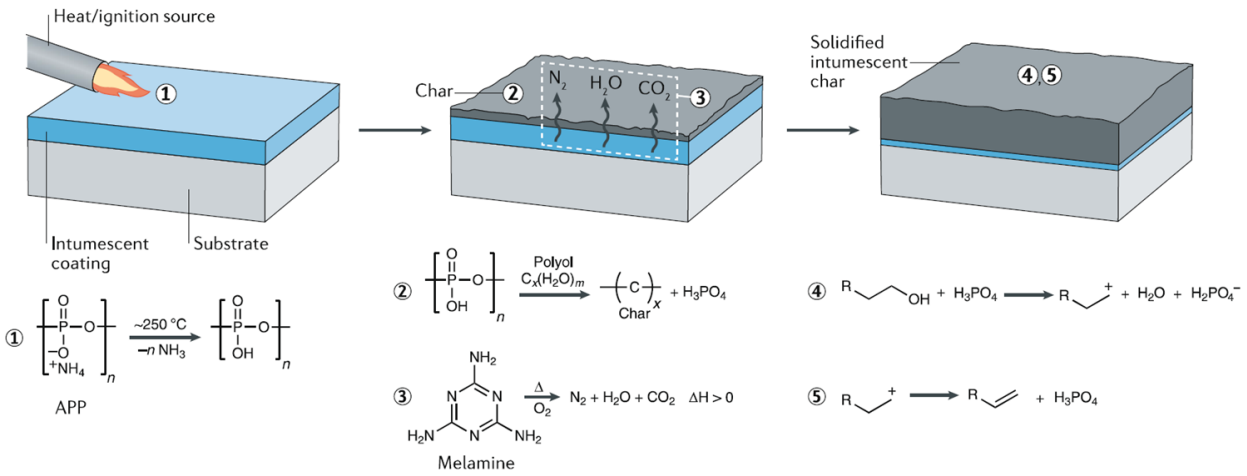

Figure 2.3. A schematic representation of the steps and components required for intumescent flame retardant systems acting in the condensed phase. The equations demonstrate the sequential activation of the intumescent coating using ammonium polyphosphate (APP) as an example acid source, a polyol as an example carbon source, and melamine as an example blowing agent.[24]

2.4.3 Nanocomposites

The highly stable inorganic filler (e.g. clay, carbon nanomaterials, etc.) of nanocomposite coatings provides a thermal barrier and protects the underlying material from decomposing upon exposure to heat. These inorganic materials form ceramic shields that confine the melt and prevent dripping of a flammable material.[44] The material is capable of thermally protecting the flammable substrate long enough for other flame retardant chemistries to help counteract the spread of fire and extinguish the flame.[45]

2.5 Measuring Efficacy

Self-extinguishing behavior is the most visually impactful and obvious ways to measure the success of a flame retardant. However, developing quantifiable criteria for a successful flame retardant is influenced by the fire conditions that the material is expected to encounter. [30,46] These flame retardant standards vary slightly from country to country and are continuously revised depending on the safety regulations in place. The most common standard tests rely on a pass or

fail criteria for certain time-dependent parameters, such as, time to ignition or time to peak heat release, or compare quantitative values of, for example, total heat release (THR) and total smoke release (TSR) for treated and untreated materials (**Table 2.1**). Other standard tests rely on identifying a specific rating based on the reaction of a material to a controlled flame. The results of the various flame retardant surface treatments should be viewed as the benchmark for developing and improving existing flame retardant technology. To be considered successful, flame retardant surface treatments must not only pass these standardized flame tests, but must be less toxic, more cost-efficient, and easily applicable for a given use as compared to currently available halogenated flame retardants.

Table 2.1. Summary of standardized flame retardant tests.

Tests and standard protocol numbers	*Description of Test*
Cone Calorimetry *(ASTM E1354, ISO 5660)*	Evaluates flame retardancy of materials by exposing 10 x 10 cm^2 samples to a radiative heat flux (≤100 kW m^{-2}) in the presence of an ignition source. Most common heat flux used is 35 or 50 kW m^{-2}, similar to those commonly found in developing fires.[47] Provides information such as time to ignition (TTI), peak heat release rate (HRR), total heat release (THR), total smoke release (TSR), and residual mass. Calculations based on Thornton's Rule that the net heat of combustion is directly proportional to the amount of oxygen consumed (~13.1 kJ g^{-1} for most materials).[48]
Microscale Combustion Calorimetry *(MCC, ASTM D7309)*	Milligram-scale samples are pyrolyzed and the resulting products are sent through a combustor where Thornton's Rule is used to calculate peak HRR and THR. Often employed on substrates and textiles that are too thin and/or difficult to be measured by cone calorimetry or used to screen gas-phase active flame retardants.
UL-94 *(ASTM D3801, UL-94V, IEC 60695-11-10)*	The flame of a Bunsen burner is applied (at a 45° angle) to the bottom of a vertically hung sample for 10 seconds and then removed. A 10-second flame is applied a second time if the sample self-extinguishes within 30 seconds of the first flame application. Results are based on one of three ratings: V-0 (best rating), V-1, or V-2.[49] (A less aggressive version of the test is in the horizontal orientation)

2.6 Polyelectrolyte Coatings

The most active area of flame retardant research is in the field of coatings made by layer-by-layer (LbL) assembly. This technique predominantly relies on electrostatic interactions between polyelectrolytes and/or charged nanoparticles, and is amenable to a variety of donor/acceptor interactions.[50,51] The sequential process involves the alternate immersion of a charged substrate (via plasma, corona, and/or chemical treatment) in aqueous solutions containing components necessary for improving flame retardancy (**Figure 2.4a**). Most coatings via LbL assembly can be approximated to be a polyelectrolyte complex (PEC). This assumption can be made because nearly all LbL films (particularly in the field of flame retardants) involve at least one polyelectrolyte component. Polyelectrolyte complexes are the insoluble precipitates formed when two oppositely charged polyelectrolytes are mixed.[52] The interface between a growing LbL film and a polyelectrolyte solution incrementally builds a PEC on a surface throughout this process. PECs and LbL films behave as heavily crosslinked materials owing to the electrostatic crosslinks that the ionic bonds cause.[53]

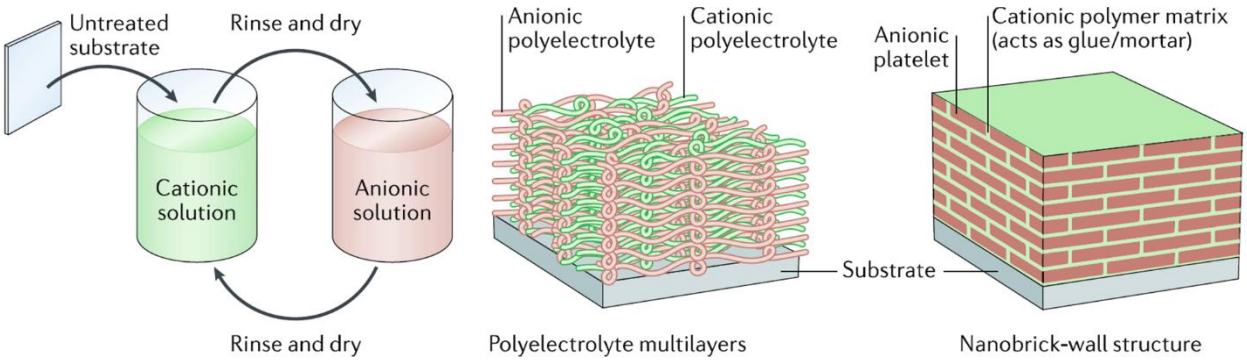

Figure 2.4. A schematic representation of the layer-by-layer procedure used to develop polyelectrolyte multilayers or a nanobrick wall structure, depending on the components used.

The formation of PECs, and by extension LbL films, is driven by entropy from the expulsion of counterions held by either charged component of the film.[54] This entropic gain of

expelling the counterions outweighs the losses of segmental motion and diffusional freedom of the polyelectrolyte chains. This is schematically illustrated in **Figure 2.5**, showing the new ionic bonds formed between chains. Typically, most of the ionic bonding sites of each polyelectrolyte species is "intrinsically compensated", meaning that the ionic site is paired with a complementary site on the other polyelectrolyte species in the film/complex. Depending on the conditions of LbL film growth/polyelectrolyte complexation, some of the ionic sites may be "extrinsically compensated" by the held counterions which serve to plasticize the film and can affect its morphology as a result.[55,56]

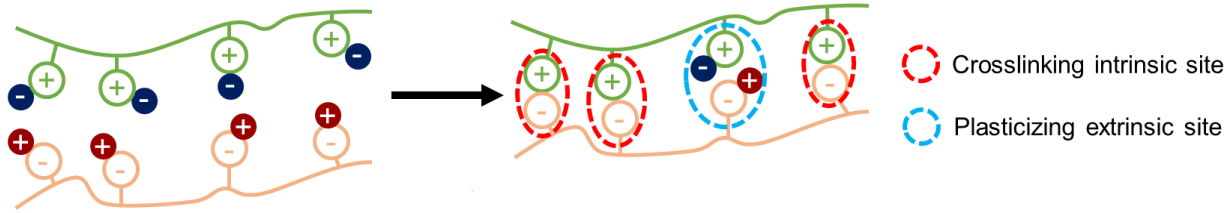

Figure 2.5. Schematic of the formation of a bulk polyelectrolyte complex. Held counterions are expelled, yielding an increase in entropy. Some counterions remain and plasticize the resultant complex in extrinsic ion-pairings sites.

Versatility is one of the factors that has led to the success and popularity of layer-by-layer assembly as a research area for flame retardants. For example, the technique can be adapted to include three-component trilayers[57–64] or four-component quadlayers,[61,64–68] of flame retardant materials. The thickness of the coating can be adjusted by using aqueous solutions of varying pH or ionic strength (**Figure 2.6**) and typically ranges from 100 nm to 1 μm. Although practically endless combinations of chemistries exist for layer-by-layer assembly, those already used to construct multilayer fire-protective coatings can be categorized by the distinctive flame retardant mechanisms employed (i.e. passive barriers or intumescent). Recently, a subclass of flame retardant coatings based upon polyelectrolytes based on buffer-cured polyelectrolyte complexes have been developed, primarily incorporating intumescent chemistry. These coatings were

designed to circumvent the large number of steps required by LbL coatings and have risen in popularity/prevalence in recent years. Owing to the extensive literature on this topic, only the most notable systems in terms of novelty, self-extinguishing behavior, low peak HRR and reduction of THR are discussed here. There is an emphasis on coatings that improve flame retardancy of polymeric substrates that are difficult to protect against fire because of their inherent chemistry and reaction to heat.

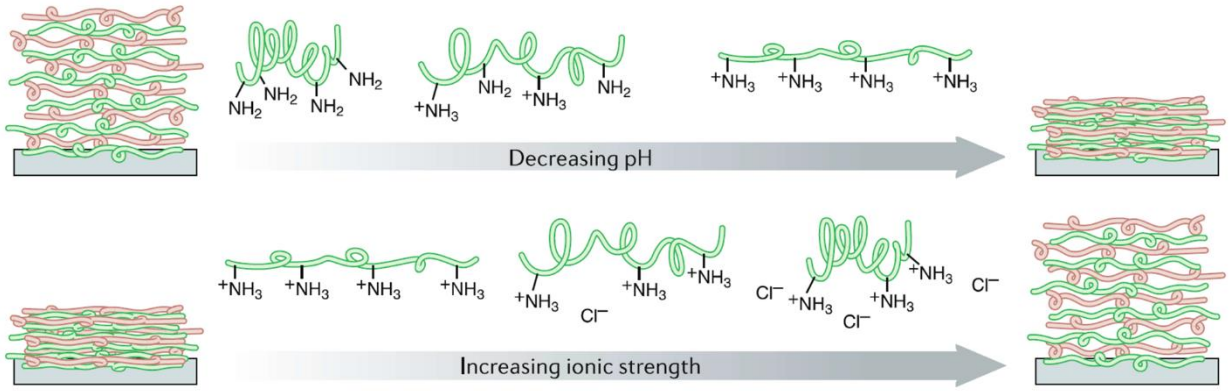

Figure 2.6. A schematic illustrating the influence that solution pH and ionic strength have on the morphology and thickness of an amine-based polyelectrolyte.

2.6.1 Passive Barriers

Flammable substrates alternately immersed into aqueous clay dispersions and polymeric solutions, create a passive barrier on the surface. This structure is often referred to as a 'nanobrick wall' owing to the polymer acting as mortar holding together aligned clay nanoplatelets. High clay-content coatings act primarily in the condensed phase as a thermal barrier. Nanobrick wall coatings act in a manner similar to the in-situ formation of a ceramic barrier from silicate nanoparticles at the interface of bulk material during pyrolysis.[69] The first well-studied layer-by-layer flame retardant coating translated this ceramic barrier mechanism onto the surface of cotton fabric using a clay-based multilayer coating consisting of negatively-charged laponite clay and positively-charged branched polyethylenimine (PEI).[70] Analogous systems have replaced PEI with

other nitrogen-rich polymers or replaced laponite with various inorganic nanomaterials.[71–76] The high thermal stability of inorganic nanomaterials have been found to be rather futile for protecting cellulosic materials, as evidenced by mediocre improvements in flammability. This poor performance is a consequence of the dehydration of the cellulosic materials during pyrolysis, which ideally depends on catalyzing inorganic acids found in intumescent mechanisms, because the flammable substrate serves as a carbon source for promoting char.[77,78]

Unlike other polymers used for textiles, the degradation of polyurethane foam starts at temperatures too low for the activation of most flame retardant chemistries, and, as a result, these foams benefit greatly from passive barrier protection. The first LbL assembled coating to improve the flame retardancy of polyurethane foam comprised four bilayers of PEI-dispersed carbon nanofibers and poly(acrylic acid).[79] This system reduced the peak HRR by 40% and laid the foundation for the passive barriers that have been developed since, most of which consist of different clays,[60,80–84] graphene oxide,[62,63,85,86] carbon nanotubes,[59,60,87,88] titanate tubes,[89] or molybdenum disulfide[90]. In particular, multilayers consisting of montmorillonite or vermiculite clay with either chitosan, PEI, or starch, have been deposited on polyurethane foam to protect against fire.[80,82] The protection observed when using vermiculite nanoplatelets (paired with chitosan in particular) were superior to montmorillonite owing to its much larger aspect ratio combined with the char forming abilities of chitosan. The char residue formed prevents the foam from melt dripping and collapsing. The application of this well-known chitosan/clay nanocoating was also evaluated as a thermal shield by demonstrating that an 8-bilayer coated polyurethane foam sample withstands a heat flux of 116 kW m^{-2}, while maintaining a tremendous temperature differential (>200°C) across a 2.5-cm distance.[91]

Despite the excellent flame retardant properties achieved with a few bilayers of these inorganic-organic materials,[80,92,93,84] the search for better flame retardant chemistries for polyurethane foam continues. Most of these inorganic-organic nanocoatings do not self-extinguish, but instead result in flashover, leading to the spread of fire via heat transfer and mass transfer. This flashover behavior is less pronounced in systems that, instead of depending solely on passive barrier protection, rely on the formation of water and non-flammable gases to physically put out the fire.[92,81,61,94–97] A recent study demonstrated that a magnesium silicate clay encompassing zeolitic water reduces the peak HRR (76%) and THR (27%) when used in conjunction with negatively-charged alginate and paired with PEI.[97] Coatings on polyurethane foam that lack passive barrier modes of action, however, often show minimal flame retardant improvement and lead to thermal shrinkage of the foam,[45,81,98,99] with few studies resulting in self-extinguishing behaviour.[100,101]

2.6.2 Intumescent Polyelectrolyte Multilayers

Intumescent chemistries have been used in multilayer films, such as when a 20-bilayer polyallylamine (PAAm)/sodium hexametaphosphate (PSP) nanocoating was applied to cotton fabric, which decreases the peak HRR and THR of cotton fabric by 43% and 51%, respectively.[78] When subjected to vertical flame testing, the treated fabric self-extinguishes because of an intumescent-like behavior ascribed to the cotton substrate acting as a carbon source, the PSP as the inorganic acid, and PAAm as the blowing agent. Bubble formation during burning is attributed to a micro-intumescent mechanism,[102] which has led to numerous iterations for an assortment of textiles.[103–105] In one case, DNA's inherent intumescent-like chemistry (i.e. phosphates acting as an acid source and its high nitrogen content) was used to protect cotton.[106] Most intumescent

multilayer coatings use amine-rich polysaccharides as the cationic component because the polysaccharides can promote char formation. Polyelectrolyte multilayer films have been developed based entirely on polysaccharides, comprising phosphorylated cellulose derivatives as the anionic component and chitosan as the cationic component.[107,108] A later study reported that increasing the loading of phosphorus can enhance the flame retardant abilities of polysaccharide-based materials, more so than phosphorylated derivatives can achieve alone.[105] A 20-bilayer coating consisting of chitosan and APP on cotton fabric decreased the peak HRR and THR with respect to uncoated cotton by 80% and 82%, respectively when evaluated by micro combustion calorimetry. The success of these intumescent coatings on cotton and ramie fabrics has led to the application of similar coating chemistries to various cotton-synthetic fiber blends. The intumescent coatings that were successful on cotton were not as effective on the blends because of the intrinsic difference in chemistry of the blended substrates that are believed to require a combination of gas phase and condensed-phase action to self-extinguish.[67]

2.6.3 Buffer-Cured Polyelectrolyte Complexes

A drawback of layer-by-layer assembly, which researchers are attempting to overcome, is the number of processing steps necessary to deposit a flame retardant coating. In one study, a mixture of PEI and PSP, both at pH 7, was used to form a complex on an immersed fabric substrate through sedimentation as the two components formed a polyelectrolyte complex that slowly settled out of solution and onto the fabric.[109] The deposited coating is analogous to a previous reported layer-by-layer assembled PAAm/PSP system studied.[78] This sedimentation process has been improved upon in subsequent years, and it was found that at a slightly higher pH (9-12 depending on the polymer used) a polyamine and polyphosphate can coexist in solution. This water-soluble

polyelectrolyte complex is then applied to a substrate and, after drying, the dried polyelectrolyte mixture is cured with a buffer that charges the polyamine and forms a solid coating on the fabric (**Figure 2.7**). This improved process enabled a solution containing 5 wt% PEI and 10 wt% PSP, cured at pH $\leq$ 4, to impart self-extinguishing behavior and pass a vertical flame test.[110] In a separate study, this process was applied to nylon/cotton blends, with incorporation of melamine,[111] and yielded a wash-durable complex (owing to the use of higher pK_a of polyallylamine compared with PEI).[112] Similar motifs have been used to form polyelectrolyte complex coatings from entirely bio-derived materials.[113]

Other polyelectrolyte complex coatings have taken advantage of ability to be deposited quickly. For example, carbon fibers coated with a polyelectrolyte complex of chitosan and APP (mimicking the sedimentation strategy[109]), were incorporated into an epoxy resin to impart substantial improvements in flame retardancy; more specifically, a 50% reduction in peak HRR and a 30% reduction in smoke production.[114] In another example, wood with a polyelectrolyte complex coating of PEI and PSP showed self-extinguishing behavior in open flame testing.[16] In both of these cases, the number of processing steps for the substrate (either the epoxy or wood), would have been prohibitively difficult to implement using layer-by-layer assembly, but the polyelectrolyte complex coating enabled a facile improvement in fire safety.

An important future direction for polyelectrolyte complex coatings is the incorporation of clay (or other nanoparticles). This incorporation has been accomplished by using a polyelectrolyte complex 'gel' of chitosan and montmorillonite to coat an acrylic fabric.[115] The gel was applied using a doctor blade. It is worth noting that in this case, the term polyelectrolyte complex is used more broadly (because only one classical polyelectrolyte is involved). Although a clay nanoplatelet is a crystalline material, it has many surface charges and is a polyelectrolyte in the broadest sense.

This chitosan and montmorillonite coating prevented the melt-dripping of the acrylic fabric, and also imparted self-extinguishing behavior in a horizontal flame test. This advancement will hopefully enable the development of more particle-containing polyelectrolyte complex systems, as pure intumescent coatings alone have been shown to be ineffective flame retardants for many important substrates, such as polyurethane foam.[45]

CHAPTER III

RENEWABLE NANOBRICK WALL COATINGS FOR FIRE PROTECTION OF WOOD*

3.1 Introduction

In 2017, there were nearly 500,000 structure fires reported in the United States. Of these fires, about 72% were home structure fires, which were responsible for 77% of all fire deaths and $7.7 billion in property damage.[116] Wood is a major component in both home construction and home décor, such as floors and ceiling/wall paneling, due to its aesthetic appeal and good mechanical properties.[2] Furthermore, wood is a renewable resource, so there is growing interest in it for both construction and the development of new technologies.[117] It is for these reasons that it is of high importance to develop effective, environmentally-benign flame retardants for wood, especially as society seeks to avoid the use of halogenated molecules and other toxic flame retardants.[118–120]

Recently, the use of flame retardant nanocoatings deposited via layer-by-layer (LbL) assembly have risen to prominence due to their environmental friendliness and efficacy.[121,122] The LbL process consists of exposure (dipping or spraying) of a substrate to a plurality of solutions of cationic and anionic macromolecules/nanoparticles. These multilayer films are typically held together via electrostatic interaction and impart a variety of functionality.[51,123,124] The appeal of this water-based coating technique lies in its versatility, as it enables construction of conformal coatings across a wide variety of different substrates and utilizes ambient processing conditions. This versatility has enabled effective flame retardant coatings of two-dimensional substrates, such

*Reprinted with permission from Kolibaba, T.J.; Brehm, J.T.; Grunlan, J.C., Renewable Nanobrick Wall Coatings for Fire Protection of Wood, *Green Materials* **2020**, *8*, 131-138.

as plastic films,[125,126] as well as conformal coatings of complex three-dimensional fabric and open-celled polyurethane foam.[127–131] There has also been some recent development of coatings for wood to reduce its flammability.[132–134]

The deposition of multilayered nanocoatings onto wood has been previously studied, although it was primarily restricted to the assembly of LbL coatings on wood fibers.[135–137] More recently, studies have been performed on bulk wood substrates.[138–142] One of the key insights from these studies has been that the heterogeneous surface of wood leads to very slow diffusion of polyelectrolytes.[138,140] This necessarily means that LbL deposition time is longer for wood than for most other substrates (sometimes hours per bilayer).[140] Surface pretreatments have been used on other substrates as a way to improve surface coverage of multilayer coatings as well as modulate thickness.[143–145] In the present study, two different surface pretreatments of wood are performed to improve the growth of a thick-growing nanobrick wall coating composed of environmentally-sourced chitosan (CH) and vermiculite (VMT) clay. Exposing wood to a sodium hydroxide solution prior to depositing two bilayers of CH/VMT results in a significant increase in time to ignition and notable decrease in total heat release. This use of a simple surface treatment provides a way to effectively apply functionality to wood using layer-by-layer assembly.

3.2 Experimental

3.2.1 Materials and Substrates

Chitosan (CH, Item FGC-1, 95% deacetylated, 50-60 cps) was purchased from the GTC Bio Corporation (Qingdao, Shandong Province, China). Microlite 963^{++} vermiculite clay (VMT, 7.8 wt% in water) was purchased from Specialty Vermiculite Corporation (Cambridge, MA, USA). Acetonitrile (Certified ACS, 99.9%) was purchased from Fisher Chemical (Waltham, MA,

USA). Hexylamine (99%) and succinic anhydride (SA, 99%) were purchased from Alfa Aesar (Tewksbury, MA, USA). Hydrochloric acid (ACS reagent, 37%), sodium hydroxide (ACS reagent, ≥97.0%), acetone (ACS reagent, ≥99.5%), and *N*,*N*-dimethylbenzylamine (≥99%) were purchased from Sigma-Aldrich (St. Louis, MO, USA). All aqueous solutions were prepared in 18 MΩ deionized (DI) water. Commercial pine boards (1x10 "Premium Kiln-Dried Square Edge Whitewood Common Board", actual thickness 1.9 cm) were purchased at a local Home Depot (College Station, TX, USA) and cut to either 10 x 5 x 1.9 cm rectangles (for open flame and mechanical testing) or 10 x 10 x 1.9 cm squares (for cone calorimetry). All dimensions are longitudinal x radial x tangential.

3.2.2 Pretreatment of Wood

Cut wood pieces were stored in a 70 °C oven prior to use. Untreated and base-treated samples were soaked in DI water for 12 hours prior to coating to increase the surface area of the wood substrate.[138] Base-treated samples were transferred from DI water and placed in a sealed container of stirring 0.1 M NaOH for 30 minutes, after which they were removed and the coating was immediately applied (i.e. without rinsing off residual NaOH). Succinic anhydride-treated wood samples were prepared by immersing wood pieces in a sealed container filled with a 0.33 M solution of SA in acetonitrile. To this mixture was added 2 mol% (relative to SA) *N*,*N*-dimethylbenzylamine as a catalyst.[146] After rolling the mixture for 24 hours, the acetonitrile solution was poured off, and the wood was rolled in a sealed container full of acetone twice for one hour each to rinse off residual SA and catalyst. The acetone was then poured off and the wood pieces were dried in a 70 °C convection oven overnight. These samples were rehydrated in DI water for 12 hours prior to coating.

3.2.3 Deposition of Coatings

A 0.1 wt% solution of chitosan in 50 mM hexylamine, which was adjusted to pH 1.8 with 5 M HCl and allowed to stir overnight, was adjusted to pH 6 with 1 M NaOH prior to use. The rinse solution of 50 mM hexylamine was adjusted to pH 6 with 5 M HCl. A suspension of 1 wt% VMT was rolled overnight and allowed to settle for 4 hours, after which the supernatant was adjusted to pH 10 with 1 M NaOH (Note: NaOH solution was added dropwise to avoid excessive amounts of VMT crashing out of solution). A final rinse solution of pH 10 water was made by diluting 1 M NaOH. Wood samples were attached by screw to a holder and were coated via a robotic dipping system.[147] Samples were first immersed in the CH + hexylamine solution, followed by three sequential dip rinses in 50 mM hexylamine solutions. To complete a bilayer (BL), the samples were then dipped in the VMT solution, followed by three sequential dip rinses in pH 10 water. All dips were for 30 minutes, and all samples were coated with 2 BL of CH/VMT. The coating process is summarized in **Figure 3.1**. After coating, samples were allowed to equilibrate at ambient temperature/humidity for three days before being placed in a 70 °C oven to more completely dry.

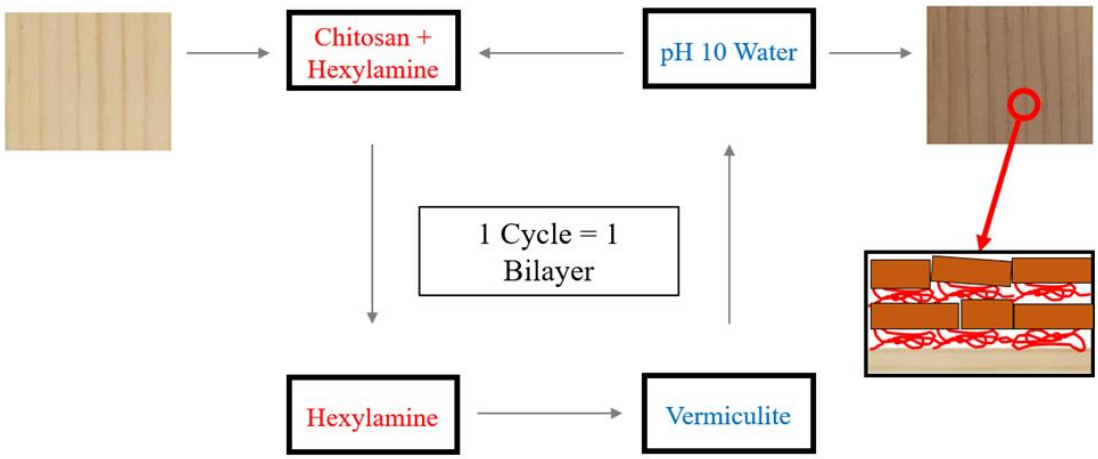

Figure 3.1. Schematic showing the layer-by-layer assembly process. Inset shows a schematic of the nanobrick wall structure on the surface of coated wood. The red lines represent chitosan and the brown blocks represent clay platelets.

3.2.4 Sample Characterization

Flame tests were performed with a home-built torch testing setup in a fume hood, with the airflow shut off and the sash set to a height of 30 cm. Wood samples were stored in a drybox prior to testing, and held vertically by wire mesh and exposed to flame from a MagTorch Model MT 48 EXT propane blowtorch (Magna Industries, Inc. Cleveland, OH, USA) fed by a Bernzomatic 400 g propane tank (Worthington Industries, Columbus, OH, USA). The torch was set so that the inner flame was 2.5 cm and the wood pieces were placed 0.5 cm away from the torch's emitter. Flame was impinged upon the sample for 30 seconds, after which the flame was removed and the sample was allowed to burn until the sample either self-extinguished or the flame burned itself out. Once smoldering had ceased, and the samples were cool to the touch, the residue was collected and weighed. Infrared spectroscopy was carried out by cutting thin slices (ca. 1 mm) from the exterior of the wood and placing them atop an Alpha Platinum-ATR FTIR spectrometer (Bruker, Billerica, MA, USA). Scanning electron microscopy (SEM) was performed with a Model JSM-7500F FE-SEM (JEOL, Tokyo, Japan) after sputter-coating the surface with a 5 nm thick Pd-Pt alloy to reduce charging. SEM images were taken along the grain of the wood, while EDS imaging (Oxford Instruments, High Wycombe, United Kingdom) was performed across the grain (i.e. a cross-sectional view was taken). Cone calorimetry experiments were performed by the University of Dayton Research Institute (Dayton, OH, USA) utilizing a FTT Dual Cone Calorimeter according to ASTM E-1354/ISO 5660. Samples were placed in an aluminum foil pan and exposed to a heat flux of 35 kW/m^2, with an exhaust flow of 24 L/s. No grid was used to prevent sample deformation. Mechanical testing was performed with a MTS Insight Electromechanical Testing System (MTS Systems Corporation, Eden Prairie, MN, USA) utilizing a 30 kN load cell. Samples were set up in a 3-point bending arrangement, with a spacing of 75 mm between the lower points. Samples were

held at ambient temperature and humidity (ca. 22 °C and 20-40% humidity) for seven days prior to performing mechanical testing. For the sake of consistency, samples that were not coated were also hydrated and screwed onto the holder (as if to be coated) prior to equilibrating with the coated samples before testing. Moisture content of wood was determined via thermogravimentric analysis (TGA Q50, TA Instruments, New Castle, DE, USA). Samples were heated isothermally at 110 °C for 20 minutes under a purge flow of 60 mL/s air with a balance flow of 40 mL/s nitrogen.

3.3 Results and Discussion

3.3.1 Surface Treatment and Coating Deposition

Wood is known for having an extremely heterogeneous surface that results in slow adsorption kinetics, thus necessitating long immersion times for layer-by-layer deposition.[138,140] For this reason, a thick-growing nanobrick wall system that utilizes buffered dip rinses was chosen.[148] This buffered system has been shown to deposit a nanobrick wall coating 200-fold thicker than a non-buffered system.[130,149] Hexylamine was chosen as the buffer because it results in the thickest coating.[148] In an effort to further optimize the growth of this system, two different surface treatments were implemented, which are summarized in **Figure 3.2**. These surface treatments are meant to increase the charge density of the wood's surface. The succinic anhydride treatment imparts carboxylate groups on the wood's surface, which have a pKa of around 4.5. When the SA-treated wood is immersed in the chitosan solution (at pH 6), most of the carboxylates are deprotonated, leading to higher surface charge density than unmodified wood. The base-treated wood simply has charges from cellulose, hemicellulose, and lignin being deprotonated by the base, leaving behind negatively-charged alkoxide groups.[150] The more charge-dense surface is thought

to help minimize the so-called “island growth” phase of LbL film deposition that leads to very uneven surface coverage in the first few deposited layers.[51,143]

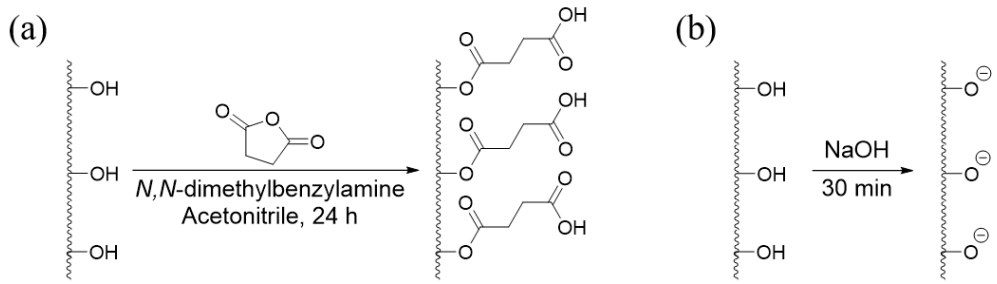

Figure 3.2. Functionalization of wood by reaction with succinic anhydride (a) and with sodium hydroxide (b).

The surface treatments appear to make the coatings more uniform, as can be seen from the digital photographs of the coated wood specimens (**Figure 3.3d-f**). It is clear that the coverage of the coating is considerably less uniform for the untreated, coated substrate (**Figure 3.3d**). The anhydride treatment does not visually appear to have a dramatic effect on the coating coverage (**Figure 3.3e**), while the base treatment results in a very uniform coating (**Figure 3.3f**). It can also be seen that the base-treated and coated wood is considerably darker in color. This suggests that the coating has infiltrated further into the wood and the darkened color is reflective of the brown color of the VMT, which is a common occurrence in such coatings.[148] The treatments do not alter the visual appearance of the wood. The untreated, SA-treated, and base-treated wood are very similar in appearance (**Figure 3.3a-c**).

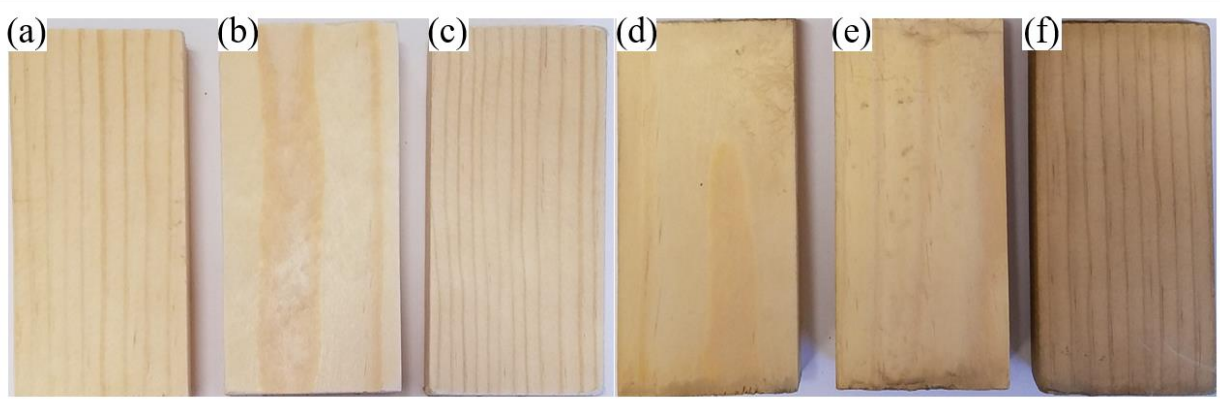

Figure 3.3. Digital images of the wood samples: **(a-c)** Before coating and **(d-f)** after coating. Treatment conditions shown here are: **(a,d)** untreated wood, **(b,e)** SA-treated wood, and **(c,f)** base-treated wood.

Further evidence of the effectiveness of the surface treatments in improving film deposition can be seen in the weight changes caused by both the coatings and the pretreatments. **Table 3.1** shows that the SA treatment increases the weight of the wood without any coating added, suggesting successful functionalization of the wood's surface with carboxylate groups. This is further confirmed by IR spectroscopy, which clearly shows an increase in the intensity of the stretches at 2924 cm^{-1} and 1730 cm^{-1}, indicating addition of alkyl C-H bonds and carbonyl functionality (**Figure 3.4**) to the wood's surface. The SA treatment also slightly improves the weight gain of the coating, suggesting successful chemical alteration and an increase in the surface charge density via the attached carboxylate groups (**Figure 3.2a**). The sodium hydroxide pretreatment lowers the weight of the wood due to the degradation and removal of lignin, with a concurrent increase porosity and surface area.[151] This increased surface area creates sites for chitosan (and subsequently VMT) to adsorb. This combination of chemical and physical alteration of the wood explains why the coating weight gain of the base-treated wood is increased by nearly 100% relative to the succinic anhydride pretreatment.

Table 3.1. Weight gain of treatment and coating of wood and subsequent torch-test performance.

Treatment	*Wt. Gain (%)*	*Coating Wt. Gain (%)*	*Afterflame Time (s)*	*Torch Test Residue (%)*
None	-	-	151 ± 50	90 ± 3
SA	0.9 ± 0.1	-	163 ± 80	90 ± 2
Base	-0.6 ± 0.1	-	60 ± 20	91 ± 1
2 BL	0.69 ± 0.03	0.69 ± 0.03	60 ± 45	93 ± 1
SA + 2 BL	1.7 ± 0.1	0.8 ± 0.1	18 ± 2	94.1 ± 0.2
Base + 2 BL	0.9 ± 0.1	1.5 ± 0.1	46 ± 8	95.0 ± 0.6

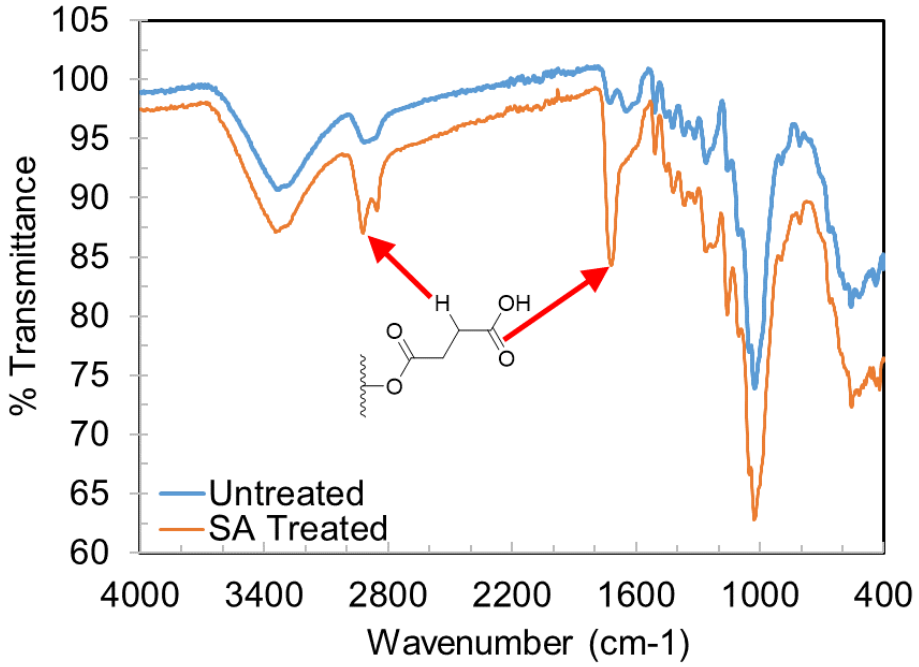

Figure 3.4. FTIR spectra of untreated and SA-treated wood, along with a schematic structure of the SA-modified wood surface, with arrows pointing out key changes in the spectrum indicative of successful functionalization.

3.3.2 Open Flame Testing

Torch testing indicates that the coatings and pretreatments alter the burning behavior of wood. **Table 3.1** summarizes the results of this testing. Untreated and SA treated wood both have very long afterflame times (defined as the time period for which the wood continued to burn after removal of the blowtorch), while the base treatment appears to considerably reduce the afterflame time. This may be a result of the base treatment's preferential erosion of lignin, which leaves

behind cellulose and hemicellulose. Lignin has a considerably higher char yield than cellulosic materials.[152,153] The absence of the char layer that forms when untreated and SA treated wood are burned leads to faster consumption of the exposed material and thus a shorter afterflame time. On the whole, this indicates that the base treatment alone causes the wood combustion to be more violent.

All three coated samples performed better in torch testing, reducing mass loss by 30-50% relative to uncoated wood. Coated wood also exhibits lower burn times than uncoated samples (with the exception of the base-treated, uncoated wood). This is due to the clay in the coating forming a physical barrier to both heat and gas transfer, which leads to the flame being extinguished sooner.[130] The performance of the coatings was most closely related to the amount of coating present, with the untreated, coated wood providing the least protection, while the base-treated, coated wood, with the highest coating weight, provided the greatest reduction in mass loss upon burning.

3.3.3 Coating Morphology

Images of the surface treatments and the multilayer coatings on the wood's surface are shown in **Figure 3.5**. As expected, SA treatment does little to alter the surface of the wood (**Figure 3.5b**). The base treatment significantly alters the wood's surface (**Figure 3.5c**), creating increased porosity. Pores are visible in the untreated (**Figure 3.5a**) and SA-treated (**Figure 3.5b**) wood, but the base treatment appears to better expose them. Greater porosity serves to explain the large increase in coating weight gain in the wood, as the opening of these pores creates more surface area on which the LbL film can grow. The eroded material is likely lignin, leaving behind cellulosic material and a scaffold of microfibrils.[2,151] The presence of just two bilayers of CH/VMT

dramatically alters the surface morphology by "smoothing" it out. It is certainly noteworthy that both the untreated and SA-treated wood still appear to have a few large holes in the coating (**Figure 3.5d,e**). These gaps in the coating likely contribute to their worse performance in the torch test as compared to the base-treated wood. Clay-based coatings operate by forming a barrier to prevent gas transfer, and holes harm the ability of the coating to protect the underlying substrate from combustion.[130,154] In contrast, it was not possible to find any holes in the base-treated wood samples. Doubling the amount of material deposited likely plays a large role in filling in these holes and forming a smooth, insulating barrier to gas and heat transfer.

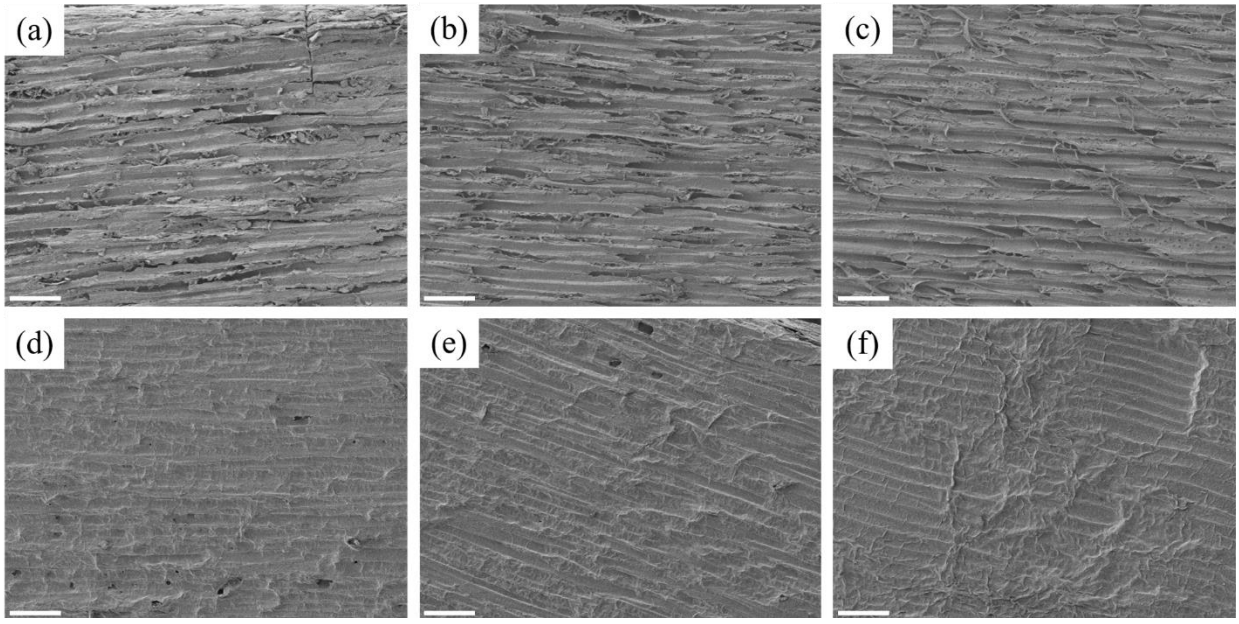

Figure 3.5. SEM images of the wood samples: **(a-c)** Before coating and **(d-f)** after coating. Images include untreated **(a,d)**, SA-treated **(b,e)**, and base-treated **(c,f)** samples. Scale bars are 200 μm.

EDS was utilized to study the depth of penetration of the coating by detecting the signal generated from the silicon and magnesium in VMT. Images and calculated depth of coating penetration are shown in **Figure 3.6**. It appears that the coating's depth of penetration increases following treatment by either SA or base. The approximately doubled depth of penetration for the

base-treated wood matches its approximately doubled coating weight gain, shown in **Table 3.1**. This is not the case for SA-treated wood, where the coating depth of penetration is increased by > 50%, but the increase in weight gain from the coating was negligible. The decreased afterflame time in open flame testing in this sample may be a result of this decreased coating density. A larger volume of wood is coated by clay in the SA-treated system. Despite the coating necessarily being thinner, this causes more of the combustible material to have some amount of coating on it, limiting gas transfer, which decreases the afterflame time because the oxygen supply runs out sooner. This lower-density coating is the likely explanation for the modest improvement in post-burn residue and large decrease in afterflame time, since there is less inorganic material present at the combustion zone, which leads to more of the organic material being exposed to thermal degradation.

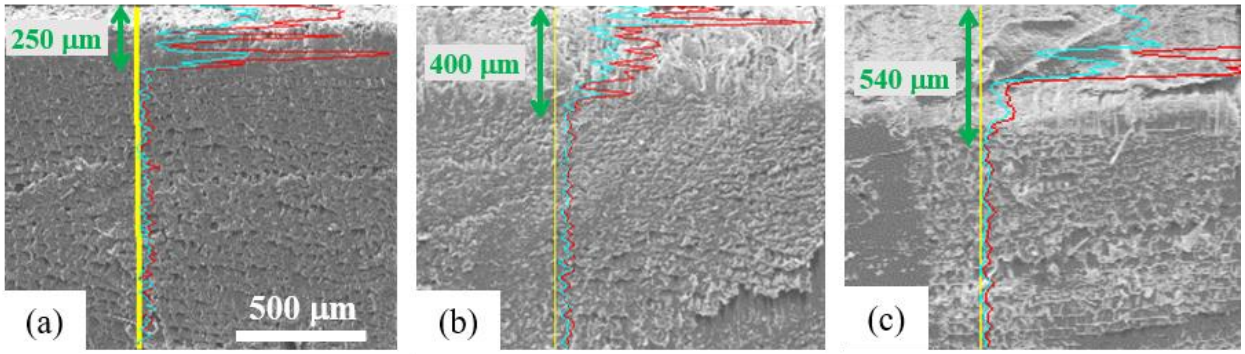

Figure 3.6. SEM images of wood cross-sections overlayed with EDS signals for silicon (red) and magnesium (teal). Depth of penetration for the coating is shown to the left of the EDS signals for coated wood samples with **(a)** no treatment, **(b)** SA-treatment, and **(c)** base-treatment.

3.3.4 Cone Calorimetry

Response of the wood to an incident heat flux was measured using a cone calorimeter, which measures heat release rate (using oxygen consumption calorimetry).[155,156] **Table 3.2** summarizes these data. Time to ignition (TTI) is how much time under the incident heat flux it

takes for a sample to ignite. Peak heat release rate (pkHRR) and average heat release rate (average HRR) are the maximum rate of heat release during combustion and the average rate of heat release, respectively. Total heat release (THR) is the total energy released upon complete combustion of the material in cone calorimetry. These pieces of information are summarized in **Table 3.2** for uncoated and untreated wood (i.e. control), untreated wood coated with 2 BL CH/VMT and base-treated and coated wood.

Table 3.2. Cone calorimetry data for wood samples.

Sample	*TTI (s)*	*pkHRR (kW/m^2)*	*Average HRR (kW/m^2)*	*THR (MJ/m^2)*	*% Residue*
Control	40 ± 9	220 ± 3	101 ± 5	90 ± 2	16.4 ± 0.6
2 BL	37 ± 4	270 ± 20	88 ± 3	83 ± 6	18 ± 1
Base + 2 BL	80 ± 30	320 ± 30	83 ± 3	73.9 ± 0.9	23 ± 2

As shown in **Table 3.2**, even in the absence of pretreatment, the 2 BL CH/VMT nanocoating provides protection by reducing average HRR (13%) and THR (8%), while increasing post-burn residue (10%). The increase in pkHRR appears to be somewhat alarming, especially since this is usually viewed as a value of critical importance when evaluating the performance of flame retardant coatings on textiles and foams.[121,157–159] This seemingly anomalous behavior can be explained by the plot shown in **Figure 3.7a**. Once the heat flux is applied, a sudden decrease to HRR < 0 is observed before a large increase followed by a fast decline to a baseline level as the wood burns. This trend is because coated and uncoated wood immediately forms a char layer when it is exposed to the heat flux. When the uppermost layer of char eventually forms cracks through which gas can flow, a large but short output of flammable gases occurs, yielding a brief increase in HRR.[160,161] Due to the negative values read prior to this spike in HRR, it is likely that the sudden influx confounds the measurement, meaning that pkHRR is likely not as important of a parameter for this particular type of sample. When the base-treatment precedes the 2 BL coating the TTI is doubled. This is an important result, as an increased ignition time dramatically reduces the danger

that a particular material poses in the event of a fire. It is for this reason that even uncoated wood has been studied for use in safer home design.[162] The base-treated, coated wood significantly reduces average HRR (18%) and THR (18%), and increases post-burn residue (40%) relative to the uncoated and untreated control.

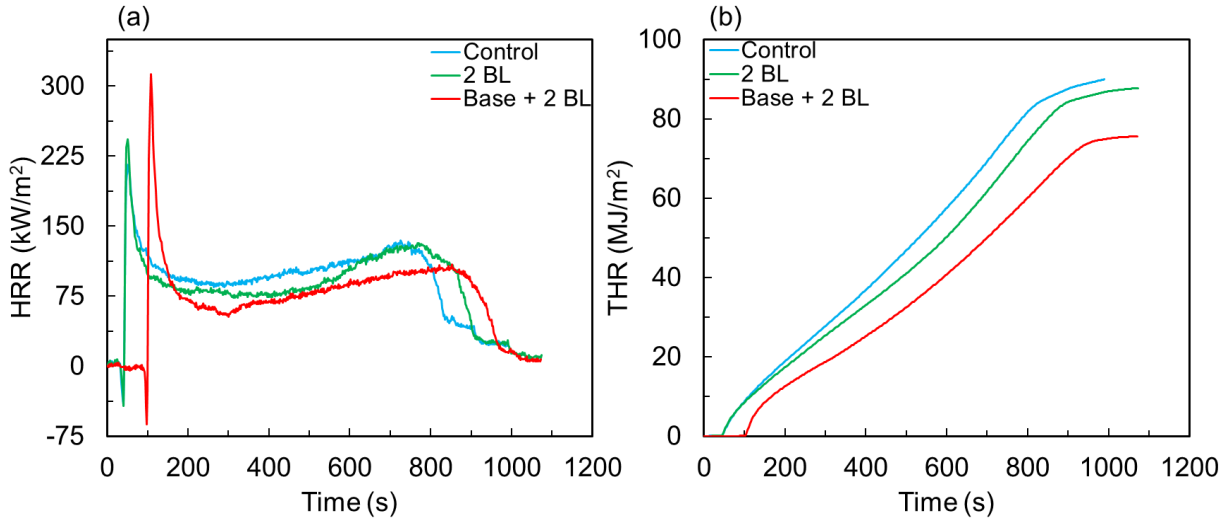

Figure 3.7. (a) Heat release rate and **(b)** total heat release as a function of time. Traces are of representative individual samples.

The plots in **Figure 3.7** show that the surface treatment is very important in reducing wood flammability. The base-treated, coated wood exhibits a substantial delay in its TTI, likely owing to the much smoother, complete barrier that is formed (**Figure 3.5f**). Lacking any of the holes that were visible for coated, untreated and SA-treated samples, the base-treated wood's coating forms a much better barrier to both heat and gas transfer, and delays ignition about twice as long as the other coatings do (on average). **Figure 3.7b** reflects what was observed in the torch testing data from **Table 3.1**, which is that any form of coating helps improve burning behavior, but the base-treatment yields the greatest improvement. The dramatic decrease in THR from the untreated to the base-treated wood is remarkable. It is expected that the coated, SA-treated wood falls between

the untreated and base-treated samples, likely lying closer to the untreated owing to its lower coating weight.

3.3.5 Mechanical Testing

The mechanical properties of wood samples were tested in 3-point bending, with the results summarized in **Table 3.3**. It is evident from these data that regardless of the pretreatment (or lack thereof), the flexural modulus decreases by ~100 MPa when the 2 BL coating is deposited. Pretreatment in the absence of coating also appears to reduce the modulus of the wood, with the base treatment resulting in a more significant decrease of ~130 MPa. In contrast, pretreatment affects flexural strength very little, while the coated samples exhibit more reduced strength as the degree of surface modification increases. The erosion of lignin and other supportive material as a result of the base treatment is likely the reason for the lowered modulus in these samples. It is unclear what leads to the reduced modulus for the SA-treated samples. It is possible that the addition of the succinic acid pendant groups causes a disruption in the crystallinity of the cellulose in the wood.[163] Reduction in crystallinity is widely known to reduce the strength and modulus.

Table 3.3. Mechanical properties of wood samples.

Treatment	*Flexural Modulus (MPa)*	*Flexural Strength (MPa)*
None	830 ± 90	42 ± 5
SA	740 ± 20	41 ± 1
Base	670 ± 90	40 ± 1
2 BL	700 ± 30	41 ± 3
SA + 2 BL	660 ± 50	35 ± 5
Base + 2 BL	540 ± 80	31 ± 2

The observed reduction in both flexural modulus and strength in the coated, base-treated wood is likely not enough to disqualify many of the potential end-uses for this coating system. Wood utilized for a weight-bearing application is not designed to approach anywhere close to the

ultimate strength of the wood. Therefore, even these erosions of wood's modulus/strength will be insignificant in wood's construction applications. Furthermore, the surface area:volume ratio would be much less in any industrial/residential application, which would dilute the effects of this system on the mechanical properties of the wood, while still providing excellent fire protection, because the coating is localized on the exterior of the wood. Additionally, many applications of wood are aesthetic (e.g. wall/ceiling paneling, building siding, etc.) and do not require much, if any, weight bearing capacity. In fact, it is thought that these aesthetic uses of wood could contribute to protecting a building from a fire.[162]

3.4 Conclusions

In summary, two bilayers of a thick-growing CH/VMT nanobrick wall coating were deposited on wood with altered surface chemistry. While carboxylation via conjugation with succinic anhydride is successful, it provides only modest improvement in coating deposition and reducing flammability, while lowering mechanical strength. Treatment with 0.1 M NaOH for 30 minutes significantly increases the coating weight and depth of penetration, which improves the flame retardant performance of the coating. This simple, water-based treatment provides a means to effectively functionalize wood and improve the safety of wood construction.

CHAPTER IV

ENVIRONMENTALLY BENIGN POLYELECTROLYTE COMPLEX THAT RENDERS WOOD FLAME RETARDANT AND MECHANICALLY STRENGTHENED*

4.1 Introduction

The United States National Fire Protection Association reports that fire departments responded to more than one million fires in 2016.[164] These fires resulted in 3,390 civilian deaths and 14,650 civilian injuries. The vast majority of deaths (81%) resulted from home structure fires, along with 73% of the injuries. A key material in the construction of most homes is wood, owing to its renewability and good mechanical properties.[2] Numerous methods to apply flame retardant (FR) compounds have been developed in the past. Many of these have relied upon the use of halogenated compounds, which have been shown to accumulate in the environment and cause poor health effects.[165,166] Several groups have recently created coatings to impart flame resistance to wood without using these harmful compounds.[167,168,134,169,132,133] These have been primarily inorganic coatings, incorporating phosphorus-containing small molecules or clays onto/into the wood in order to provide flame shielding and a reduction in overall flammability.

In related work, a variety of common household substrates (e.g. foam and textiles) have used polyelectrolyte complexes (PECs) to combat flammability. PECs are most often deposited via the layer-by-layer (LbL) assembly method, where the substrate is alternately immersed in polycation and polyanion solutions, with rinse steps in between.[121,122] Due to the large number of processing steps, and the extremely heterogeneous surface of wood that leads to very slow

*Reprinted with permission from Kolibaba, T.J.; Grunlan, J.C. Environmentally Benign Polyelectrolyte Complex that Renders Wood Flame Retardant and Mechanically Strengthened, *Macromolecular Materials and Engineering* **2019**, *304*, 1900179.

adsorption of polyelectrolytes in each deposition step,[138] While it was shown in Chapter III to be effective, LbL assembly seems an impractical option for protecting wood.[15] It was recently found that for optimal growth, much longer dip times are necessary, requiring up to two hours for the deposition and rinse cycle of a single polyelectrolyte, equating to four hours per bilayer.[140] Most intumescent LbL coatings typically require more than 10 bilayers to be effective.[158,170–173] On a wood substrate, applying this many bilayers would take more than one day.

One way to circumvent the large number of processing steps required by the LbL method has been to utilize water-soluble polyelectrolyte complex coatings. This strategy involves creating a stable solution of two polyelectrolytes by adjusting the pH so that only one species is highly charged. In this state, the PEC will be water soluble and can be easily applied to a surface, which is then exposed to a buffer solution that charges the uncharged polyelectrolyte.[110–112] Due to the length of time required to deposit an effective LbL coating to impart flame retardancy to a wood substrate, a polyelectrolyte complex strategy was adopted here to protect construction lumber with an intumescent coating. This coating, comprised of polyethylenimine and sodium hexametaphosphate (and cured with a citric acid buffer), is deposited with relatively little processing time and few processing steps, while also preserving the visual aesthetic of the wood substrate. The PEC imparts effective FR properties to wood, including self-extinguishing behavior in open flame tests, increased time to ignition, and reduced peak heat release rate. Additionally, the PEC increases both the modulus and the strength of the coated wood.

4.2 Experimental

4.2.1 Chemicals and Substrates

Branched polyethylenimine (PEI, M_w ~25,000 g mol^{-1}), sodium hexametaphosphate (PSP, crystalline, +200 mesh, 96%), hydrochloric acid (HCl, ACS reagent, 37%), sodium hydroxide (NaOH, ACS reagent, 97%) and citric acid monohydrate (CA, reagent grade, 98%) were purchased from Sigma Aldrich (St. Louis, MO, USA) and used as received. A commercial 2x4 "Premium Kiln-Dried Whitewood Stud" (actual dimensions 3.8 x 8.9 cm) was purchased at a local Home Depot (College Station, TX, USA) and cut across the grain into 6.4 mm thick slices (slices were 3.8 x 8.9 x 0.64 cm, radial x tangential x longitudinal). Wood slices were soaked in stirring 18 MΩ deionized (DI) water for 72 hours and then dried and stored in a 70 °C oven prior to use.

4.2.2 Polyelectrolyte Complex Deposition

Dried wood slices were immersed in DI water for at least 12 hours before use to hydrate cell walls prior to coating, which increases the surface area of the wood up to 1000X.[138] Two equal mass solutions, 15 wt% PEI (adjusted to pH 9 with 5 M HCl) and 30 wt% PSP (at its natural pH), were prepared separately. The 100 mM CA curing buffer solution was created by dissolving an appropriate amount of CA in DI water, followed by adjusting the pH to 3 with 1 M NaOH. The separate PEI and PSP solutions were mixed to form a pearlescent polyelectrolyte complex solution, with final concentration of 7.5 wt% PEI and 15 wt% PSP, which was utilized immediately after mixing.

Wood samples were immersed into the stirring PEC solution for a given length of time, referred to as the 'dip time' (1 or 60 minutes). After the initial coating was deposited, it was cured by immediately immersing samples into the 100 mM CA buffer for a given length of time, referred

to as the 'cure time' (1 or 10 minutes), with periodic stirring. Coated samples are referred to as $PEC_{x,y}$, where x is the dip time and y is the cure time. $PEC_{1,1}$ is the sample that was dipped in the complex for one minute and cured for one minute. After curing, samples were immersed in stirring DI water for one hour before being dried for 72 hours in a 70 °C oven. The complete coating process is summarized in **Figure 4.1**. Wood samples were stored in a drybox until they were characterized.

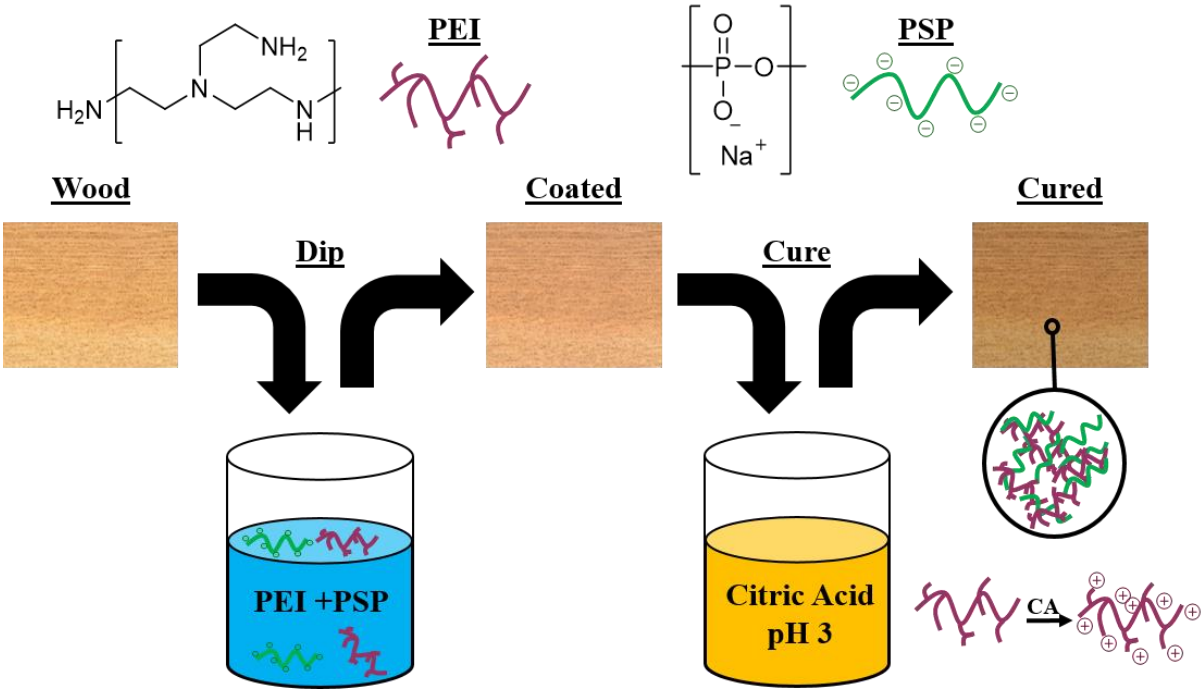

Figure 4.1. Schematic of the deposition process of the PEC coating onto the wood substrate, along with the structures of the polyelectrolytes utilized in this study.

4.2.3 Characterization of Coated Wood

Flame tests were performed with a homebuilt torch testing setup in a fume hood, with the airflow shut off and the sash set to 30 cm. Wood samples were held vertically by wire mesh and exposed to the flame (parallel to the grain) from a butane torch (Bernzomatic ST2200, Worthington Industries, Columbus, OH, USA). The inner blue flame of the torch was approximately 2.2 cm

long. The torch's emitter was positioned 1.8 cm from the wood sample for 45 seconds, after which the torch was removed and the sample was allowed to continue burning until the fire burned itself out or the coating self-extinguished the flame (i.e. the afterflame time). After all smoldering had ceased, the residue was collected and weighed. Thermogravimetric analysis (TGA) was carried out with a Q-50 thermogravimetric analyzer (TA Instruments, New Castle, DE, USA). Samples were heated at 100 °C for 30 minutes to remove any residual water, and then heated at 10 °C min^{-1} up to 800 °C under a purge flow of 60 mL s^{-1} air with a balance flow of 40 mL s^{-1} nitrogen.

Scanning electron microscope (SEM) images of the wood surface were taken with a Model JSM-7500F FE-SEM (JEOL, Tokyo, Japan) after sputtering the surface with a 5 nm thick Pd-Pt alloy. SEM images were taken with an end-grain orientation. Energy dispersive spectroscopy (EDS) data were acquired from the SEM via an Oxford EDS system (Oxford Instruments, High Wycombe, United Kingdom). Cross sectional samples for EDS measurement were acquired from the interior part of coated substrates to ensure that the phosphorus signals measured were a result of coating diffusion through the bulk of the sample and not a result of diffusion through the edges.

Cone calorimetry experiments were conducted by the University of Dayton Research Institute utilizing an FTT Dual Cone Calorimeter according to ASTM E-1354-16. Samples were placed in an aluminum foil pan and exposed to a heat flux of 35 kW m^{-2} (exhaust flow 24 L s^{-1}). No grid was used to prevent sample deformation by the incident heat. It should be noted that typical dimensions for the sample holder in cone calorimetry are 10 x 10 cm. The substrates utilized in this study are smaller than normal cone calorimetry samples, so a larger percentage of their surface area was exposed to the atmosphere. Mechanical testing was performed with a MTS Insight Electromechanical Testing System (MTS Systems Corporation, Eden Prairie, MN, USA) utilizing

a 2.5 kN load cell. Samples were set up in a 3-point bending arrangement, with a spacing of 45 mm between the lower points.

4.3 Results and Discussion

4.3.1 Polyelectrolyte Complex Deposition

At high pH, the charge density of polyethylenimine is not sufficient to initiate complex formation with hexametaphosphate, which provides time for the solution to effectively coat the wood samples. Once the PEI and PSP have adsorbed onto the wood's surface, the acidic buffer (well below the pKa of PEI's amine groups) protonates the PEI and causes it to have substantial positive charge. The strong positive charge of the PEI, coupled with the negative charge of the PSP leads to an entropy-driven complexation of the two polyelectrolytes. A film forms over the surface of the wood that is initially sticky to the touch, but after drying feels no different from uncoated wood and visibly appears the same, as shown in **Figure 4.2**. This deposited complex is extremely insoluble at this point, owing to the strong ionic crosslinks formed by the interaction of the charged groups of PEI and PSP. These crosslinks render the coating resistant to dissolution by any further water exposure.[112]

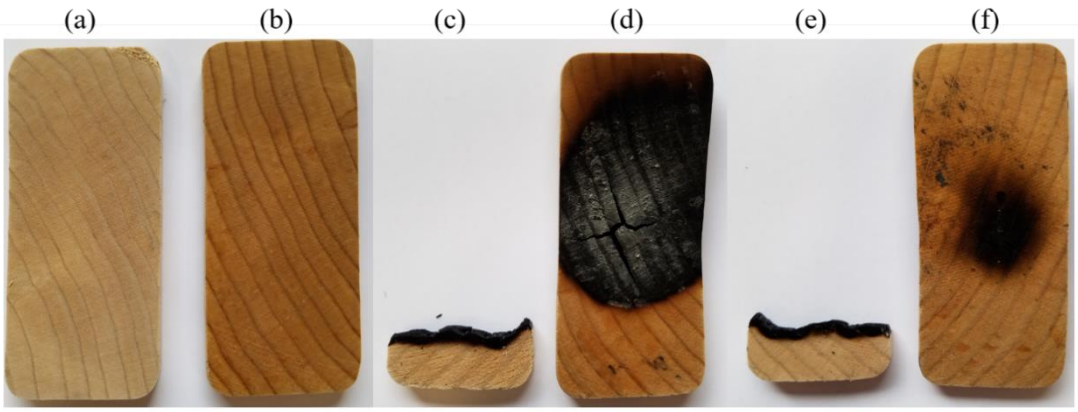

Figure 4.2. Images of uncoated **(a, c, e)** and coated **(b, d, f)** wood before **(a, b)** and after **(c-f)** butane torch testing. Shown is the side of the samples that faced the torch **(c, d)**, as well as the side opposite the torch flame **(e, f)**.

The amount of coating that is deposited on the wood varies with both the length of time immersed in the polyelectrolyte solution and the length of cure time, as summarized in **Table 4.1**. This variation in coating weight is due to the heterogeneous nature of the wood surface, which leads to very slow diffusion relative to the time required to deposit analogous coatings on textile substrates.[140] With the short immersion time, so little polyelectrolyte adsorbs onto the surface of the wood that the curing time makes little appreciable difference in the weight gain. With longer immersion time in the polyelectrolyte solution, the coating is better able to coalesce and adhere to the substrate when immersed in the curing buffer solution for a longer period of time. This assertion is supported by the fact that $PEC_{60,10}$ treated wood has almost 50% more weight gain than $PEC_{60,1}$ (**Table 4.1**).

Table 4.1. Weight gain and torch test performance for wood samples.

Dip Time	**Control**	**1 m**		**60 m**	
Cure Time	N/A	1 m	10 m	1 m	10 m
Weight Gain (%)	-	1.3 ± 0.3	1.3 ± 0.5	4.2 ± 0.2	5.9 ± 1.0
Afterflame (s)	246 ± 18	171 ± 23	139 ± 92	53 ± 73	4.3 ± 0.6
Residue (%)	15.8 ± 0.6	52 ± 17	65 ± 18	78 ± 16	90.4 ± 0.6

.

EDS data provide further insight into the rate of diffusion of the PEC into the wood during the dipping step. **Figure 4.3** shows a map of the linear density of phosphorus overlayed onto a SEM image of a cross section of the wood. Phosphorus is an ideal analyte because it is not a major component of uncoated wood, so the only significant source of phosphorus is from the PSP in the PEC. It is apparent from the data that in coated samples, the intensity of the phosphorus signal is highest towards the exterior face of the wood and decreases closer to the interior. It is also evident that increasing the dip time increases the depth of coating infiltration into the wood from **Figure 4.3a** and **Figure 4.3c**, which demonstrate a roughly 2.5 fold increase in coating penetration upon increase of dipping time from 1 to 60 minutes.

.

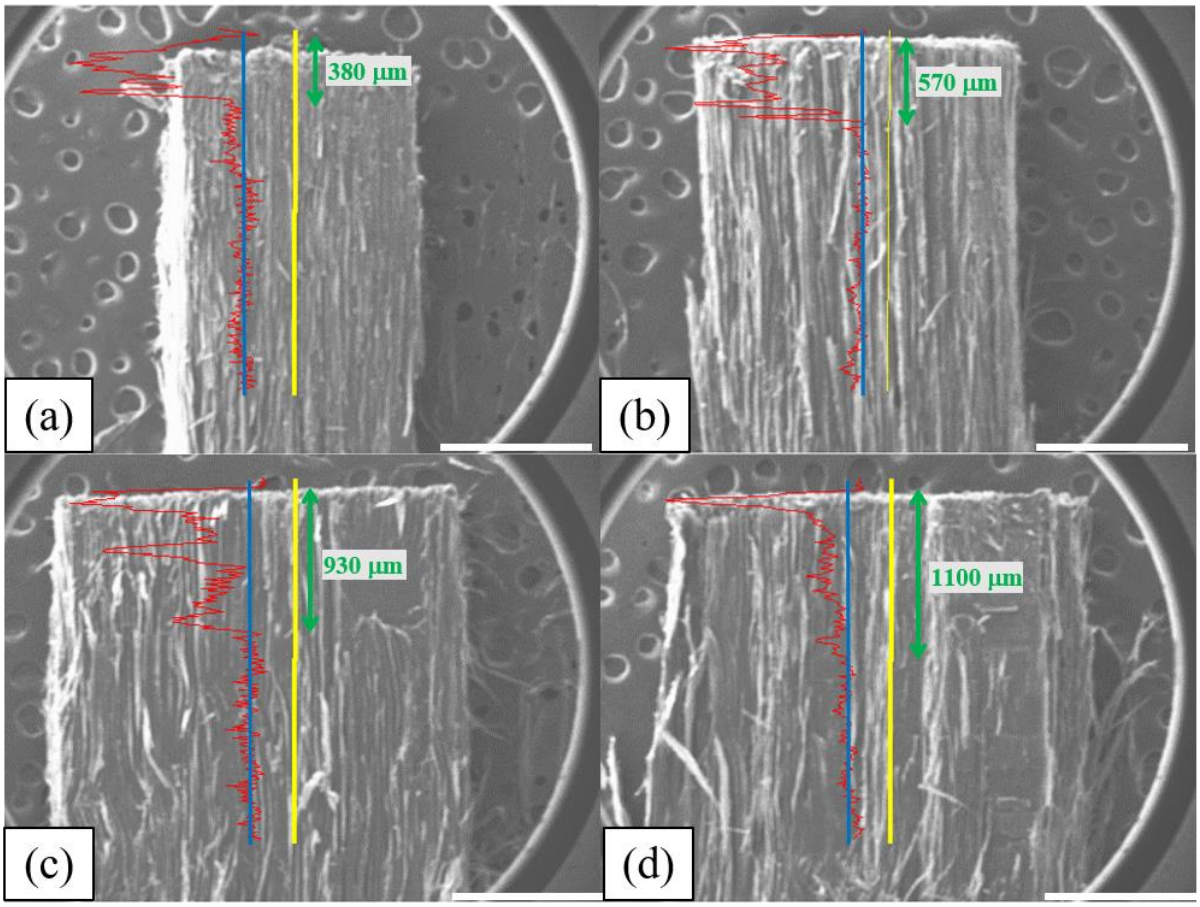

Figure 4.3. EDS traces signifying intensity of the phosphorus Kα peak as a function of distance through cross sections of **(a)** $PEC_{1,1}$, **(b)** $PEC_{1,10}$, **(c)** $PEC_{60,1}$, and **(d)** $PEC_{60,10}$. White scale bars are all 1 mm. Blue lines are to guide the eye as to the approximate level of background noise where there is no phosphorus signal. Green lines indicate the areas determined to be of relevant phosphorus content, along with the measured length.

Interestingly, a longer cure time also appears to increase the depth of penetration of the polyelectrolyte complex. In the case $PEC_{1,1}$ as compared to $PEC_{1,10}$, a roughly 50% increase in depth of coating penetration (from 380 µm to 570 µm) is observed with an increased cure time. This may be due to the ionic strength of the buffer plasticizing the complex and allowing continued diffusion through the wood. It is well known that increasing the ionic strength of a solution screens the charges of polyelectrolytes and decreases the stiffness of the complex.[174–176] Complexes similar

to PEI/PSP have been shown to form coacervates upon initial exposure to acidic conditions before drying, and it is possible that this liquid-like coacervate state is what initially forms when the material is exposed to buffer, maintaining a high degree of mobility to diffuse into and coat the wood's interior.[177] At a longer dip time, $PEC_{60,1}$ and $PEC_{60,10}$ show only a modest (~20%) increase in coating depth of penetration (from 930 to 1100 μm). The smaller increase is likely due to the length of time it takes for citric acid to diffuse that far into the substrate and cure/plasticize the PEC. The depth of penetration is likely also tied to the grain orientation of the studied wood, as the solution is able to travel along the wood's fluid channels, reaching much greater depths in a shorter time period. Similar coating penetration could be more quickly obtained by utilization of commercial pressure-treatment systems.

4.3.2 Flame Retardant Performance

The PEI/PSP coating's mechanism of action begins with the thermal decomposition of the PSP, which is protonated by nearby ammonium groups from PEI.[178] This degradation generates phosphoric acid that catalyzes char formation on the surface of the wood substrate. This endothermic char-forming process releases water, which serves to dilute the flame's oxygen supply. Furthermore, the char insulates the wood, preventing escape and ignition of flammable gases. This intumescent mechanism works to slow flame spread as well as thermal decomposition, causing the substrate to self-extinguish once the flame source is removed.

The effectiveness of this polyelectrolyte coating is related to the extent of protonation of the amine groups. Previous work has shown that polyphosphates are ineffective flame retardants without the ammonium species nearby to cause formation of the phosphoric acid catalyst.[112] This phenomenon is illustrated by comparing $PEC_{1,1}$ and $PEC_{1,10}$, which have very similar weight gain. $PEC_{1,10}$ performed slightly better during torch tests, likely due to the PEI in the coating having a

higher degree of ionization which provides more acidic protons to initiate the intumescence process. For the wood samples studied, weight gain correlates strongly to torch test performance, with higher weight corresponding to shorter afterflame periods, as well as a higher overall residue after testing (Table 1). $PEC_{60,10}$ performed the best, adding just 5.9 wt% and self-extinguishing in less than five seconds after flame removal, leaving behind more than 90% of the starting sample weight.

TGA allows for the investigation of how the bulk wood responds to the surface treatment. A thermogram of both uncoated and coated wood samples is shown in **Figure 4.4**. It is evident from these data that the surface coating still has a considerable effect on the bulk wood's thermal stability despite the coating being restricted primarily to a depth of ~1 mm (~1/3 of the total wood sample). The differential thermogram (**Figure 4.4b**) demonstrates that the decomposition pathway is changed by the coating. While uncoated wood has a single degradation step, indicated by a single peak in the differential weight loss, the coated wood shows two degradation steps. The first is believed to be the decomposition of the polyphosphate, analogous to the demonstrated decomposition mechanism of cotton fabric coated with a similar polyamine-polyphosphate coating.[178] The second peak is most likely decomposition of the wood at the center of the sample that was not influenced by the coating process. The lower intensity and area of these two peaks relative to the uncoated wood indicates that the coating causes wood to degrade more slowly, meaning it would contribute less overall energy to propagating a fire.

.

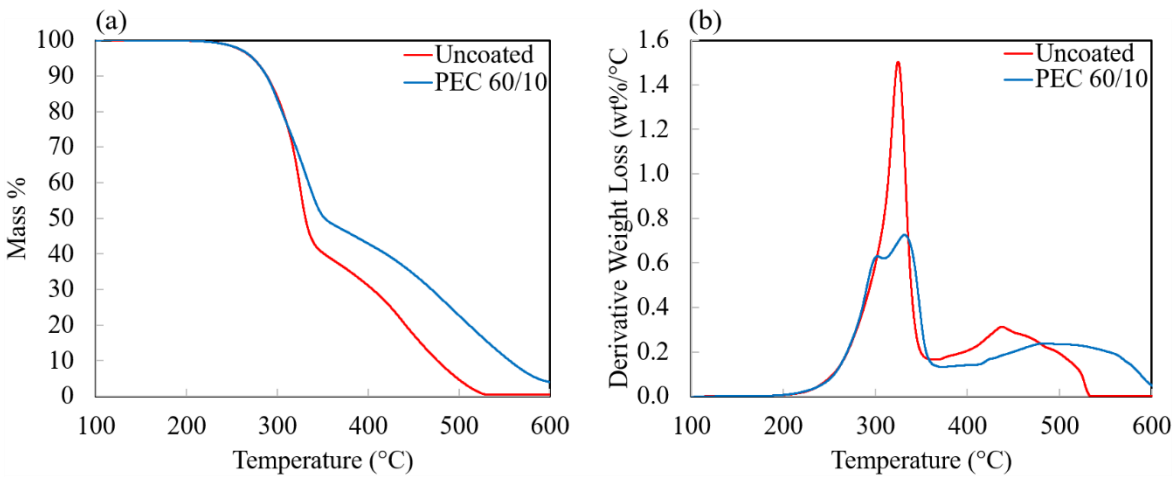

Figure 4.4. Thermograms displaying **(a)** mass vs temperature and **(b)** mass loss rate vs temperature for uncoated (red trace) and $PEC_{60,10}$ coated (blue trace) wood pieces.

4.3.3 Coating Morphology

Figure 4.5 shows SEM images of the uncoated and coated ($PEC_{60,10}$) wood samples. The uncoated sample shows the expected porous morphology of wood, with a highly irregular and rough surface. The coated substrate appears different, with much larger feature sizes and the appearance of there being less overall surface area, which is more easily seen in the magnified images (**Figure 4.5d** and **Figure 4.5e**). The reduction in flammability of the wood can partially be attributed to this reduced surface area, allowing a smaller amount of oxygen to reach the surface and feed the spread of flame. Furthermore, this coating is very smooth, lacking much of the texture of uncoated wood. This smooth surface will likely create a better insulating layer when the char-forming process begins, with fewer cracks through which flammable gasses can escape. This should disrupt the combustion cycle and aids in the coating's self-extinguishing behavior.

.

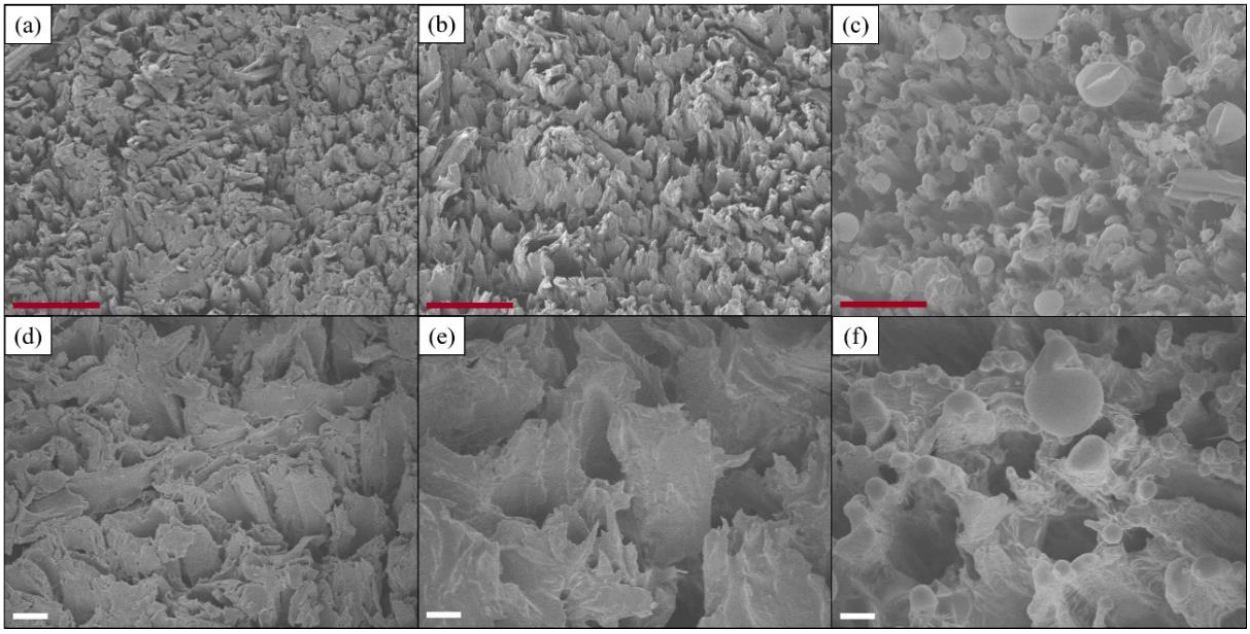

Figure 4.5. (a,d) Surface SEM images of uncoated wood, **(b,e)** $PEC_{60,10}$ coated wood before torch testing, and **(c,f)** the coated wood after the torch test. Red scale bars **(a,b,c)** are 100 μm, while white scale bars **(d,e,f)** are 10 μm.

Figure 4.5c and **Figure 4.5f** show the structure of $PEC_{60,10}$ treated wood following burning. The bubbles characteristic of the microintumescence phenomenon are clearly visible.[178] These bubbles indicate successful charring of the surface, catalyzed by the decomposition of PSP when it is exposed to the flame. Furthermore, the SEM images show that some of these bubbles seem to block the pores in the wood's underlying structure (**Figure 5f**), limiting gas transfer to the sample's interior and further disrupting the combustion process.

4.3.4 Cone Calorimetry

The cone calorimetry data shown in **Table 4.2** demonstrates the influence of the PEC coating on the flame retardancy of wood. Time to ignition (TTI) and peak heat release rate (pkHRR) reflect how long it takes for a sample to ignite, and the highest heat release rate of the

sample as it burns, respectively. The former relates to how much exposure a material can have to a heat flux prior to ignition, while the latter relates to how much a material will contribute to propagating a fire once it has ignited and begins to burn. Generally, a longer TTI and lower pkHRR correspond to lower flammability.[121] The coated samples demonstrate an increase in TTI (+27%) and a decrease in pkHRR (-10.8%), meaning the coated wood is more fire resistant. Total heat release (THR) is how much total energy a material contributes to a fire event. The coated wood's 34.5% reduction in THR indicates less energy available to perpetuate a fire. Finally, the coated wood had a 62% greater residue following cone calorimeter testing than the uncoated wood, suggesting it will maintain greater structural stability if this material were used in home construction.

Table 4.2. Cone calorimetry data for wood samples.

	Uncoated	**PEC$_{60,10}$**	***Change***
TTI (s)	49 ± 9	62 ± 6	*+ 27%*
pkHRR (kW m^{-2})	379 ± 9	338 ± 18	*- 10.8%*
THR (MJ m^{-2})	29.0 ± 0.8	19.0 ± 0.7	*- 34.5%*
TSR(m^2 m^{-2})	209 ± 9	210 ± 12	*Unchanged*
Residue (%)	26 ± 3	42 ± 3	*+ 62%*

It should be noted that the flammability properties of wood differ dramatically based upon the orientation of the wood grain to the incident heat flux. This study performed cone calorimetry testing with the heat flux aligned parallel to the grain of the wood, which dramatically increases its susceptibility to thermal degradation.[179,180] In home construction, the grain is usually not going to be oriented towards the flame source, and as a result the absolute performance of these samples would likely improve considerably, while the relative performances would likely remain the same.

It is also important to note that the wood samples bent considerably over time as the heat flux was applied. This is problematic because the heat release rate (HRR) is normalized by surface area (units of kW m^{-2}). The coated and uncoated samples were likely changing dimensions at different rates, which would expose a greater surface area that wasn't accounted for by the cone calorimetry analysis. This dimensional change and its difference between samples explains some of the noise in the plot of HRR as a function of time (**Figure 4.6**). Torch testing reveals that the coated sample bends more than the control upon exposure to flame, which would cause its surface area to increase more rapidly, and lower the apparent HRR over time. Still images from videos of torch testing (**Figure 4.7**) reveal significant differences in the degree of deformation after just a few seconds of direct flame exposure.

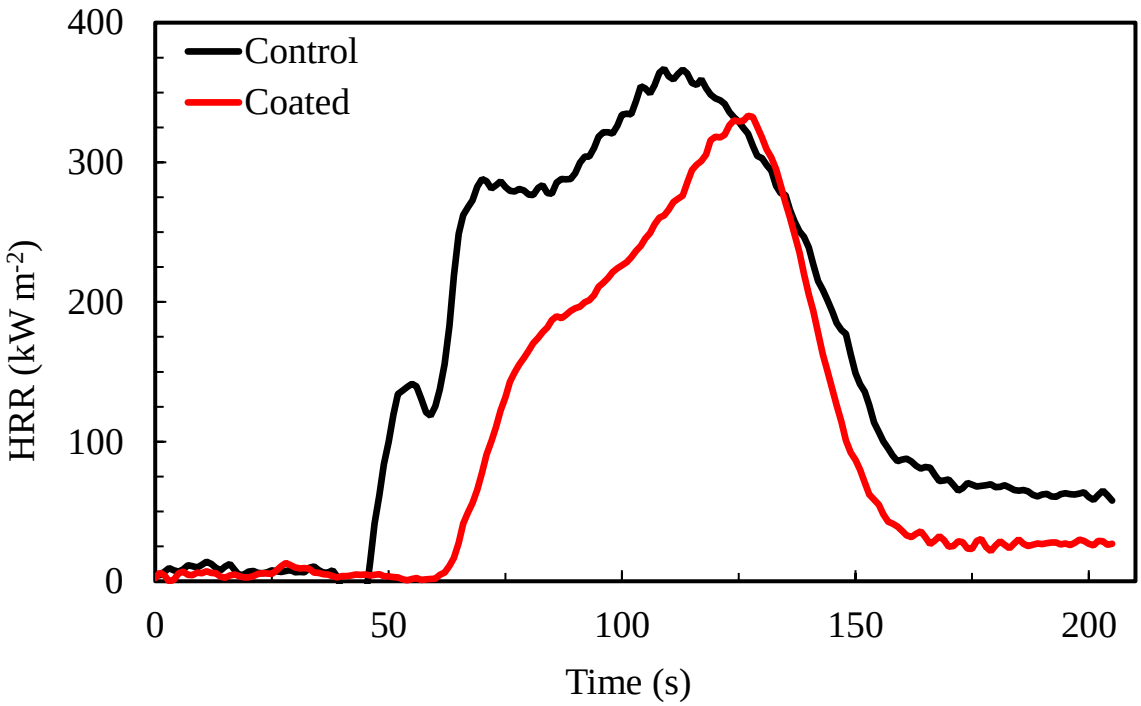

Figure 4.6. Heat release rate as a function of time for uncoated wood (black trace) and wood coated with $PEC_{60,10}$ (red trace), as measured by cone calorimetry. These traces are the average of four trials each.

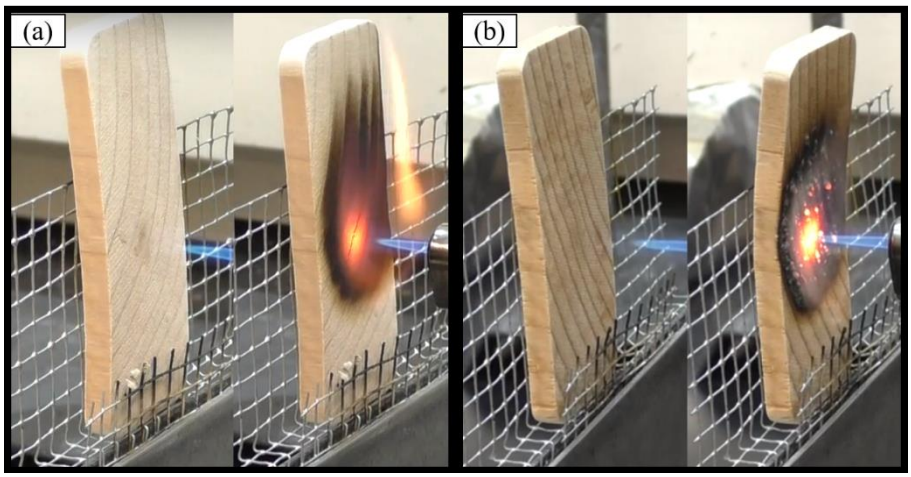

Figure 4.7. Still images of wood samples 0 and 20 seconds into handheld torch testing. The uncoated control **(a)** shows very little bending 20 seconds into the test, while the $PEC_{60,10}$ coated sample **(b)** has visible deformation towards the flame source.

The uncoated sample undergoes very little bending as it burns, as can be seen in the righthand portion of **Figure 4.7a**. In contrast, the $PEC_{60,10}$ coated sample significantly deforms after 20 seconds of flame exposure. This may be due to the intumescent mechanism, which proceeds through a phosphate-catalyzed dehydration step.[178] This intumescent process proceeds very quickly, removing lots of water from the cell walls of the wood at the point of flame exposure, which causes shrinking of the cells and the observed warping of the wood. Similar bending would almost certainly occur under the heat flux of the cone calorimeter, thereby altering any surface-area-normalized quantities. The bending observed here would increase the apparent surface area of the coated sample and decrease HRR, pkHRR, TSR, and THR relative to the uncoated wood.

4.3.5 Mechanical Testing

The data in **Table 4.3** show the flexural modulus and flexural strength (defined as flexural stress at the wood's breaking point) of both uncoated and $PEC_{60,10}$ coated wood. Flexural stress-strain curves are shown in Supporting Information (**Figure 4.8**). It is evident that the PEC coating

considerably improves the mechanical properties of the wood, which is likely due to the high PEC modulus.[181,182] Ion pairing between polycation and polyanion forms crosslinks that serve to increase the modulus/strength of the complex and, by extension, the coated substrate.[183] These improved properties are likely surface area dependent (i.e. a less dramatic increase would be observed on construction-scale pieces of wood), but is nonetheless a promising indication that this flame retardant PEC coating will not degrade wood's mechanical performance.

Table 4.3. Mechanical behavior of wood samples.

3-Point Bend Test	**Uncoated**	**$PEC_{60,10}$**	***Change***
Flexural Modulus (MPa)	21 ± 1	36 ± 6	*+ 71%*
Flexural Strength (MPa)	4.0 ± 0.4	5.0 ± 0.5	*+ 25%*

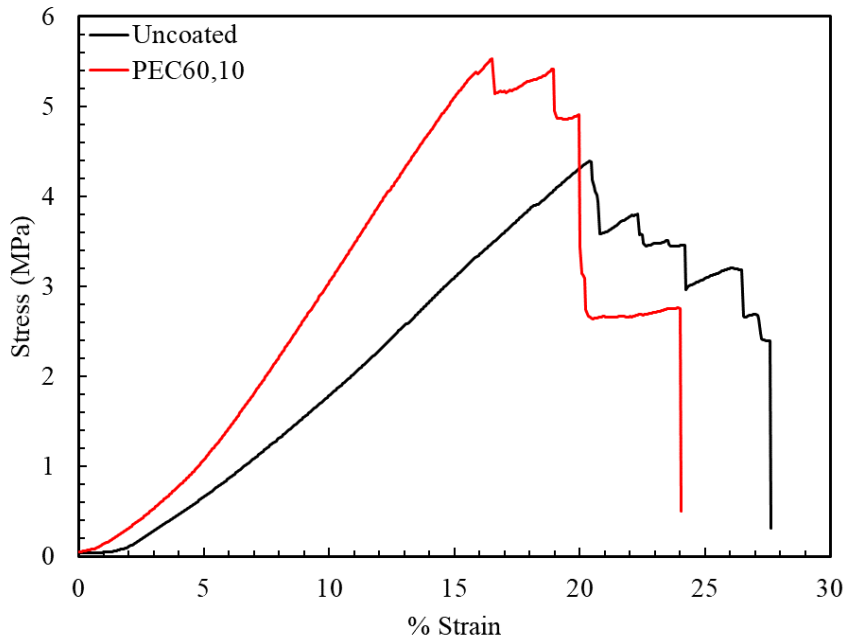

Figure 4.8. Flexural stress as a function of flexural strain for uncoated wood (black trace) and wood coated with $PEC_{60,10}$ (red trace), as measured by a 3-point bend test.

4.4 Conclusions

A polyelectrolyte complex coating was deposited on wood in two steps that substantially reduces its flammability, while simultaneously improving flexural modulus and strength. Due to slow diffusion kinetics of the wood's surface, it was determined that longer PEC immersion time and citric acid cure time correlated to greater coating weight and associated improvement in flame retardant metrics. The coating's microintumescent mechanism of action was evidenced by SEM images that reveal a bubbling up of the charred surface that blocks the transfer of volatile gasses and oxygen to or from the substrate. Cone calorimetry revealed only modest improvements in TTI, pkHRR, and THR relative to the uncoated wood, but these data were confounded by dimensional changes during heating that likely masked some of the coating's flame retardant benefit. This simple two-step deposition process provides an opportunity for producing flame retardant wood with relatively little processing time and under ambient conditions.

CHAPTER V

SELF-EXTINGUISHING ADDITIVE MANUFACTURING FILAMENT FROM A UNIQUE COMBINATION OF POLYLACTIC ACID AND A POLYELECTROLYTE COMPLEX*

5.1 Introduction

3D printing, also known as additive manufacturing (AM), has found widespread use in a multitude of different fields, such as aerospace and medicine.[4–6] In particular, fused filament fabrication (FFF) has matured considerably as an AM technique and has become ubiquitous. Objects printed via FFF are made layer-by-layer 'from the bottom-up', with a thermoplastic filament being extruded by a print head that can move in two dimensions, depositing material onto a bed which moves in the third, vertical dimension. Parts are assembled by depositing sequential layers of filament, which can consist of a variety of thermoplastics such as polylactic acid (PLA), acrylonitrile-butadiene-styrene (ABS), ethylene vinyl acetate (EVA), and nylon. The proliferation of additive manufacturing in general, and FFF in particular, has largely ignored the inherent flammability of these commodity thermoplastics, the ignition of which is capable of starting fires that can cause considerable property damage and put lives at risk.[7,8]

As fused filament fabrication printers continue to become more commonplace, there exists a need to develop methods to reduce its inherent fire hazard. There are some available commercial options, such as utilizing inherently flame resistant polyether ether ketone (PEEK), but this requires printing temperatures far above those of most existing printers. There is also concern that PEEK can begin to decompose during printing, which compromises the integrity of the part.[184]

*Reprinted with permission from Kolibaba, T.J.; Shih, C.; Lazar, S.; Tai, B.L.; Grunlan, J.C., Self-Extinguishing Additive Manufacturing Filament from a Unique Combination of Polylactic Acid and a Polyelectrolyte Complex, *ACS Materials Letters* **2020**, *1*, 15-19.

Combining flame retardant (FR) ingredients into existing filaments has been studied, but requires increased printer complexity or a substantial number of added ingredients.[185–187] An ideal FR filament for FFF would utilize minimal additive and would be printable under the same conditions (i.e. print temperature, speed, and filament diameter) as commercially available filaments.

Polyelectrolyte complex (PEC) treatments deposited either in a single step or layer-by-layer have recently been shown to impart excellent flame retardant behavior to wood, epoxy, and various fibers.[171,115,114,16] A PEC is the precipitate formed from a mixture of a polycation and a polyanion, held together via ionic interactions that act as physical crosslinks. Until now, PECs have been limited to imparting FR properties as nanocoatings, which is not particularly appealing for FFF filaments because it could interfere with the fusion process between layers of deposited filament. Recently, conventional methods have been used to extrude PECs by taking advantage of their 'saloplasticity'.[174,188] In short, PECs can be plasticized by the addition of water and salt (the identity and concentration of salt needed are a function of the ion-pairing strength between the polyelectrolytes and the desired processing temperature), which makes them amenable to extrusion.[175] Despite this breakthrough, the applications of PECs in AM has been limited primarily to the application of PEC hydrogels or have utilized non-FFF methods such as pseudo digital light processing.[189–191]

Bulk composites of polyelectrolyte complexes and thermoplastics have yet to be rigorously studied, despite some promising results from chitosan/phytic acid complexes when incorporated into bulk ethylene-vinyl acetate.[192] Here we report the first ever 3D-printed composite composed of a plasticized PEC of polyvinylamine (PVA) and sodium polyphosphate (PSP) incorporated into PLA, which can be printed with an ordinary FFF printer. Printed parts self-extinguish in open flame testing and the peak heat release rate of the material in microscale combustion calorimetry

is reduced by 42%. Unmodified PLA burns completely, while the PLA-PEC undergoes significant charring that aids in maintaining part integrity.

5.2 Experimental

5.2.1 Materials and Chemicals

Hydrochloric acid (HCl, ACS reagent, 37%), sodium hydroxide (NaOH, ACS reagent, 97%), and sodium hexametaphosphate (PSP, 65-70% P_2O_5 basis) were purchased from Sigma-Aldrich (St. Louis, MO, USA). Polyvinyl amine (PVA, Lupamin 9095) was acquired from BASF. Polylactic acid (PLA) filament (Natural clear, 1.75 mm) was purchased from 3D Solutech (Seattle, WA, USA). All solutions were prepared in deionized (DI) 18 M□ water.

5.2.2 Polyelectrolyte Complex Formation

To form the polyelectrolyte complex, two separate, equal volume solutions of 0.25 M PVA and 0.25 M PSP (both with respect to repeat unit molar mass) were adjusted to pH 7, using 5 M HCl and 5 M NaOH, respectively. These two solutions were then simultaneously mixed under vigorous stirring. The PEC immediately formed and began to precipitate from solution. The mixture stirred for 30 minutes to allow complete formation/precipitation of the complex. After the complex had fully formed, the stirring was stopped to allow for settling of PEC particles. The supernatant from the mixture was decanted, and the PEC was collected and chopped into ~1 cm pieces with scissors. These pieces were then placed into a jar full of deionized water and rolled for several days, with the water being changed every 8-16 hours, until the conductivity of the supernatant read <10 □S/cm with a handheld conductivity meter (Traceable®, VWR, Radnor, PA, USA), to ensure complete removal of all expelled counterions from the complexation process.[52]

The PEC pieces were then dried in a 120 °C oven overnight, followed by grinding into a fine powder with a coffee grinder.

5.2.3 Filament Extrusion

Chopped pieces (ca. 1-2 cm) of PLA filament were mixed with PEC powder in a 3:1 weight ratio in 4-5g batches in scintillation vials. Water was added in a weight equal to that of the PEC powder, which was left to absorb the moisture overnight. The PLA-PEC mixture was then fed into a twin-screw compounder/extruder (HAAKE MiniCTW, Thermo Fisher Scientific, Waltham, MA, USA), set to 185 °C, and mixed at 200 rpm (until a stable torque value ~1 Nm was reached, typically after 15-20 minutes) before being extruded through a 1.7 mm die in constant-torque mode at 0.07 Nm.

5.2.4 Printing

Pieces of filament ~20 cm long (either pure PLA or PLA-PEC) were fed into a LulzBot Mini 3D printer (Aleph Objects, Inc. Loveland, CO, USA) with a 1.75 mm hot-end channel. To facilitate quality printing with the PLA-PEC, the printer was slightly modified to have a heater block with a longer melting channel (~2 cm) and a larger extrusion nozzle (0.6 mm) to facilitate the slight variation in filament diameter from the extruder utilized. In addition, a nylon tube (with a 2 mm inner diameter, with a cutout for the feeder to engage and feed filament without buckling) that was attached between the filament entrance and the heat sink to guide filament into the hot-end. PLA and PLA-PEC parts were printed with these modifications at a 200 °C nozzle temperature and a bed temperature of 50 °C (both normal for pure PLA) at 3000 mm/s, with 0.5 mm filament retraction. 3D models for printing were generated via SolidWorks software (Dassault

Systemes, Waltham, MA, USA), while a slicing software (Simplify3D, Cincinnati, OH, USA) was utilized to set up process parameters and plan a printing path.

5.2.5 Characterization

Thermal transitions of the filaments were measured using a differential scanning calorimeter (Q20 DSC, TA Instruments, New Castle, DE, USA) by heating the sample at 10 °C/min to 200 °C, then cooling to 0 °C at 5 °C/min to erase thermal history, followed by the reported scan from 0 – 200 °C at 10 °C/min (or 2 °C/min). Mechanical properties were measured using a dynamic mechanical analyzer (Q800 DMA, TA Instruments, New Castle, DE, USA) in a single-cantilever arrangement, with a strain rate of 1 Hz and strain amplitude of 0.1%, while increasing temperature 2 °C/min from 30-150 °C. Thermal stability of filaments was determined using a thermogravimetric analyzer (Q50 TGA, TA Instruments, New Castle, DE, USA) under a 60 mL/min sample purge flow of air and 40 mL/min balance flow of N_2. Samples were heated at a rate of 10 °C/min to 700 °C, following a 30 minute isothermal hold at 100 °C to remove any water. Microscale combustion calorimetry experiments were performed by the University of Dayton Research Institute utilizing method A of ASTM D7309 (pyrolysis under nitrogen), heating from 150-600 °C at 1 °C/min. Open flame testing was performed with a butane blowtorch (Bernzomatic ST2200, Worthington Industries, Columbus, OH, USA), with its emitter set so that the inner blue flame was 2 cm in length. Printed parts were suspended from the side by a metal clip and the flame was impinged upon the bottom of the sample from a distance of 3 cm for 5 s, at which time the flame was removed and the 3D printed part was allowed to burn until either the material self-extinguished or until the flame burned itself out.

5.3 Results and Discussion

5.3.1 Preparation and Printing of Composite Filament

A salt free, stoichiometric PEC was generated in a manner similar to previously published methods.[52] The complex was precipitated by simultaneously mixing equal volumes of 0.25 M PVA and 0.25 M PSP solutions (with respect to repeat unit molar mass) at neutral pH. Figure 1a shows the structures of the polyelectrolytes used. The precipitate was then soaked in deionized (DI) water for several days (changing water every ~12 hours) to extract all expelled counterions. After drying, the PEC was ground into a powder and mixed in a 1:3 ratio of PEC to PLA for filament extrusion at 185 °C. Prior to extrusion, the PLA-PEC mixture was hydrated with water (an amount equal to the mass of PEC) overnight to plasticize the PEC and facilitate more effective melt-mixing in the dual-function compounder/extruder. Water is known to cause PECs to transition from a brittle powder into rubbery solids.[53] In particular, it is known that polyamine-polyphosphate complexes tend to weakly associate or dissociate under high-salinity conditions.[193] As a result, it was not necessary to add any salt to the complex for further plasticization. The rubbery PEC is able to effectively mix with melted PLA in the compounder to form a homogenous PLA-PEC filament upon extrusion.

This composite filament can be printed in a commercial 3D printer utilizing FFF (**Figure 5.1c**). Pictures of printed PLA-PEC parts can be seen in **Figure 5.1b**, they are of similar detail and quality to those of the pure PLA parts lying next to them. PLA-PEC parts are printed at 3000 mm/min, while neat PLA prints at 3600 mm/min. The similarity of printing speed means the composite filament can be efficiently implemented in conventional printers. The PLA-PEC is also printed with the same hot-end and bed temperatures as unmodified PLA. In order to achieve the highest possible print quality, slight modifications were made to the length of the melting channel,

extrusion nozzle size, and filament retraction of the printer. These modifications reduce the backpressure on the filament during printing and yield better part fidelity. The yellow color that is observed in the printed part is a result of the color of the incorporated PEC, which is a yellow powder when dry. The homogenous color of the parts suggests good mixing of the two components.

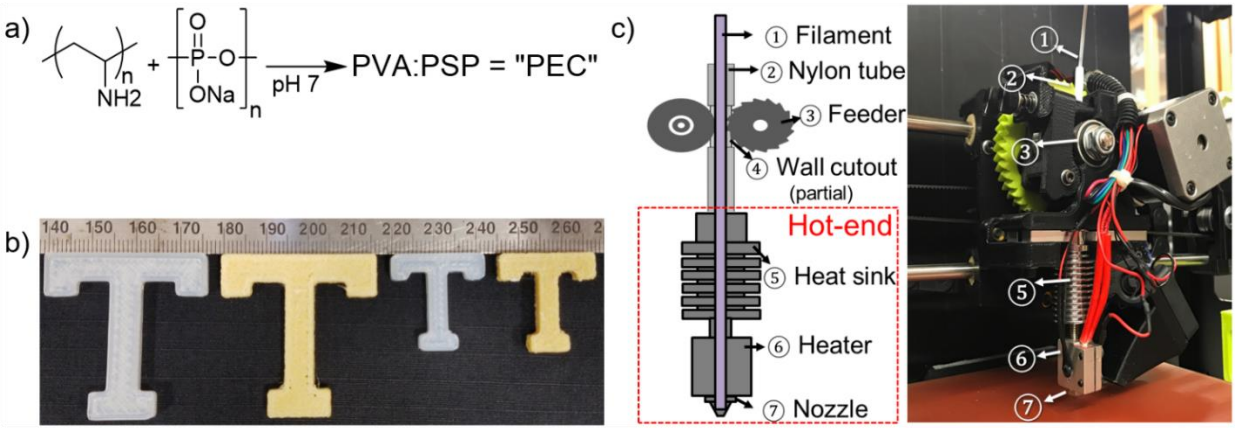

Figure 5.1. (a) Polyelectrolytes used to form the PEC utilized in this study. **(b)** Pictures of printed PLA (translucent) and PLA-PEC (yellow) parts. **(c)** Schematic of the printer head utilized in in this study.

5.3.2 Thermal Analysis

The composite filament's thermal properties were analyzed by differential scanning calorimetry (DSC). **Figure 5.2a** shows the differential thermograms of neat PLA and the PLA-PEC composite. There is a minimal change in T_g and T_m of PLA (**Table 5.1**), suggesting that the incorporation of the PEC does not substantially alter the interactions between PLA chains. Once dry, the PEC itself does not have a glass transition, indicating that the ~ 2 °C change observed in T_g is not due to plasticization of PLA by the PEC.[53] The presence of the PEC does inhibit cold crystallization during the warming of the PLA-PEC. This is likely due to the mixture of polyelectrolyte chains with the pure PLA, which inhibits or modifies some intermolecular interactions and thus prevents cold crystallization at the heating rate utilized (10 °C/ min).

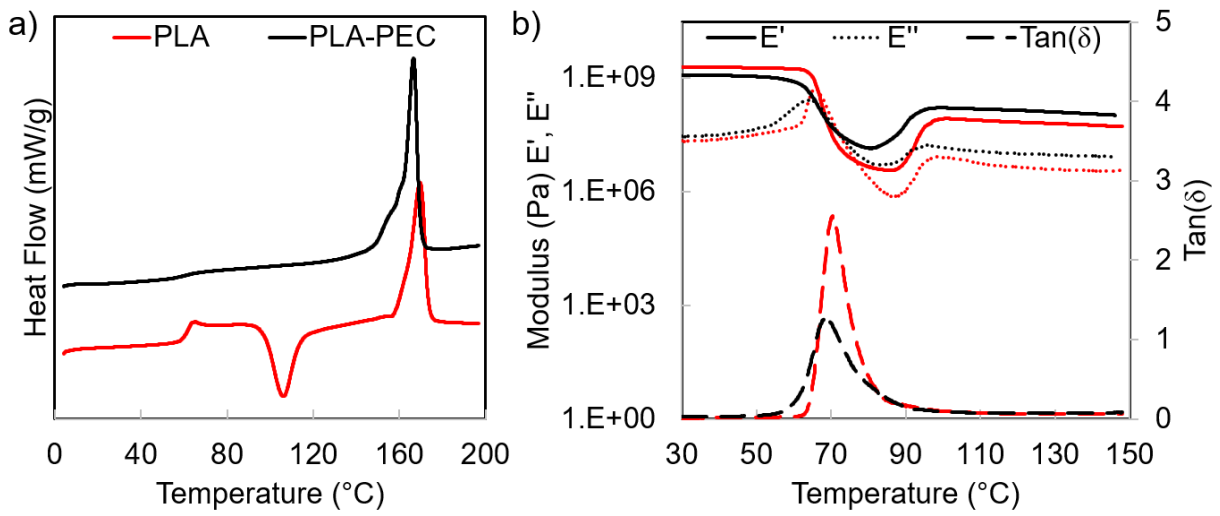

Figure 5.2. (a) Second-heating DSC trace of PLA (red) and PLA-PEC (black). **(b)** DMA data of PLA and PLA-PEC. Solid lines are storage modulus, dotted lines are loss modulus, and dashed lines are tan(δ).

Table 5.1. Thermal properties of PLA and PLA-PEC.

Sample	T_g (°C)	T_c/T_m (°C)	$\Delta H_c/\Delta H_m$ (J/g)	Crystallinity[a)] (%)
PLA	62	97/162	22.4/28.4	6.5
PLA-PEC	60	–/161	–/37.3	53.5

[a)]The enthalpy of fusion for a PLA crystal of infinite size was taken to be 93 J/g.[194]

The incorporation of PEC does alter the crystallinity of PLA. The shoulder in the melting peak can be clearly observed in **Figure 5.2a**, and **Table 5.1** shows a considerable increase in the degree of crystallinity of the PLA-PEC composite. Effects like this have been observed before in flame retarded PLA.[195] This increase in crystallinity is likely a result of the polyelectrolyte complex providing nucleation sites for the growth of crystalline regions within the composite.[196] It is also observed in **Figure 5.2a** that the melting peak for PLA-PEC has a shoulder, which is indicative of some crystalline regions with less order.[195] The presence of more disordered regions of crystallinity is likely due to the dispersion of the PEC in the PLA matrix limiting the growth and organization of some crystalline phases.

Dynamic mechanical analysis (DMA) of the two filaments (**Figure 5.2b**) further reveals important information about the PLA-PEC composite. The peaks of tan(δ) are within ~ 2 °C of each other, further supporting the observation that the PEC has little influence on the T_g of the composite. The initial storage modulus of PLA-PEC is slightly lower than that of neat PLA. This disparity can be explained by disruptions to the intermolecular forces and/or entanglements within PLA because of the presence of the PEC. The overall similarity in E' and E'' suggests that PLA-PEC will be a good substitute for any uses intended for neat PLA. Once the material approaches T_g, it appears as though the properties of the composite filament changes more slowly, indicated by the wider peak of tan(δ).

After passing through the glass transition, PLA-PEC has a higher storage modulus. This increased storage modulus after T_g is likely a result of the tough PEC helping to reinforce the PLA matrix. This retention of toughness above T_g is important for fire safety, making the material less likely to melt drip. Melt dripping contributes to the spread of fire and is a major factor in fire-related death and property damage.[197] Beyond ~100 °C, an increase in storage modulus is observed for both materials, which is likely a result of cold crystallization.[198,199] In DSC, the PLA-PEC composite did not exhibit cold crystallization behavior. The lower heating rate, combined with the strain of the DMA experiment could lead to nucleation of crystalline phases, which would toughen the material. However, this is uncertain, as PLA-PEC fails to exhibit cold crystallization in DSC when the heating rate is set to match the DMA experiment (2 °C/min as opposed to 10 °C/min, **Figure 5.3**). Despite these small differences, the two filaments largely possess very similar mechanical properties, indicating that the composite filament could be a very effective substitute for PLA in most applications.

.

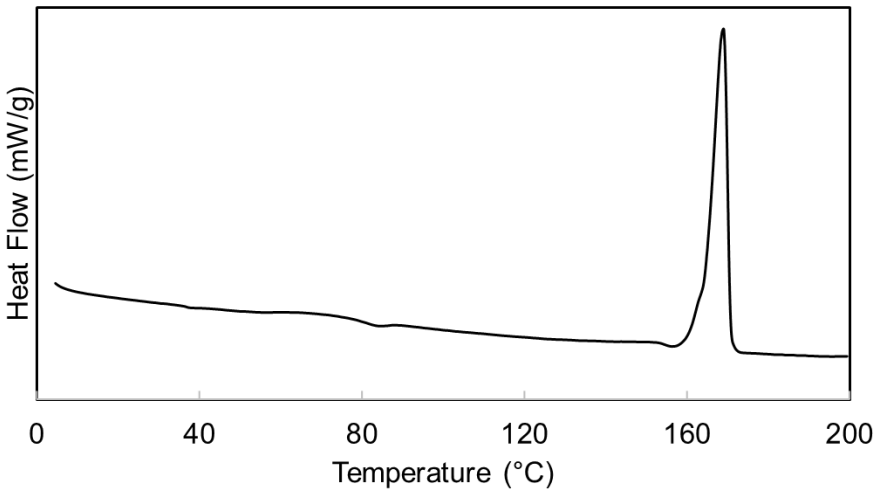

Figure 5.3. Second-heating DSC trace for PLA-PEC with heating rate of 2 °C/min.

5.3.2 Thermal Stability

In order to better understand the combustion behavior of the filaments, thermogravimetric analysis (TGA) was performed under an oxidizing atmosphere (**Figure 5.4a**). The earlier onset of decomposition for PLA-PEC is expected, having occurred when polyamine-polyphosphate coatings are applied to other substrates.[16,178,200] This earlier onset of decomposition, occurring around 250 °C, is a result of the polyphosphate decomposing and initiating the intumescence process, which forms char and suppresses combustion by protecting the underlying substrate and blocking heat/mass transfer.[178] This phenomenon can be seen in **Figure 5.4a** in the derivative curve of the thermogram, which shows that the PLA-PEC peak rate of mass loss is reduced by nearly 30%. The remaining mass at 400 °C, after the primary decomposition step at 350 °C, is improved sevenfold by the incorporation of the PEC. These data support the PEC's involvement in suppressing thermal degradation that serves to protect printed parts from fire. TGA of the PEC in the absence of PLA (**Figure 5.4b**) highlights its resistance to thermal degradation and high char yield, even up to 700 °C.

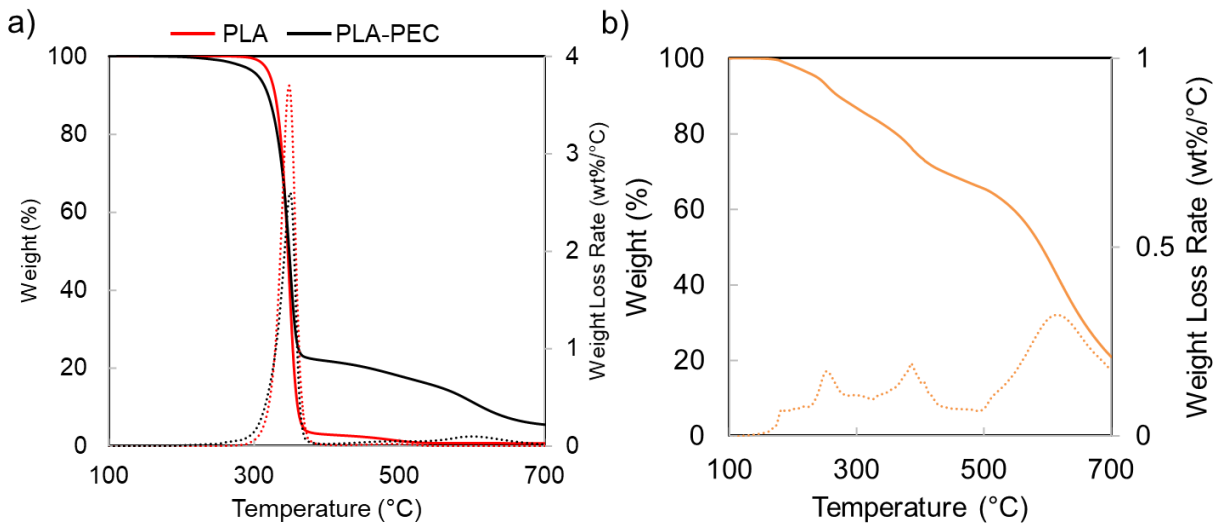

Figure 5.4. TGA mass (solid lines) and derivative (dashed lines) curves. **(a)** PLA (red) and PLA-PEC (black) thermograms under air overlayed to highlight contrasts in their degradation behavior. **(b)** Thermogram of PVA:PSP under air.

5.3.3 Microscale Combustion Calorimetry

Microscale combustion calorimetry (MCC) offers further insight into the filament decomposition. MCC measured several parameters related to a material's ability to spread flame such as heat release rate (HRR), peak heat release rate (pkHRR), total heat release (THR), and the temperature at which pkHRR is reached.[201] One of the most important figures of merit from MCC is the pkHRR, since this is the most relevant to how much a burning item contributes to propagating a fire. A plot of HRR as a function of temperature is shown in **Figure 5.5**, with the relevant flammability data summarized in **Table 5.2**. There is only a single heat release peak observed, which correlates with the TGA data (**Figure 5.4a**), showing a single step decomposition. The onset of degradation occurs slightly sooner for PLA-PEC, agreeing with the TGA data. The increased width of the PLA-PEC curve is more pronounced in MCC, as opposed to TGA, and the composite exhibits a 42% lower pkHRR relative to PLA. The total heat release is lowered by nearly 20%. These two values indicate that the composite filament is substantially less likely to propagate fires

in the event of combustion, and contributes less overall energy to the fire. Furthermore, the char yield is improved from <1% all the way to ~14%, which is a 1600% increase in the residue. This can be seen from the images of the char residues after burning (**Figure 5.5b,c**), where it's evident that PLA-PEC has considerably more residue visible. This suggests that more filament will be left behind after fire exposure, in addition to releasing less heat in the process.

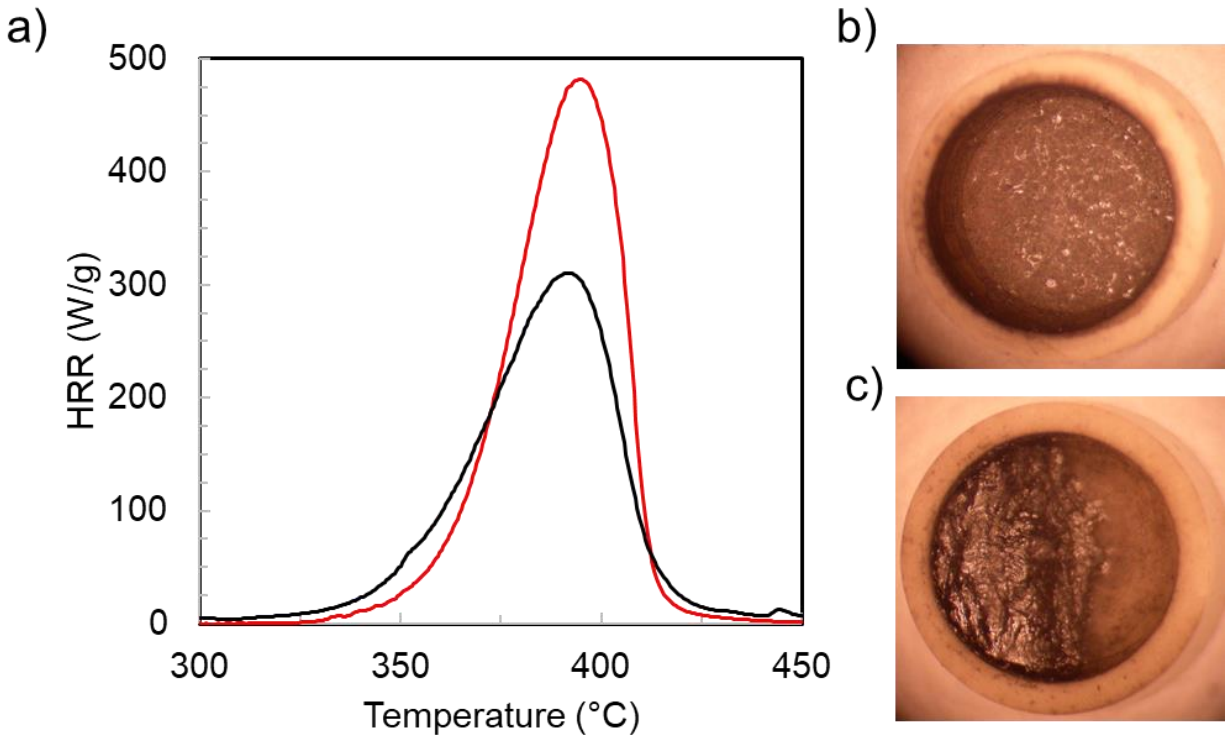

Figure 5.5. (a) MCC plot of PLA (red) and PLA-PEC (black). **(b,c)** Image of the char residue of PLA and PLA-PEC, respectively.

Table 5.2. Micro combustion calorimetry results for PLA and PLA-PEC filaments.

Sample	Char Yield (wt. %)	pkHRR (W/g)	pkHRR Temp (°C)	THR (kJ/g)
PLA	0.8 (± 0.2)	530 (± 40)	392 (± 5)	16.8 (± 0.1)
PLA-PEC	13.6 (± 0.3)	309 (± 3)	391 (± 0)	13.6 (± 0.1)
Change	+1600%	-42%	-	-19%

5.3.4 Open Flame Testing

The performance of printed parts in open flame tests was also evaluated, with time lapse images shown in **Figure 5.6**. It is clear that the PEC's intumescent FR mechanism is taking place from the instant that the flame touches the PLA-PEC part (bottom row of images), as small bubbles and char formation are easily observed. By the time the torch's flame is removed from the part (third image from left in each row), pure PLA has begun to form a melt pool that leads to melt dripping as combustion continues. The PLA-PEC part instantly self-extinguishes upon removal of the flame, with none of the part melting away. Inspection of the PLA-PEC flame test video reveals a bubbling over of the surface and a visible expansion of the bottom of the part during flame exposure. This expansion recedes when the flame is removed and the part largely maintains its original shape. This suggests that the presence of the PEC (and likely the protective char formed because of the PEC's involvement in the intumescence process) serves to protect the structure of the part and prevents melting, which dramatically improves its fire safety.

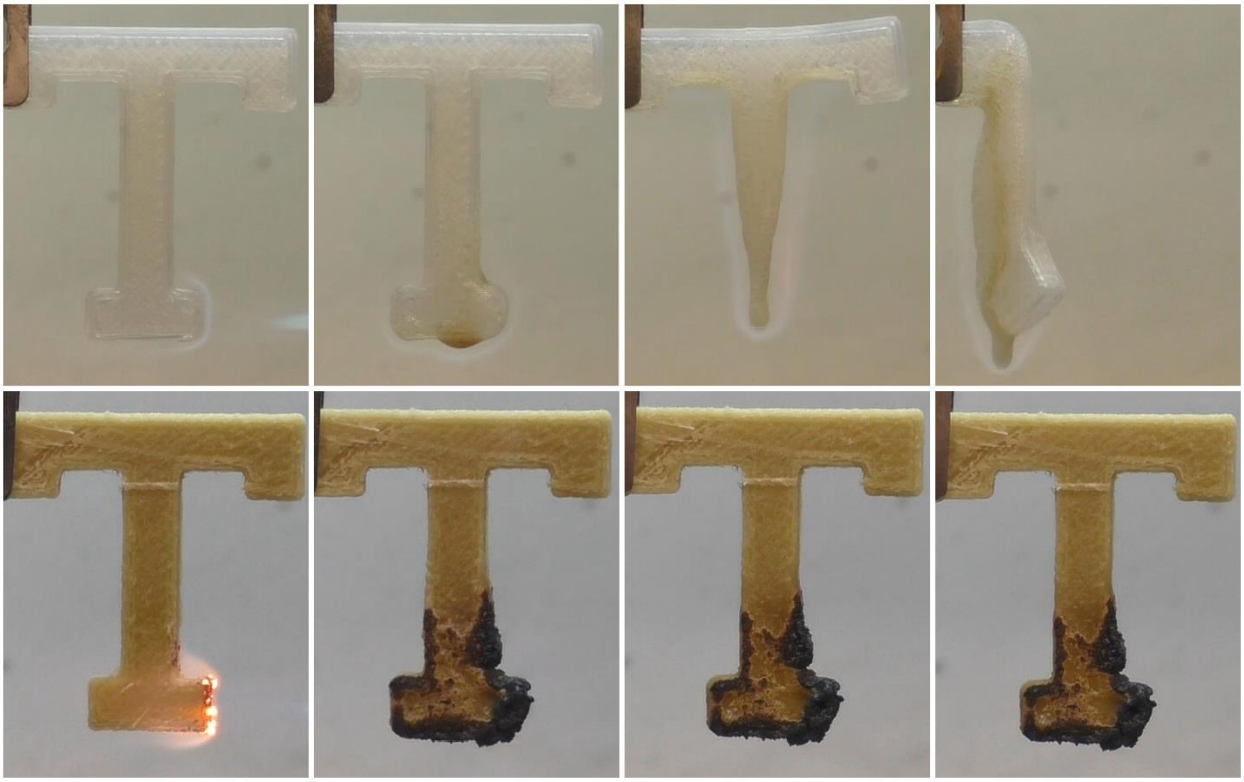

Figure 5.6. Time lapse still frames from open flame testing of 3D printed parts: the moment of flame impingement, immediately after flame removal, 20 s after flame removal, and 30 s after flame removal (moving from left to right). The top row of images is PLA alone, while the bottom row is PLA-PEC.

5.4 Conclusions

In conclusion, a polyelectrolyte complex was successfully incorporated into a common PLA 3D-printing filament at a 25 wt% loading. This was accomplished by taking advantage of the plasticizing effect water has on the complex, which enables thorough mixing and effective extrusion of high-quality filament. The ability of this filament to be printed using a commercial 3D printer was demonstrated. Furthermore, the thermal and physical properties of the filament were investigated, and found to differ little from the commercial PLA starting material. Analysis of the composite filament's thermal stability reveals a dramatic reduction in both the rate and extent of degradation relative to neat PLA. Additionally, calorimetry measurements revealed a 42% reduction in pkHRR. Finally, open flame testing demonstrated the self-extinguishing

behavior of the PLA-PEC filament, even after incorporation into a part. This work demonstrates the first 3D printed composite comprised of a thermoplastic and a PEC. There is tremendous opportunity to further improve this technology and broaden its application to other polymeric filaments.

CHAPTER VI

CONCLUSIONS AND FUTURE WORK

6.1 Polyelectrolyte Complexes for Fire Protection of Materials

This dissertation has outlined several novel methods of protecting materials through the application of polyelectrolyte complexes (PECs). In particular, it highlights the use of these materials to provide fire protection to structurally intricate materials, namely wood and additively manufactured parts. Materials can be coated with a PEC in the form of a coating applied via layer-by-layer assembly or through a two-step process in which a water-soluble PEC is cured via exposure to an acidic buffer. Additive manufacturing filaments are not readily amenable to coatings, but a PEC can be mixed into a thermoplastic as a bulk additive. In every case, treatment with a PEC was found to significantly improve the resistance of the underlying or base material to fire exposure, including self-extinguishing behavior in some cases. The efficacy of these PEC treatments is further buoyed by the fact that most polyelectrolytes are environmentally benign, and in some cases biologically-sourced and/or biodegradable. This enables treatments that meet or exceed the performance of the halogenated materials that they seek to replace, while also meeting fire safety standards of the current commercially available flame retardant treatments.

Chapter III highlighted a layer-by-layer treatment of wood with a renewable nanobrick wall coating comprised of chitosan (CH) and vermiculite clay (VMT). The growth rate of this coating was found to be heavily influenced by the surface chemistry of the wood, with both carboxylation and base treatment providing improved coating uptake via increased negative surface charge prior to immersion in the coating solutions. Two bilayers of thick growing CH/VMT on base-treated wood resulted in a doubled time to ignition in cone calorimetry, along

with an 18% reduction in the total heat release. It was found that the pretreatment and the coating process both decrease the mechanical strength of the wood.

Chapter IV demonstrated a two-step procedure to deposit a polyelectrolyte complex coating on wood surfaces. Longer dip and cure times were found to be more effective as a result of the slow diffusion kinetics at the surface of wood. This polyethylenimine/poly(sodium phosphate) (PEI/PSP) coating added just 6 wt% to the wood and imparted it with self-extinguishing behavior. Additionally, this coating decreased the peak heat release rate and total heat release by 11% and 35% respectively. In contrast to the coating demonstrated in Chapter III, this PEI/PSP complex improved flexural modulus and flexural strength of the wood in three-point bend testing.

Chapter V present a bulk polyelectrolyte complex comprised of polyvinylamine and poly(sodium phosphate), that was mixed with polylactic acid (PLA) to form a composite filament for additive manufacturing. The composite filament was able to be utilized in a commercial 3D printer under identical conditions to neat PLA. The presence of the PEC enabled self-extinguishing behavior in the printed parts during open flame testing and prevented melt-dripping. In microscale combustion calorimetry the composite filament exhibited a 42% lower peak heat release rate as compared to neat PLA.

There are several potential directions in which this research could be furthered. Most notably, the process of depositing flame retardant nanocoatings could be improved through the development of methods to replace the buffer cure step, which is summarized below. Additionally, the principles of polyelectrolyte complexation could be utilized to enable the additive manufacturing of intrinsically flame retardant PEC parts. A proposal to achieve this is outlined below.

6.2 Alternative Curing Methods to Enable One-Step Polyelectrolyte Complex Nanocoatings

The buffer-cured complexes outlined in Chapter IV and in other work represent a considerable reduction in processing steps as compared to the layer-by-layer assembled counterparts of these coatings.[16,110,112,176,202] While the number of handling steps is reduced, all of these techniques require at least two drying steps (after the deposition of the soluble complex/coacervate and again after the buffer/rinse exposures) which requires considerable amounts of energy and has the potential to limit the commercial applications of these techniques. Ideally, a method could be developed that would circumvent the buffer curing and thus the second drying step.

PECs exist along a spectrum ranging from solid, insoluble complex (the phase utilized to ensure durable coatings) to fully dissolved polymer solutions (like the dip solutions in the published buffer-cured PEC coating systems).[52] This spectrum is traversed by modulating the ionic bonds between polyelectrolytes, either by adding salt which screens charges or by manipulating the pH of a solution containing at least one weak polyelectrolyte.[54,175] A few methods to accomplish this will be briefly discussed here, including salt removal from a high-salinity polyelectrolyte complex solution, evaporation of a volatile acid or base, and incorporation of a photoacid generator.

6.2.1 Removal of Salt from a Polyelectrolyte Complex Solution

A blueprint for a salt removal strategy was recently published. In this study, a solution of poly(diallyldimethylammonium chloride) and poly(styrene sulfonae) was formed at high salinity to ensure full dissolution of the PEC.[203] This solution was then cast onto a substrate and then immediately immersed in a lower-salinity bath. This immersion caused the salt concentration in the cast film to suddenly decrease, causing the two polyelectrolytes to precipitate and form a

complex. These particular complexes then served as effective filtration membranes owing to their porous architecture. Since intumescent flame retardant coatings are not as structurally dependent as nanobrick wall coatings, this strategy would likely be effective if applied to polyamine/polyphosphate systems. The key issue to overcome in this case will be the adhesion of the coating to the substrate during the water immersion. Depositing some kind of priming layer and/or concurrent crosslinking during the salt removal may be ways to accomplish this.

6.2.2 Evaporation of Volatile Acids or Bases

In Chapter IV it was shown that the phase of a polyelectrolyte complex can be controlled by the pH of the solution. Weak polyelectrolytes like polyethylenimine and poly(acrylic acid) are typically incorporated in these types of complex solutions since their charge density is dependent upon pH.[16,176] Unfortunately, these techniques necessitate a second "curing" step to increase the charge density of the weak polyelectrolyte and drive subsequent complex formation. This situation requires two drying steps, following soluble PEC deposition and again following curing, which is impractical and energy-intensive.

Recently, it was shown that PECs could be electrospun from a solution containing either ethanol (to act as a charge screening agent and change proton affinity) or formic acid (to directly lower solution pH).[204,205] The electrospinning process drives off the volatile materials and renders a solid complex as the mixture dries. There is a possibility that these techniques could be applied to polyethylenimine/poly(sodium phosphate) mixtures (using ammonia or triethylamine to raise the pH prior to drying and the resultant thermal curing). One complication facing this strategy is the pH sensitivity of polyphosphates and their tendency to hydrolyze.[110,206] This means that the shelf-stability of the coating solution will likely be poor, and potentially neutralizes the entire concept. Charge screening with ethanol (or other volatile hydrophilic small molecules) will not

present these same hydrolysis issues. With that said, polyphosphates are not soluble in alcohols to any appreciable extent so reaching the proper concentration for an effective coating may not be possible. Alternatives to polyphosphates could be explored, such as poly(vinylphosphonic acid), but they are considerably more expensive.

6.2.3 Photoacid Generators

Another potential method to sidestep the curing step of PEC coatings is the incorporation of photoacid generators (PAGs) into the coating solution. A photoacid generator is a compound that has negligible acidity under normal conditions. When these materials are exposed to a particular wavelength of (typically ultraviolet) light, they undergo irreversible reactions that transform them into extremely potent acids.[207] PAGs are typically used as part of photoresist formulations in semiconductor manufacturing. An enormous variety of them have been developed, including water-soluble versions.[208]

In theory, incorporation of PAGs into a polyamine/polyphosphate mixture could enable a very simple two step coating process. The coating solution in question would begin with a higher pH polyamine/polyphosphate mixture with inert PAG added. After dipping a substrate in this solution, it could be exposed to ultraviolet irradiation to activate the PAG. This would protonate the polyamine, forming a solid complex on the substrate, which could then have a subsequent rinse step to remove the activated PAG and loosely adhered material. This PEC-coated fabric would only require one drying step at the end of this process and would then be ready for characterization and wear. Determining exact PAG concentration and processing conditions would be the most difficult portion of this research, but could lead to an enormous improvement in the amount of time and processing steps required to deposit flame retardant polyelectrolyte coatings.

6.3 In-Situ Formation of Polyelectrolyte Complexes from Digital Light Processing

6.3.1 Introduction

Additive manufacturing (AM), also known as 3D printing, has drawn considerable interest in recent years due to its capability to rapidly develop prototypes and functional parts for a variety of fields including medicine, aerospace, and chemistry.[5,6,209] Recently vat photopolymerization, also known as digital light processing (DLP) has risen to prominence among AM techniques due to its capability to produce parts with very high resolution, surface finish, and accuracy.[210] DLP printing operates by projecting a patterned UV light source over a resin containing both mono- and di-functional monomers/oligomers with some form of photoresponsive initiator. Exposure to UV light leads to crosslinking at the site of irradiation on a build platform, which is then moved and fresh resin is polymerized to form the next layer of material (**Figure 6.1**). Monomers utilized in DLP are typically epoxy and acrylate-based, so they can be photochemically cured into a thermoset via cationic or radical polymerization mechanisms (or both).[211]

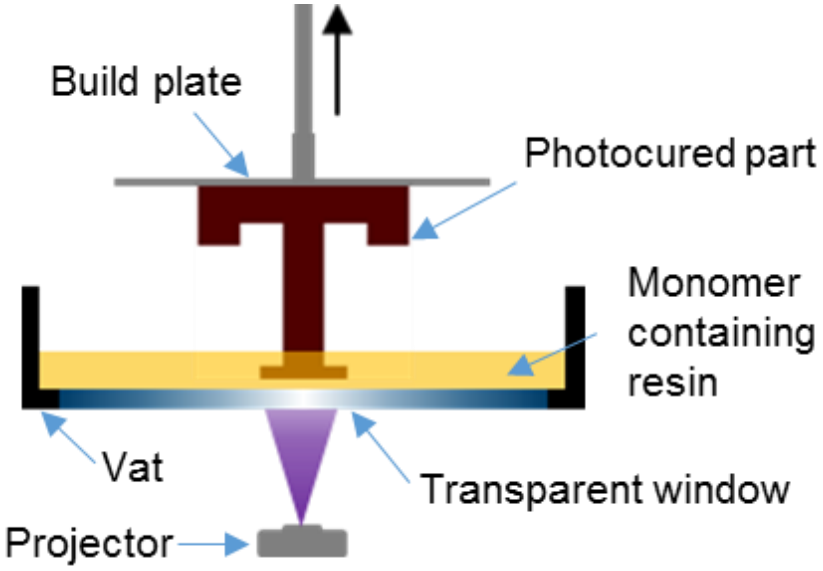

Figure 6.1. Schematic of a DLP 3D printer utilizing vat photopolymerization.

Polyelectrolyte complexes (PECs) have received significant attention recently due to their stimuli-responsive nature,[212,213] ability to separate/purify waste water,[214,215] and utility as vectors for drug delivery.[216–218] PECs can be formed in many ways, most commonly by mixing two oppositely charged macromolecules to form a bulk complex physically that is crosslinked by ionic bonds (**Figure 6.2**). A variety of PECs have been prepared via layer-by-layer assembly to form functional nanocoatings with wide ranging applications.[51,121,122,219,220] In particular, PECs consisting of cationic polyamines and anionic polyphosphates have acted as flame retardant coatings and bulk additives for a variety of substrates, considerably improving the safety of materials such as textiles, flexible foams, wood, and even additively manufactured parts.[16,17,45,110] More recently, methods have been developed to take advantage of the 'saloplasticity' of PECs, which has enabled the processing of bulk PECs with more conventional methods such as extrusion.[174,188] Despite the advances in PEC processing, making parts with particular shapes from a PEC remains challenging, requiring hard-to-scale photolithography techniques that are effective in only two dimensions.[191]

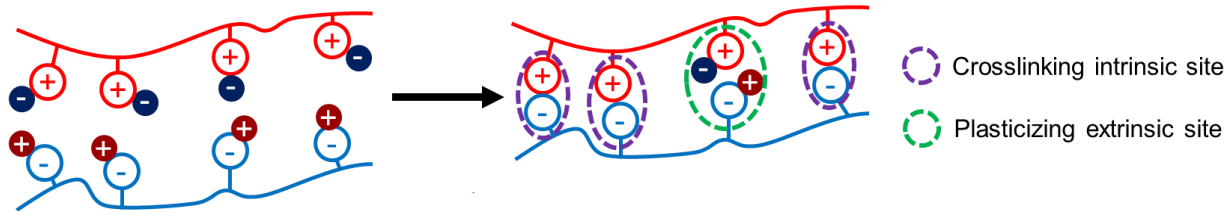

Figure 6.2. Schematic of the formation of a polyelectrolyte complex by mixing a polycation (red) with a polyanion (blue). The resultant complex is held together by the ionic bonds formed (intrinsic ion-pair sites shown in purple ovals). The complex can be plasticized by extrinsic ion-pairing sites (green oval) where the original counterions are compensating polyelectrolyte charge.

Recently, polyelectrolytes were successfully printed via DLP with high resolution and their mechanical properties were modulated via copolymerization with an uncharged hydrophilic monomer.[221] With a fundamental understanding of how hydration, salinity, and polymer chemistry

influence complex formation in the DLP process, vat photopolymerization of polyelectrolyte complexes could be enabled, which has never been done before. The initial objective of this project will be to use DLP-based additive manufacturing to produce the first ever 3D printed PEC parts with high spatial resolution. Next, the mechanical behavior of these PEC parts will be studied in response to varying composition, salinity, and pH to understand the nature of these photopolymerized assemblies. Finally, knowledge acquired from the first two objectives will be leveraged to additively manufacture PECs that are intrinsically flame retardant, with tunable mechanical properties.

6.3.2 Research Plan

Vat photopolymerization of a polyelectrolyte complex: The first phase of this research project will seek to form a polyelectrolyte complex via digital light processing additive manufacturing. Poly(styrene sulfonate) (PSS) will be utilized as the anionic component of the complexes created in this project. Due to the sensitivity of DLP resins to viscosity, PSS will be synthesized in-house to control molar mass and consequently the viscosity of the resins studied.[222] The synthesis of PSS will be performed via a free-radical polymerization initiated by ammonium persulfate under inert atmosphere (**Figure 6.3a**). While free-radical chemistry does not afford tremendous control over molecular weight, the relative ratio of monomer to initiator will be sufficient to modulate resin viscosity.[223] Synthesized PSS will be characterized by NMR spectroscopy and gel permeation chromatography.

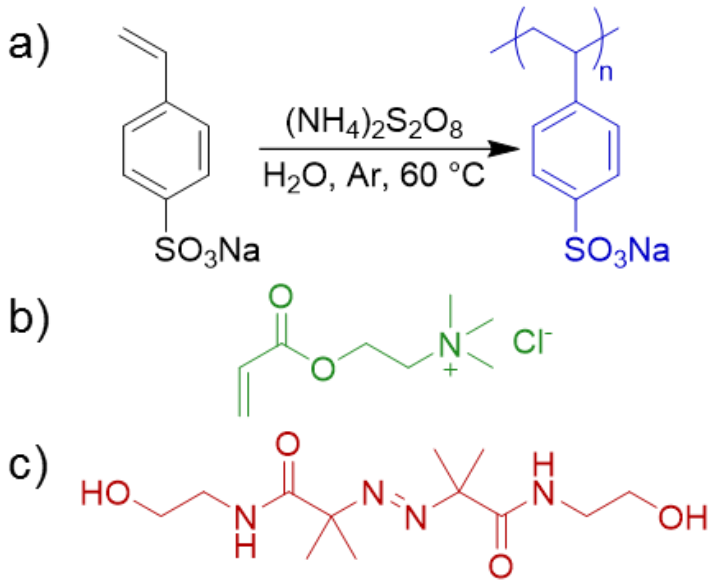

Figure 6.3. (a) Polymerization of sodium 4-styrenesulfonate to yield PSS. **(b)** Structure of the TMA monomer to be used in the proposed work. **(c)** Structure of water-soluble photoinitiator VA-086.

The cationic component of the complex will be trimethylammoniumethyl acrylate (TMA), shown in **Figure 6.3b**, which has previously been successfully printed and is commercially available.[221] TMA is chemically similar to poly(diallyldimethylammonium chloride), a polycation we have worked with before.[224,225,176] As the PSS and acrylate monomer will be in an aqueous solution, a water-soluble photoinitiator is ideal and the VA-086 photoinitiator (**Figure 6.3c**) is one of the best characterized. This initiator absorbs light near 400 nm (a common wavelength for DLP printers), well above PSS's deeper-UV absorbance, and it is also biocompatible, increasing the potential opportunities for printed PEC parts.[222,226,227]

Printing will take place with a commercial DLP printer utilizing a 400 nm light source. Resin formulations will contain synthesized PSS, TMA, and VA-086 dissolved in water. Concentration of the photoinitiator will start at 2 wt%, with the PSS and TMA mixed in a stoichiometric ratio (with respect to PSS's monomer molar mass) to account for an additional 80 wt% of the solution (approximately 2 M concentration of each ionic species), with the balance being deionized water. Prior to the initiation of polymerization by exposure to UV light, this

mixture will be unlikely to exhibit any of the properties of a polyelectrolyte complex. The small molecule TMA will behave more like the sodium ions in the solution than a polycation before it is polymerized, ensuring a soluble and homogeneous printing resin. Areas irradiated by light will undergo polymerization of TMA to poly(trimethylammoniumethyl acrylate) (PTMA). Once the PTMA reaches a critical molar mass it will be able to complex with the PSS in solution, yielding an insoluble complex in the area of irradiation.[228] Shape control will be afforded by changing the projected pattern on the resin as the build plate moves upward (see **Figure 6.1**).

Inhibition of polymerization by oxygen presents a potential barrier to this research plan.[222,229] Growing polymer chains can be terminated by oxygen in the air, yielding an unreactive peroxyl radical. This inhibition can be overcome in a variety of ways. First, since all components of the resin are low-volatility, argon can be bubbled into the system to displace oxygen and minimize chain inhibition during polymerization. Additionally, tertiary amines can nullify oxygen inhibition by reviving terminated chains and reinitiating polymerization.[229] A tertiary amine can be introduced into the reaction by replacing a small amount (1-5 mol %) of the TMA with its tertiary analog dimethylaminoethyl acrylate (DMA) or by simply adding triethylamine.

Composition and behavior of additively manufactured PECs: Once the ability to successfully to print PECs is established, their composition and properties will be studied in detail. Composition of the printed polyelectrolyte complex as a function of resin composition (i.e. PSS:TMA:photoinitiator ratio) will be analyzed by NMR spectroscopy. Despite the insolubility of PECs in water, the ionic bonds between polymers can be disrupted when exposed to solution of sufficient salinity. As a result, composition can be analyzed by dissolving pieces of the printed part in 2 M KBr in D_2O.[53] The aromatic protons of PSS and the methyl protons of PTMA will serve as good markers for integration. Composition will also be analyzed as a function of polymerization

duration. If the polyelectrolytes are incorporated unequally into the resultant part, there is a potential for compositional change throughout the printing process. Parts will be printed and various slices will be analyzed to determine the extent of this disparity, if any exists.

The mechanical properties (e.g. elastic modulus and tensile strength) of the printed parts will be analyzed as a function of salinity (both in the printing media and via introduction of printed parts into solutions of varying salinity) through the use of an Instron Universal Testing Machine. Bulk PECs are known for having varying mechanical properties on the basis of salt exposure.[188] In addition, macroscopic dimensional change will be analyzed by exposing printed parts to solutions of varying salinity. The proposed complex will have relatively low water content, meaning that printed complexes will be unlikely to undergo significant shrinking after printing.[174] Even so, exposure to water would likely cause swelling in a predictable way (varying with salinity). These changes in mechanical strength, elasticity, and size will all be studied to provide a good understanding and ability to predict behavior.

Finally, comonomers can be incorporated into the resin. It has previously been shown that precursors to other water-soluble polymers can be incorporated when photopolymerizing polyelectrolytes.[221] Incorporation of a comonomer (specifically *N*-vinylpyrrolodinone, NVP, shown in **Figure 6.4a**) will be studied with regard to mechanical performance of printed parts. NVP will replace TMA, while holding the TMA:PSS monomer ratio constant. A good understanding of salinity, hydration, and copolymerization will greatly aid in the utility of PEC parts, with desirable mechanical behavior and dimensional stability.

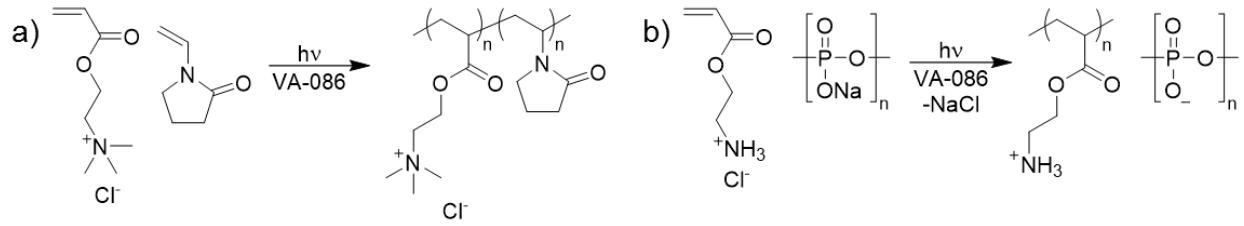

Figure 6.4. (a) Incorporation of NVP into reaction with TMA to yield more mechanically durable polycations for subsequent PEC formation with PSS. **b)** Photopolymerization of protonated amine AEA yields PAEA, which can complex with polyphosphate to yield an intrinsically flame retardant PEC.

Flame-retardant PEC by DLP: As was previously mentioned, the most effective polyelectrolyte complexes for flame retardant applications consist of polyamines and polyphosphates.[16,17,110,192] These can be printed utilizing the knowledge gained in the proposed work (Section 2.1 and 2.2). Specifically, PSS will be replaced by poly(sodium phosphate) (PSP) and TMA will be replaced by its protonated analog, 2-aminoethylacrylate (AEA) (to yield a new protonated amine-containing polycation PAEA). A protonated amine is necessary for a flame retardant PEC in order to provide the acidic proton source for intumescence to take effect (**Figure 6.4b**).[112,178,230]

The incorporation of PSP will likely alter some aspects of the PECs formed during printing. In general, polyphosphates possess weaker ion-pairing strength than other polyanions.[17,175] This weakness will be mitigated to some extent by the protonated polycation that will likely be stronger binding than the quaternary trimethylammonium groups in PTMA.[175] The viscosity and oxygen inhibition concerns outlined in Section 2.1 are addressed by the low molar mass of commercially available PSP and the ability to introduce free tertiary amines in AEA by adjusting pH, respectively. Physical/mechanical properties and composition of these PECs will be studied to determine the influence of polyelectrolyte identity on printed parts.

Fire testing will be critical in evaluating the success of printed parts. Overall thermal stability will be analyzed by thermogravimentric analysis, where the high phosphorus and nitrogen

content will likely produce high char yields, even under oxidative conditions. The bulk flame retardant properties of these parts will be evaluated by cone calorimetry (ASTM E1354), which will reveal time to ignition, peak heat release rate, and total heat release. In addition, vertical burning behavior will be studied according to ASTM D3801, a test to evaluate the capacity of printed parts for sustained ignition and whether or not they self-extinguish. As NVP comonomer is incorporated to alter mechanical properties, further fire studies will also be needed to understand how altering the composition changes the flame retardant behavior of printed parts.

6.3.3 Conclusion

The development of advanced manufacturing methods for polyelectrolyte complexes promises to yield important outcomes. The proposed work seeks to develop an understanding of polyelectrolyte complexes formed through digital light processing. PECs have never been created using this technique. The high resolution afforded by DLP additive manufacturing will enable PEC structures that are currently inaccessible via any other routes. Applying this methodology to flame retardant PECs will enable highly customizable shapes for rapid prototyping of parts for aerospace and other industries that demand rigorous fire protection while avoiding harmful halogen chemistries.

REFERENCES

(1) Brushlinsky, N. N.; Ahrens, M.; Sokolov, S. V.; Wagner, P. World Fire Statistics. *International Association of Fire and Rescue Services* **2018**.

(2) Hill, C. A. S. *Wood Modification: Chemical, Thermal and Other Processes*; John Wiley & Sons, Ltd: Chichester, UK, 2006. https://doi.org/10.1002/0470021748.

(3) Dubrulle, L.; Zammarano, M.; Davis, R. D. *Effect of Fire-Retardant Coatings and Accelerated-Weathering on the Flammability of Wood-Based Materials in Wildland-Urban Interface (WUI) Communities*; National Institute of Standards and Technology, 2020. https://doi.org/10.6028/NIST.TN.2094.

(4) Paesano, A. Polymeric Additive Manufacturing: Present Status and Future Trends of Materials and Processes. *Boeing Technical Journal* **2016**, 1–12.

(5) Chen, R. K.; Jin, Y.; Wensman, J.; Shih, A. Additive Manufacturing of Custom Orthoses and Prostheses—A Review. *Additive Manufacturing* **2016**, *12*, 77–89. https://doi.org/10.1016/j.addma.2016.04.002.

(6) Liu, Z.; Wang, Y.; Wu, B.; Cui, C.; Guo, Y.; Yan, C. A Critical Review of Fused Deposition Modeling 3D Printing Technology in Manufacturing Polylactic Acid Parts. *The International Journal of Advanced Manufacturing Technology* **2019**, *102* (9–12), 2877–2889. https://doi.org/10.1007/s00170-019-03332-x.

(7) Anonymous. Don't Burn Your House down 3D Printing. A Cautionary Tale. *This Smart House*, 2018.

(8) Surette, R. 3D printer blamed for fire inside Cain Building on Texas A&M campus https://www.kbtx.com/content/news/Smoke-prompts-evacuation-of-Cain-Building-on-Texas-AM-campus-501035161.html (accessed Jun 4, 2019).

(9) Shaw, S. Halogenated Flame Retardants: Do the Fire Safety Benefits Justify the Risks? *Rev. Environ. Health* **2010**, *25*, 261–305.

(10) Segev, O.; Kushmaro, A.; Brenner, A. Environmental Impact of Flame Retardants (Persistence and Biodegradability). *Int J Environ Res Public Health* **2009**, *6*, 478–491.

(11) Watanabe, I.; Sakai, S. Environmental Release and Behavior of Brominated Flame Retardants. *Environment International* **2003**, *29*, 665–682.

(12) Birnbaum, L. S.; Staskal, D. F. Brominated Flame Retardants: Cause for Concern? *Environmental Health Perspectives* **2004**, *112*, 9–17.

(13) Westervelt, A. California's Fire Code Update: The End of Toxic Flame Retardants? https://www.forbes.com/sites/amywestervelt/2013/02/08/californias-fire-code-update-the-end-of-toxic-flame-retardants/ (accessed Jan 6, 2021).

(14) Hahladakis, J. N.; Velis, C. A.; Weber, R.; Iacovidou, E.; Purnell, P. An Overview of Chemical Additives Present in Plastics: Migration, Release, Fate and Environmental Impact during Their Use, Disposal and Recycling. *Journal of Hazardous Materials* **2018**, *344*, 179–199.

(15) Kolibaba, T. J.; Brehm, J. T.; Grunlan, J. C. Renewable Nanobrick Wall Coatings for Fire Protection of Wood. *Green Materials* **2020**, *8* (3), 131–138. https://doi.org/10.1680/jgrma.19.00037.

(16) Kolibaba, T. J.; Grunlan, J. C. Environmentally Benign Polyelectrolyte Complex That Renders Wood Flame Retardant and Mechanically Strengthened. *Macromol. Mater. Eng.* **2019**, *304* (8), 1900179. https://doi.org/10.1002/mame.201900179.

(17) Kolibaba, T. J.; Shih, C.-C.; Lazar, S.; Tai, B. L.; Grunlan, J. C. Self-Extinguishing Additive Manufacturing Filament from a Unique Combination of Polylactic Acid and a Polyelectrolyte Complex. *ACS Mater. Lett.* **2020**, *2*, 15–19. https://doi.org/10.1021/acsmaterialslett.9b00393.

(18) How the Tragedy Unfolded at Grenfell Tower. *BBC News*. May 18, 2018.

(19) Massive Fire Ravages Notre-Dame Cathedral. *BBC News*. April 16, 2019.

(20) Morgan, A. B.; Wilkie, C. A. An Introduction to Polymeric Flame Retardancy, Its Role in Materials Science, and the Current State of the Field. In *Fire Retardancy of Polymeric Materials*; Morgan, A. B., Wilkie, C. A., Eds.; CRC Press, 2010; pp 1–14.

(21) Hahladakis, J. N.; Velis, C. A.; Weber, R.; Iacovidou, E.; Purnell, P. An Overview of Chemical Additives Present in Plastics: Migration, Release, Fate and Environmental Impact during Their Use, Disposal and Recycling. *Journal of Hazardous Materials* **2018**, *344*, 179–199. https://doi.org/10.1016/j.jhazmat.2017.10.014.

(22) Green, J. Mechanisms for Flame Retardancy and Smoke Suppression -A Review. *Journal of Fire Sciences* **1996**, *14* (6), 426–442. https://doi.org/10.1177/073490419601400602.

(23) Laoutid, F.; Bonnaud, L.; Alexandre, M.; Lopez-Cuesta, J.-M.; Dubois, Ph. New Prospects in Flame Retardant Polymer Materials: From Fundamentals to Nanocomposites. *Materials Science and Engineering: R: Reports* **2009**, *63* (3), 100–125. https://doi.org/10.1016/j.mser.2008.09.002.

(24) Lazar, S. T.; Kolibaba, T. J.; Grunlan, J. C. Flame-Retardant Surface Treatments. *Nature Reviews Materials* **2020**.

(25) Wilson Jr., W. E.; Fristrom, R. M. Radicals in Flames. *APL Technical Digest* **1963**, *2* (6), 2–7.

(26) Janbozorgi, M.; Far, K.; Metghalchi, H. Combustion Fundamentals. In *Handbook of combustion*; Lackner, M., Ed.; Wiley-VCH: Weinheim, 2010; Vol. 1, pp 1–25.

(27) Boryniec, S.; Przygocki, W. Polymer Combustion Processes . 3 . Flame Retardants for Polymeric Materials; 2001.

(28) Schartel, B. Phosphorus-Based Flame Retardancy Mechanisms—Old Hat or a Starting Point for Future Development? *Materials* **2010**, *3* (10), 4710–4745. https://doi.org/10.3390/ma3104710.

(29) Kashiwagi, T. Polymer Combustion and Flammability—Role of the Condensed Phase. *Symposium (International) on Combustion* **1994**, *25* (1), 1423–1437. https://doi.org/10.1016/S0082-0784(06)80786-1.

(30) Camino, G.; Costa, L.; Luda di Cortemiglia, M. P. Overview of Fire Retardant Mechanisms. *Polymer Degradation and Stability* **1991**, *33* (2), 131–154. https://doi.org/10.1016/0141-3910(91)90014-I.

(31) Shen, K. K. Boron-Based Flame Retardants in Non-Halogen-Based Polymers. In *Non-Halogenated Flame Retardant Handbook*; Morgan, A. B., Wilkie, C. A., Eds.; 2014; pp 201–241.

(32) Kilinc, M. *Silicon Based Flame Retardants*; Morgan, A. B., Wilkie, C. A., Eds.; Scrivener Publishing Llc: Beverly, 2014.

(33) Brown, S. C. Flame Retardants: Inorganic Oxide and Hydroxide Systems. In *Plastic Additives An A-Z Reference*; Springer Science + Business Media Dorcrecht, 1998; pp 287–296.

(34) Morgan, A. B.; Cusack, P. A.; Wilkie, C. A. Other Non-Halogenated Flame Retardant Chemistries and Future Flame Retardant Solutions. *Non-Halogenated Flame Retardant Handbook* **2014**, 347–403.

(35) Salmeia, K.; Gaan, S.; Malucelli, G. Recent Advances for Flame Retardancy of Textiles Based on Phosphorus Chemistry. *Polymers* **2016**, *8* (9), 319. https://doi.org/10.3390/polym8090319.

(36) Salmeia, K.; Fage, J.; Liang, S.; Gaan, S. An Overview of Mode of Action and Analytical Methods for Evaluation of Gas Phase Activities of Flame Retardants. *Polymers* **2015**, *7* (3), 504–526. https://doi.org/10.3390/polym7030504.

(37) Schartel, B.; Perret, B.; Dittrich, B.; Ciesielski, M.; Krämer, J.; Müller, P.; Altstädt, V.; Zang, L.; Döring, M. Flame Retardancy of Polymers: The Role of Specific Reactions in the Condensed Phase: FR Polymers: Role of Condensed Phase. *Macromol. Mater. Eng.* **2016**, *301* (1), 9–35. https://doi.org/10.1002/mame.201500250.

(38) Velencoso, M. M.; Battig, A.; Markwart, J. C.; Schartel, B.; Wurm, F. R. Molecular Firefighting-How Modern Phosphorus Chemistry Can Help Solve the Challenge of Flame Retardancy. *Angew. Chem. Int. Ed.* **2018**, *57* (33), 10450–10467. https://doi.org/10.1002/anie.201711735.

(39) Klatt, M. *Nitrogen-Based Flame Retardants*; Morgan, A. B., Wilkie, C. A., Eds.; Scrivener Publishing Llc: Beverly, 2014.

(40) Schartel, B.; Wilkie, C. A.; Camino, G. Recommendations on the Scientific Approach to Polymer Flame Retardancy: Part 2—Concepts. *Journal of Fire Sciences* **2017**, *35* (1), 3–20. https://doi.org/10.1177/0734904116675370.

(41) Horacek, H.; Grabner, R. Advantages of Flame Retardants Based on Nitrogen Compounds. *Polymer Degradation and Stability* **1996**, *54* (2–3), 205–215. https://doi.org/10.1016/S0141-3910(96)00045-6.

(42) Vandersall, H. L. Intumescent Coating Systems, Their Development and Chemistry. *Journal of Fire Flammability* **1971**, *2*, 97–140.

(43) Guin, T.; Krecker, M.; Milhorn, A.; Grunlan, J. C. Maintaining Hand and Improving Fire Resistance of Cotton Fabric through Ultrasonication Rinsing of Multilayer Nanocoating. *Cellulose* **2014**, *21* (4), 3023–3030. https://doi.org/10.1007/s10570-014-0286-3.

(44) Smith, R. J.; Holder, K. M.; Ruiz, S.; Hahn, W.; Song, Y.; Lvov, Y. M.; Grunlan, J. C. Environmentally Benign Halloysite Nanotube Multilayer Assembly Significantly Reduces Polyurethane Flammability. *Advanced Functional Materials* **2018**, *28* (27), 1703289.

(45) Holder, K. M.; Huff, M. E.; Cosio, M. N.; Grunlan, J. C. Intumescing Multilayer Thin Film Deposited on Clay-Based Nanobrick Wall to Produce Self-Extinguishing Flame Retardant Polyurethane. *Journal of Materials Science* **2015**, *50* (6), 2451–2458. https://doi.org/10.1007/s10853-014-8800-4.

(46) Hull, T. R. 11 - Challenges in Fire Testing: Reaction to Fire Tests and Assessment of Fire Toxicity. In *Advances in Fire Retardant Materials*; Horrocks, A. R., Price, D., Eds.; Woodhead Publishing Series in Textiles; Woodhead Publishing, 2008; pp 255–290. https://doi.org/10.1533/9781845694701.2.255.

(47) Schartel, B.; Hull, T. R. Development of Fire-Retarded Materials—Interpretation of Cone Calorimeter Data. *Fire Mater.* **2007**, *31* (5), 327–354. https://doi.org/10.1002/fam.949.

(48) Huggett, C. Estimation of Rate of Heat Release by Means of Oxygen Consumption Measurements. *Fire Mater.* **1980**, *4* (2), 61–65. https://doi.org/10.1002/fam.810040202.

(49) Laoutid, F.; Bonnaud, L.; Alexandre, M.; Lopez-Cuesta, J.-M.; Dubois, Ph. New Prospects in Flame Retardant Polymer Materials: From Fundamentals to Nanocomposites. *Materials Science and Engineering: R: Reports* **2009**, *63* (3), 100–125. https://doi.org/10.1016/j.mser.2008.09.002.

(50) Decher, G.; Hong, J. D. Buildup of Ultrathin Multilayer Films by a Self-Assembly Process: II. Consecutive Adsorption of Anionic and Cationic Bipolar Amphiphiles and Polyelectrolytes on Charged Surfaces. *Berichte der Bunsengesellschaft für physikalische Chemie* **1991**, *95* (11), 1430–1434. https://doi.org/10.1002/bbpc.19910951122.

(51) Decher, G.; Schlenoff, J. B. *Multilayer Thin Films: Sequential Assembly of Nanocomposite Materials, Second Edition*; John Wiley & Sons, Ltd, 2012.

(52) Wang, Q.; Schlenoff, J. B. The Polyelectrolyte Complex/Coacervate Continuum. *Macromolecules* **2014**, *47* (9), 3108–3116. https://doi.org/10.1021/ma500500q.

(53) Zhang, Y.; Batys, P.; O'Neal, J. T.; Li, F.; Sammalkorpi, M.; Lutkenhaus, J. L. Molecular Origin of the Glass Transition in Polyelectrolyte Assemblies. *ACS Central Science* **2018**, *4* (5), 638–644. https://doi.org/10.1021/acscentsci.8b00137.

(54) Fu, J.; Schlenoff, J. B. Driving Forces for Oppositely Charged Polyion Association in Aqueous Solutions: Enthalpic, Entropic, but Not Electrostatic. *Journal of the American Chemical Society* **2016**, *138* (3), 980–990. https://doi.org/10.1021/jacs.5b11878.

(55) Yang, M.; Shi, J.; Schlenoff, J. B. Control of Dynamics in Polyelectrolyte Complexes by Temperature and Salt. *Macromolecules* **2019**, *52* (5), 1930–1941. https://doi.org/10.1021/acs.macromol.8b02577.

(56) Li, L.; Srivastava, S.; Andreev, M.; Marciel, A. B.; de Pablo, J. J.; Tirrell, M. V. Phase Behavior and Salt Partitioning in Polyelectrolyte Complex Coacervates. *Macromolecules* **2018**, *51* (8), 2988–2995. https://doi.org/10.1021/acs.macromol.8b00238.

(57) Cain, A. A.; Nolen, C. R.; Li, Y.-C.; Davis, R.; Grunlan, J. C. Phosphorous-Filled Nanobrick Wall Multilayer Thin Film Eliminates Polyurethane Melt Dripping and Reduces Heat Release Associated with Fire. *Polymer Degradation and Stability* **2013**, *98* (12), 2645–2652. https://doi.org/10.1016/j.polymdegradstab.2013.09.028.

(58) Li, Y.-C.; Kim, Y. S.; Shields, J.; Davis, R. Controlling Polyurethane Foam Flammability and Mechanical Behaviour by Tailoring the Composition of Clay-Based Multilayer Nanocoatings. *J. Mater. Chem. A* **2013**, *1* (41), 12987. https://doi.org/10.1039/c3ta11936j.

(59) Kim, Y. S.; Davis, R. Multi-Walled Carbon Nanotube Layer-by-Layer Coatings with a Trilayer Structure to Reduce Foam Flammability. *Thin Solid Films* **2014**, *550*, 184–189. https://doi.org/10.1016/j.tsf.2013.10.167.

(60) Pan, H.; Pan, Y.; Wang, W.; Song, L.; Hu, Y.; Liew, K. M. Synergistic Effect of Layer-by-Layer Assembled Thin Films Based on Clay and Carbon Nanotubes To Reduce the Flammability of Flexible Polyurethane Foam. *Ind. Eng. Chem. Res.* **2014**, *53* (37), 14315–14321.

(61) Yang, Y.-H.; Li, Y.-C.; Shields, J.; Davis, R. D. Layer Double Hydroxide and Sodium Montmorillonite Multilayer Coatings for the Flammability Reduction of Flexible Polyurethane Foams. *J. Appl. Polym. Sci.* **2015**, *132* (14), n/a-n/a. https://doi.org/10.1002/app.41767.

(62) Zhang, X.; Shen, Q.; Zhang, X.; Pan, H.; Lu, Y. Graphene Oxide-Filled Multilayer Coating to Improve Flame-Retardant and Smoke Suppression Properties of Flexible Polyurethane Foam. *J. Mater. Sci.* **2016**, *51* (23), 10361–10374.

(63) Pan, H.; Lu, Y.; Song, L.; Zhang, X.; Hu, Y. Construction of Layer-by-Layer Coating Based on Graphene Oxide/β-FeOOH Nanorods and Its Synergistic Effect on Improving Flame Retardancy of Flexible Polyurethane Foam. *Composites Science and Technology* **2016**, *129*, 116–122. https://doi.org/10.1016/j.compscitech.2016.04.018.

(64) Li, Y.-C.; Yang, Y.-H.; Kim, Y. S.; Shields, J.; Davis, R. D. DNA-Based Nanocomposite Biocoatings for Fire-Retarding Polyurethane Foam. *Green Materials* **2014**, *2* (3), 144–152. https://doi.org/10.1680/gmat.14.00003.

(65) Liu, X.; Qin, S.; Li, H.; Sun, J.; Gu, X.; Zhang, S.; Grunlan, J. C. Combination Intumescent and Kaolin-Filled Multilayer Nanocoatings That Reduce Polyurethane Flammability. *Macromol. Mater. Eng.* **2019**, *304* (2), 1800531. https://doi.org/10.1002/mame.201800531.

(66) Carosio, F.; Di Blasio, A.; Cuttica, F.; Alongi, J.; Malucelli, G. Self-Assembled Hybrid Nanoarchitectures Deposited on Poly(Urethane) Foams Capable of Chemically Adapting to Extreme Heat. *RSC Adv.* **2014**, *4* (32), 16674–16680. https://doi.org/10.1039/C4RA01343C.

(67) Alongi, J.; Carosio, F.; Malucelli, G. Influence of Ammonium Polyphosphate-/Poly(Acrylic Acid)-Based Layer by Layer Architectures on the Char Formation in Cotton, Polyester and Their Blends. *Polymer Degradation and Stability* **2012**, *97* (9), 1644–1653. https://doi.org/10.1016/j.polymdegradstab.2012.06.025.

(68) Kumar Kundu, C.; Wang, W.; Zhou, S.; Wang, X.; Sheng, H.; Pan, Y.; Song, L.; Hu, Y. A Green Approach to Constructing Multilayered Nanocoating for Flame Retardant Treatment of Polyamide 66 Fabric from Chitosan and Sodium Alginate. *Carbohydrate Polymers* **2017**, *166*, 131–138. https://doi.org/10.1016/j.carbpol.2017.02.084.

(69) Zanetti, M.; Kashiwagi, T.; Falqui, L.; Camino, G. Cone Calorimeter Combustion and Gasification Studies of Polymer Layered Silicate Nanocomposites. *Chem. Mater.* **2002**, *14* (2), 881–887. https://doi.org/10.1021/cm011236k.

(70) Li, Y.-C.; Schulz, J.; Grunlan, J. C. Polyelectrolyte/Nanosilicate Thin-Film Assemblies: Influence of PH on Growth, Mechanical Behavior, and Flammability. *ACS Applied Materials & Interfaces* **2009**, *1* (10), 2338–2347. https://doi.org/10.1021/am900484q.

(71) Li, Y.-C.; Schulz, J.; Mannen, S.; Delhom, C.; Condon, B.; Chang, S.; Zammarano, M.; Grunlan, J. C. Flame Retardant Behavior of Polyelectrolyte−Clay Thin Film Assemblies on Cotton Fabric. *ACS Nano* **2010**, *4* (6), 3325–3337. https://doi.org/10.1021/nn100467e.

(72) Choi, K.; Seo, S.; Kwon, H.; Kim, D.; Park, Y. T. Fire Protection Behavior of Layer-by-Layer Assembled Starch–Clay Multilayers on Cotton Fabric. *J Mater Sci* **2018**, *53* (16), 11433–11443. https://doi.org/10.1007/s10853-018-2434-x.

(73) Huang, G.; Yang, J.; Gao, J.; Wang, X. Thin Films of Intumescent Flame Retardant-Polyacrylamide and Exfoliated Graphene Oxide Fabricated via Layer-by-Layer Assembly

for Improving Flame Retardant Properties of Cotton Fabric. *Ind. Eng. Chem. Res.* **2012**, *51* (38), 12355–12366. https://doi.org/10.1021/ie301911t.

(74) Ding, X.; Fang, F.; Du, T.; Zheng, K.; Chen, L.; Tian, X.; Zhang, X. Carbon Nanotube-Filled Intumescent Multilayer Nanocoating on Cotton Fabric for Enhancing Flame Retardant Property. *Surface and Coatings Technology* **2016**, *305*, 184–191. https://doi.org/10.1016/j.surfcoat.2016.08.035.

(75) Pan, H.; Wang, W.; Pan, Y.; Zeng, W.; Zhan, J.; Song, L.; Hu, Y.; Liew, K. M. Construction of Layer-by-Layer Assembled Chitosan/Titanate Nanotubes Based Nanocoating on Cotton Fabrics: Flame Retardant Performance and Combustion Behavior. *Cellulose* **2015**, *22* (1), 911–923. https://doi.org/10.1007/s10570-014-0536-4.

(76) Uğur, Ş. S.; Sarıışık, M.; Aktaş, A. H. Nano-Al2O3 Multilayer Film Deposition on Cotton Fabrics by Layer-by-Layer Deposition Method. *Materials Research Bulletin* **2011**, *46* (8), 1202–1206. https://doi.org/10.1016/j.materresbull.2011.04.005.

(77) Kandola, B. K.; Horrocks, A. R.; Price, D.; Coleman, G. V. Flame-Retardant Treatments of Cellulose and Their Influence on the Mechanism of Cellulose Pyrolysis. *Journal of Macromolecular Science, Part C: Polymer Reviews* **1996**, *36* (4), 721–794. https://doi.org/10.1080/15321799608014859.

(78) Li, Y.-C.; Mannen, S.; Morgan, A. B.; Chang, S.; Yang, Y.-H.; Condon, B.; Grunlan, J. C. Intumescent All-Polymer Multilayer Nanocoating Capable of Extinguishing Flame on Fabric. *Advanced Materials* **2011**, *23* (34), 3926–3931. https://doi.org/10.1002/adma.201101871.

(79) Kim, Y. S.; Davis, R.; Cain, A. A.; Grunlan, J. C. Development of Layer-by-Layer Assembled Carbon Nanofiber-Filled Coatings to Reduce Polyurethane Foam Flammability. *Polymer* **2011**, *52* (13), 2847–2855. https://doi.org/10.1016/j.polymer.2011.04.023.

(80) Cain, A. A.; Plummer, M. G. B.; Murray, S. E.; Bolling, L.; Regev, O.; Grunlan, J. C. Iron-Containing, High Aspect Ratio Clay as Nanoarmor That Imparts Substantial Thermal/Flame Protection to Polyurethane with a Single Electrostatically-Deposited Bilayer. *J. Mater. Chem. A* **2014**, *2* (41), 17609–17617.

(81) Smith, R. J.; Holder, K. M.; Ruiz, S.; Hahn, W.; Song, Y.; Lvov, Y. M.; Grunlan, J. C. Environmentally Benign Halloysite Nanotube Multilayer Assembly Significantly Reduces Polyurethane Flammability. *Adv. Funct. Mater.* **2018**, *28* (27), 1703289.

(82) Zhang, C.; Milhorn, A.; Haile, M.; Mai, G.; Grunlan, J. C. Nanocoating of Starch and Clay That Reduces the Flammability of Polyurethane Foam. *Green Materials* **2017**, *5* (4), 182–186. https://doi.org/10.1680/jgrma.17.00025.

(83) Laufer, G.; Kirkland, C.; Cain, A. A.; Grunlan, J. C. Clay–Chitosan Nanobrick Walls: Completely Renewable Gas Barrier and Flame-Retardant Nanocoatings. *ACS Appl. Mater. Interfaces* **2012**, *4* (3), 1643–1649. https://doi.org/10.1021/am2017915.

(84) Qin, S.; Pour, M. G.; Lazar, S.; Köklükaya, O.; Gerringer, J.; Song, Y.; Wågberg, L.; Grunlan, J. C. Super Gas Barrier and Fire Resistance of Nanoplatelet/Nanofibril Multilayer Thin Films. *Adv. Mater. Interfaces* **2019**, *6* (2), 1801424. https://doi.org/10.1002/admi.201801424.

(85) Pan, H.; Yu, B.; Wang, W.; Pan, Y.; Song, L.; Hu, Y. Comparative Study of Layer by Layer Assembled Multilayer Films Based on Graphene Oxide and Reduced Graphene Oxide on Flexible Polyurethane Foam: Flame Retardant and Smoke Suppression Properties. *RSC Adv.* **2016**, *6* (115), 114304–114312. https://doi.org/10.1039/C6RA15522G.

(86) Maddalena, L.; Carosio, F.; Gomez, J.; Saracco, G.; Fina, A. Layer-by-Layer Assembly of Efficient Flame Retardant Coatings Based on High Aspect Ratio Graphene Oxide and Chitosan Capable of Preventing Ignition of PU Foam. *Polymer Degradation and Stability* **2018**, *152*, 1–9. https://doi.org/10.1016/j.polymdegradstab.2018.03.013.

(87) Zhang, T.; Yan, H.; Peng, M.; Wang, L.; Ding, H.; Fang, Z. Construction of Flame Retardant Nanocoating on Ramie Fabric via Layer-by-Layer Assembly of Carbon Nanotube and Ammonium Polyphosphate. *Nanoscale* **2013**, *5* (7), 3013. https://doi.org/10.1039/c3nr34020a.

(88) Holder, K. M.; Cain, A. A.; Plummer, M. G.; Stevens, B. E.; Odenborg, P. K.; Morgan, A. B.; Grunlan, J. C. Carbon Nanotube Multilayer Nanocoatings Prevent Flame Spread on Flexible Polyurethane Foam. *Macromol. Mater. Eng.* **2016**, *301* (6), 665–673. https://doi.org/10.1002/mame.201500327.

(89) Pan, H.; Wang, W.; Pan, Y.; Song, L.; Hu, Y.; Liew, K. M. Formation of Layer-by-Layer Assembled Titanate Nanotubes Filled Coating on Flexible Polyurethane Foam with Improved Flame Retardant and Smoke Suppression Properties. *ACS Appl. Mater. Interfaces* **2015**, *7* (1), 101–111.

(90) Pan, H.; Shen, Q.; Zhang, Z.; Yu, B.; Lu, Y. MoS2-Filled Coating on Flexible Polyurethane Foam via Layer-by-Layer Assembly Technique: Flame-Retardant and Smoke Suppression Properties. *J Mater Sci* **2018**, *53* (12), 9340–9349. https://doi.org/10.1007/s10853-018-2199-2.

(91) Lazar, S.; Carosio, F.; Davesne, A.-L.; Jimenez, M.; Bourbigot, S.; Grunlan, J. Extreme Heat Shielding of Clay/Chitosan Nanobrick Wall on Flexible Foam. *ACS Appl. Mater. Interfaces* **2018**, *10* (37), 31686–31696. https://doi.org/10.1021/acsami.8b10227.

(92) Patra, D.; Vangal, P.; Cain, A. A.; Cho, C.; Regev, O.; Grunlan, J. C. Inorganic Nanoparticle Thin Film That Suppresses Flammability of Polyurethane with Only a Single Electrostatically-Assembled Bilayer. *ACS Appl. Mater. Interfaces* **2014**, *6* (19), 16903–16908.

(93) Mu, X.; Yuan, B.; Pan, Y.; Feng, X.; Duan, L.; Zong, R.; Hu, Y. A Single α-Cobalt Hydroxide/Sodium Alginate Bilayer Layer-by-Layer Assembly for Conferring Flame

Retardancy to Flexible Polyurethane Foams. *Materials Chemistry and Physics* **2017**, *191*, 52–61. https://doi.org/10.1016/j.matchemphys.2017.01.023.

(94) Haile, M.; Fomete, S.; Lopez, I. D.; Grunlan, J. C. Aluminum Hydroxide Multilayer Assembly Capable of Extinguishing Flame on Polyurethane Foam. *J Mater Sci* **2016**, *51* (1), 375–381. https://doi.org/10.1007/s10853-015-9258-8.

(95) Shi, X.; Yang, P.; Peng, X.; Huang, C.; Qian, Q.; Wang, B.; He, J.; Liu, X.; Li, Y.; Kuang, T. Bi-Phase Fire-Resistant Polyethylenimine/Graphene Oxide/Melanin Coatings Using Layer by Layer Assembly Technique: Smoke Suppression and Thermal Stability of Flexible Polyurethane Foams. *Polymer* **2019**, *170*, 65–75. https://doi.org/10.1016/j.polymer.2019.03.008.

(96) Carosio, F.; Fina, A. Three Organic/Inorganic Nanolayers on Flexible Foam Allow Retaining Superior Flame Retardancy Performance Upon Mechanical Compression Cycles. *Front. Mater.* **2019**, *6*, 20. https://doi.org/10.3389/fmats.2019.00020.

(97) Pan, Y.; Liu, L.; Cai, W.; Hu, Y.; Jiang, S.; Zhao, H. Effect of Layer-by-Layer Self-Assembled Sepiolite-Based Nanocoating on Flame Retardant and Smoke Suppressant Properties of Flexible Polyurethane Foam. *Applied Clay Science* **2019**, *168*, 230–236. https://doi.org/10.1016/j.clay.2018.11.014.

(98) Carosio, F.; Negrell-Guirao, C.; Alongi, J.; David, G.; Camino, G. All-Polymer Layer by Layer Coating as Efficient Solution to Polyurethane Foam Flame Retardancy. *European Polymer Journal* **2015**, *70*, 94–103. https://doi.org/10.1016/j.eurpolymj.2015.07.001.

(99) Carosio, F.; Ghanadpour, M.; Alongi, J.; Wågberg, L. Layer-by-Layer-Assembled Chitosan/Phosphorylated Cellulose Nanofibrils as a Bio-Based and Flame Protecting Nano-Exoskeleton on PU Foams. *Carbohydrate Polymers* **2018**, *202*, 479–487. https://doi.org/10.1016/j.carbpol.2018.09.005.

(100) Wang, X.; Pan, Y.-T.; Wan, J.-T.; Wang, D.-Y. An Eco-Friendly Way to Fire Retardant Flexible Polyurethane Foam: Layer-by-Layer Assembly of Fully Bio-Based Substances. *RSC Adv.* **2014**, *4* (86), 46164–46169. https://doi.org/10.1039/C4RA07972H.

(101) Laufer, G.; Kirkland, C.; Morgan, A. B.; Grunlan, J. C. Exceptionally Flame Retardant Sulfur-Based Multilayer Nanocoating for Polyurethane Prepared from Aqueous Polyelectrolyte Solutions. *ACS Macro Lett.* **2013**, *2* (5), 361–365. https://doi.org/10.1021/mz400105e.

(102) Jimenez, M.; Guin, T.; Bellayer, S.; Dupretz, R.; Bourbigot, S.; Grunlan, J. C. Microintumescent Mechanism of Flame-Retardant Water-Based Chitosan-Ammonium Polyphosphate Multilayer Nanocoating on Cotton Fabric. *J. Appl. Polym. Sci.* **2016**, *133* (32). https://doi.org/10.1002/app.43783.

(103) Laufer, G.; Kirkland, C.; Morgan, A. B.; Grunlan, J. C. Intumescent Multilayer Nanocoating, Made with Renewable Polyelectrolytes, for Flame-Retardant Cotton. *Biomacromolecules* **2012**, *13* (9), 2843–2848. https://doi.org/10.1021/bm300873b.

(104) Zhang, T.; Yan, H.; Wang, L.; Fang, Z. Controlled Formation of Self-Extinguishing Intumescent Coating on Ramie Fabric via Layer-by-Layer Assembly. *Ind. Eng. Chem. Res.* **2013**, *52* (18), 6138–6146. https://doi.org/10.1021/ie3031554.

(105) Fang, F.; Zhang, X.; Meng, Y.; Gu, Z.; Bao, C.; Ding, X.; Li, S.; Chen, X.; Tian, X. Intumescent Flame Retardant Coatings on Cotton Fabric of Chitosan and Ammonium Polyphosphate via Layer-by-Layer Assembly. *Surface and Coatings Technology* **2015**, *262*, 9–14. https://doi.org/10.1016/j.surfcoat.2014.11.011.

(106) Alongi, J.; Carletto, R. A.; Di Blasio, A.; Carosio, F.; Bosco, F.; Malucelli, G. DNA: A Novel, Green, Natural Flame Retardant and Suppressant for Cotton. *J. Mater. Chem. A* **2013**, *1* (15), 4779. https://doi.org/10.1039/c3ta00107e.

(107) Pan, H.; Song, L.; Ma, L.; Pan, Y.; Liew, K. M.; Hu, Y. Layer-by-Layer Assembled Thin Films Based on Fully Biobased Polysaccharides: Chitosan and Phosphorylated Cellulose for Flame-Retardant Cotton Fabric. *Cellulose* **2014**, *21* (4), 2995–3006. https://doi.org/10.1007/s10570-014-0276-5.

(108) Pan, H.; Wang, W.; Pan, Y.; Song, L.; Hu, Y.; Liew, K. M. Formation of Self-Extinguishing Flame Retardant Biobased Coating on Cotton Fabrics via Layer-by-Layer Assembly of Chitin Derivatives. *Carbohydrate Polymers* **2015**, *115*, 516–524. https://doi.org/10.1016/j.carbpol.2014.08.084.

(109) Cain, A. A.; Murray, S.; Holder, K. M.; Nolen, C. R.; Grunlan, J. C. Intumescent Nanocoating Extinguishes Flame on Fabric Using Aqueous Polyelectrolyte Complex Deposited in Single Step: Intumescent Nanocoating Extinguishes Flame on Fabric. *Macromolecular Materials and Engineering* **2014**, *299* (10), 1180–1187. https://doi.org/10.1002/mame.201400022.

(110) Haile, M.; Fincher, C.; Fomete, S.; Grunlan, J. C. Water-Soluble Polyelectrolyte Complexes That Extinguish Fire on Cotton Fabric When Deposited as PH-Cured Nanocoating. *Polymer Degradation and Stability* **2015**, *114*, 60–64. https://doi.org/10.1016/j.polymdegradstab.2015.01.022.

(111) Leistner, M.; Haile, M.; Rohmer, S.; Abu-Odeh, A.; Grunlan, J. C. Water-Soluble Polyelectrolyte Complex Nanocoating for Flame Retardant Nylon-Cotton Fabric. *Polymer Degradation and Stability* **2015**, *122*, 1–7. https://doi.org/10.1016/j.polymdegradstab.2015.10.008.

(112) Haile, M.; Leistner, M.; Sarwar, O.; Toler, C. M.; Henderson, R.; Grunlan, J. C. A Wash-Durable Polyelectrolyte Complex That Extinguishes Flames on Polyester–Cotton Fabric. *RSC Advances* **2016**, *6* (40), 33998–34004. https://doi.org/10.1039/C6RA03637F.

(113) Cheng, X.-W.; Guan, J.-P.; Yang, X.-H.; Tang, R.-C.; Yao, F. A Bio-Resourced Phytic Acid/Chitosan Polyelectrolyte Complex for the Flame Retardant Treatment of Wool Fabric. *Journal of Cleaner Production* **2019**, *223*, 342–349. https://doi.org/10.1016/j.jclepro.2019.03.157.

(114) Shi, X.-H.; Chen, L.; Liu, B.-W.; Long, J.-W.; Xu, Y.-J.; Wang, Y.-Z. Carbon Fibers Decorated by Polyelectrolyte Complexes Toward Their Epoxy Resin Composites with High Fire Safety. *Chin J Polym Sci* **2018**, *36* (12), 1375–1384. https://doi.org/10.1007/s10118-018-2164-1.

(115) Carosio, F.; Alongi, J. Flame Retardant Multilayered Coatings on Acrylic Fabrics Prepared by One-Step Deposition of Chitosan/Montmorillonite Complexes. *Fibers* **2018**, *6* (2), 36. https://doi.org/10.3390/fib6020036.

(116) Evarts, B. Fire Loss in the United States During 2017. **2018**, 23.

(117) Berglund, L. A.; Burgert, I. Bioinspired Wood Nanotechnology for Functional Materials. *Advanced Materials* **2018**, *30* (19), 1704285. https://doi.org/10.1002/adma.201704285.

(118) Lowden, L. A.; Hull, T. R. Flammability Behaviour of Wood and a Review of the Methods for Its Reduction. *Fire science reviews* **2013**, *2* (1), 4.

(119) Alaee, M. An Overview of Commercially Used Brominated Flame Retardants, Their Applications, Their Use Patterns in Different Countries/Regions and Possible Modes of Release. *Environment International* **2003**, *29* (6), 683–689. https://doi.org/10.1016/S0160-4120(03)00121-1.

(120) Mendis, G. P.; Weiss, S. G.; Korey, M.; Boardman, C. R.; Dietenberger, M.; Youngblood, J. P.; Howarter, J. A. Phosphorylated Lignin as a Halogen-Free Flame Retardant Additive for Epoxy Composites. *Green Materials* **2016**, *4* (4), 150–159. https://doi.org/10.1680/jgrma.16.00008.

(121) Holder, K. M.; Smith, R. J.; Grunlan, J. C. A Review of Flame Retardant Nanocoatings Prepared Using Layer-by-Layer Assembly of Polyelectrolytes. *Journal of Materials Science* **2017**, *52* (22), 12923–12959. https://doi.org/10.1007/s10853-017-1390-1.

(122) Qiu, X.; Li, Z.; Li, X.; Zhang, Z. Flame Retardant Coatings Prepared Using Layer by Layer Assembly: A Review. *Chemical Engineering Journal* **2018**, *334*, 108–122. https://doi.org/10.1016/j.cej.2017.09.194.

(123) Dubas, S. T.; Schlenoff, J. B. Factors Controlling the Growth of Polyelectrolyte Multilayers. *Macromolecules* **1999**, *32* (24), 8153–8160. https://doi.org/10.1021/ma981927a.

(124) Borges, J.; Mano, J. F. Molecular Interactions Driving the Layer-by-Layer Assembly of Multilayers. *Chemical Reviews* **2014**, *114* (18), 8883–8942. https://doi.org/10.1021/cr400531v.

(125) Hagen, D. A.; Song, Y.; Saucier, L.; Milhorn, A.; Stevens, B.; Grunlan, J. C. Balancing Polyelectrolyte Diffusion and Clay Deposition for High Gas Barrier. *Green Materials* **2016**, *4* (3), 98–103. https://doi.org/10.1680/jgrma.16.00012.

(126) Qin, S.; Pour, M. G.; Lazar, S.; Köklükaya, O.; Gerringer, J.; Song, Y.; Wågberg, L.; Grunlan, J. C. Super Gas Barrier and Fire Resistance of Nanoplatelet/Nanofibril Multilayer Thin Films. *Advanced Materials Interfaces* **2019**, *6* (2), 1801424. https://doi.org/10.1002/admi.201801424.

(127) Liu, L.; Pan, Y.; Wang, Z.; Hou, Y.; Gui, Z.; Hu, Y. Layer-by-Layer Assembly of Hypophosphorous Acid-Modified Chitosan Based Coating for Flame-Retardant Polyester–Cotton Blends. *Industrial & Engineering Chemistry Research* **2017**, *56* (34), 9429–9436. https://doi.org/10.1021/acs.iecr.7b02303.

(128) Zhang, C.; Milhorn, A.; Haile, M.; Mai, G.; Grunlan, J. C. Nanocoating of Starch and Clay That Reduces the Flammability of Polyurethane Foam. *Green Materials* **2017**, *5* (4), 182–186. https://doi.org/10.1680/jgrma.17.00025.

(129) Kumar Kundu, C.; Wang, W.; Zhou, S.; Wang, X.; Sheng, H.; Pan, Y.; Song, L.; Hu, Y. A Green Approach to Constructing Multilayered Nanocoating for Flame Retardant Treatment of Polyamide 66 Fabric from Chitosan and Sodium Alginate. *Carbohydrate Polymers* **2017**, *166*, 131–138. https://doi.org/10.1016/j.carbpol.2017.02.084.

(130) Lazar, S.; Carosio, F.; Davesne, A.-L.; Jimenez, M.; Bourbigot, S.; Grunlan, J. Extreme Heat Shielding of Clay/Chitosan Nanobrick Wall on Flexible Foam. *ACS Applied Materials & Interfaces* **2018**, *10* (37), 31686–31696. https://doi.org/10.1021/acsami.8b10227.

(131) Chen, P.; Zhao, Y.; Wang, W.; Zhang, T.; Song, S. Correlation of Montmorillonite Sheet Thickness and Flame Retardant Behavior of a Chitosan–Montmorillonite Nanosheet Membrane Assembled on Flexible Polyurethane Foam. *Polymers (Basel)* **2019**, *11* (2). https://doi.org/10.3390/polym11020213.

(132) Fu, Q.; Medina, L.; Li, Y.; Carosio, F.; Hajian, A.; Berglund, L. A. Nanostructured Wood Hybrids for Fire-Retardancy Prepared by Clay Impregnation into the Cell Wall. *ACS Applied Materials & Interfaces* **2017**, *9* (41), 36154–36163. https://doi.org/10.1021/acsami.7b10008.

(133) Guo, B.; Liu, Y.; Zhang, Q.; Wang, F.; Wang, Q.; Liu, Y.; Li, J.; Yu, H. Efficient Flame-Retardant and Smoke-Suppression Properties of Mg–Al-Layered Double-Hydroxide Nanostructures on Wood Substrate. *ACS Applied Materials & Interfaces* **2017**, *9* (27), 23039–23047. https://doi.org/10.1021/acsami.7b06803.

(134) Carosio, F.; Cuttica, F.; Medina, L.; Berglund, L. A. Clay Nanopaper as Multifunctional Brick and Mortar Fire Protection Coating—Wood Case Study. *Materials & Design* **2016**, *93*, 357–363. https://doi.org/10.1016/j.matdes.2015.12.140.

(135) Zheng, Z.; McDonald, J.; Khillan, R.; Su, Y.; Shutava, T.; Grozdits, G.; Lvov, Y. M. Layer-by-Layer Nanocoating of Lignocellulose Fibers for Enhanced Paper Properties. *Journal of Nanoscience and Nanotechnology* **2006**, *6* (3), 624–632. https://doi.org/10.1166/jnn.2006.081.

(136) Agarwal, M.; Lvov, Y.; Varahramyan, K. Conductive Wood Microfibres for Smart Paper through Layer-by-Layer Nanocoating. *Nanotechnology* **2006**, *17* (21), 5319–5325. https://doi.org/10.1088/0957-4484/17/21/006.

(137) Lin, Z.; Renneckar, S.; Hindman, D. P. Nanocomposite-Based Lignocellulosic Fibers 1. Thermal Stability of Modified Fibers with Clay-Polyelectrolyte Multilayers. *Cellulose* **2008**, *15* (2), 333–346. https://doi.org/10.1007/s10570-007-9188-y.

(138) Renneckar, S.; Zhou, Y. Nanoscale Coatings on Wood: Polyelectrolyte Adsorption and Layer-by-Layer Assembled Film Formation. *ACS Applied Materials & Interfaces* **2009**, *1* (3), 559–566. https://doi.org/10.1021/am800119q.

(139) Lu, X.; Hu, Y. Layer-by-Layer Deposition of TiO2 Nanoparticles in the Wood Surface and Its Superhydrophobic Performance. *BioResources* **2016**, *11* (2), 4605–4620.

(140) Bellanger, H.; Casdorff, K.; Muff, L. F.; Ammann, R.; Burgert, I.; Michen, B. Layer-by-Layer Deposition on a Heterogeneous Surface: Effect of Sorption Kinetics on the Growth of Polyelectrolyte Multilayers. *Journal of Colloid and Interface Science* **2017**, *500*, 133–141. https://doi.org/10.1016/j.jcis.2017.02.048.

(141) Casdorff, K.; Keplinger, T.; Bellanger, H.; Michen, B.; Schön, S.; Burgert, I. High-Resolution Adhesion Mapping of the Odd–Even Effect on a Layer-by-Layer Coated Biomaterial by Atomic-Force-Microscopy. *ACS Applied Materials & Interfaces* **2017**, *9* (15), 13793–13800. https://doi.org/10.1021/acsami.7b02564.

(142) Lozhechnikova, A.; Bellanger, H.; Michen, B.; Burgert, I.; Österberg, M. Surfactant-Free Carnauba Wax Dispersion and Its Use for Layer-by-Layer Assembled Protective Surface Coatings on Wood. *Applied Surface Science* **2017**, *396*, 1273–1281. https://doi.org/10.1016/j.apsusc.2016.11.132.

(143) Krogman, K. C.; Zacharia, N. S.; Schroeder, S.; Hammond, P. T. Automated Process for Improved Uniformity and Versatility of Layer-by-Layer Deposition. *Langmuir* **2007**, *23* (6), 3137–3141. https://doi.org/10.1021/la063085b.

(144) Elbert, D. L.; Herbert, C. B.; Hubbell, J. A. Thin Polymer Layers Formed by Polyelectrolyte Multilayer Techniques on Biological Surfaces. *Langmuir* **1999**, *15* (16), 5355–5362. https://doi.org/10.1021/la9815749.

(145) Lvov, Y.; Haas, H.; Decher, G.; Moehwald, H.; Kalachev, A. Assembly of Polyelectrolyte Molecular Films onto Plasma-Treated Glass. *The Journal of Physical Chemistry* **1993**, *97* (49), 12835–12841. https://doi.org/10.1021/j100151a033.

(146) Matsuda, H. Preparation and Utilization of Esterified Woods Bearing Carboxyl Groups. *Wood Sci. Technol.* **1987**, *21*, 75–88.

(147) Jang, W.-S.; Grunlan, J. C. Robotic Dipping System for Layer-by-Layer Assembly of Multifunctional Thin Films. *Review of Scientific Instruments* **2005**, *76* (10), 103904. https://doi.org/10.1063/1.2084447.

(148) Guin, T.; Krecker, M.; Milhorn, A.; Hagen, D. A.; Stevens, B.; Grunlan, J. C. Exceptional Flame Resistance and Gas Barrier with Thick Multilayer Nanobrick Wall Thin Films. *Advanced Materials Interfaces* **2015**, *2* (11), 1500214. https://doi.org/10.1002/admi.201500214.

(149) Laufer, G.; Kirkland, C.; Cain, A. A.; Grunlan, J. C. Clay–Chitosan Nanobrick Walls: Completely Renewable Gas Barrier and Flame-Retardant Nanocoatings. *ACS Applied Materials & Interfaces* **2012**, *4* (3), 1643–1649. https://doi.org/10.1021/am2017915.

(150) Bialik, E.; Stenqvist, B.; Fang, Y.; Östlund, Å.; Furó, I.; Lindman, B.; Lund, M.; Bernin, D. Ionization of Cellobiose in Aqueous Alkali and the Mechanism of Cellulose Dissolution. *The Journal of Physical Chemistry Letters* **2016**, *7* (24), 5044–5048. https://doi.org/10.1021/acs.jpclett.6b02346.

(151) Kim, J. S.; Lee, Y. Y.; Kim, T. H. A Review on Alkaline Pretreatment Technology for Bioconversion of Lignocellulosic Biomass. *Bioresource Technology* **2016**, *199*, 42–48. https://doi.org/10.1016/j.biortech.2015.08.085.

(152) Alongi, J.; Malucelli, G. Thermal Degradation of Cellulose and Cellulosic Substrates. In *Reactions and Mechanisms in Thermal Analysis of Advanced Materials*; Tiwari, A., Raj, B., Eds.; John Wiley & Sons, Inc.: Hoboken, NJ, USA, 2015; pp 301–332. https://doi.org/10.1002/9781119117711.ch14.

(153) Ferry, L.; Dorez, G.; Taguet, A.; Otazaghine, B.; Lopez-Cuesta, J. M. Chemical Modification of Lignin by Phosphorus Molecules to Improve the Fire Behavior of Polybutylene Succinate. *Polymer Degradation and Stability* **2015**, *113*, 135–143. https://doi.org/10.1016/j.polymdegradstab.2014.12.015.

(154) Kim, Y. S.; Li, Y.-C.; Pitts, W. M.; Werrel, M.; Davis, R. D. Rapid Growing Clay Coatings to Reduce the Fire Threat of Furniture. *ACS Applied Materials & Interfaces* **2014**, *6* (3), 2146–2152. https://doi.org/10.1021/am405259n.

(155) Huggett, C. Estimation of Rate of Heat Release by Means of Oxygen Consumption Measurements. *Fire and Materials* **1980**, *4* (2), 61–65. https://doi.org/10.1002/fam.810040202.

(156) Babrauskas, V. Development of the Cone Calorimeter - A Bench-Scale Heat Release Rate Apparatus Based on Oxygen Consumption. *Fire and Materials* **1984**, *8* (2), 81–95. https://doi.org/10.1002/fam.810080206.

(157) Wang, L.; He, X.; Wilkie, C. A. The Utility of Nanocomposites in Fire Retardancy. *Materials* **2010**, *3* (9), 4580–4606. https://doi.org/10.3390/ma3094580.

(158) Laufer, G.; Kirkland, C.; Morgan, A. B.; Grunlan, J. C. Intumescent Multilayer Nanocoating, Made with Renewable Polyelectrolytes, for Flame-Retardant Cotton. *Biomacromolecules* **2012**, *13* (9), 2843–2848. https://doi.org/10.1021/bm300873b.

(159) Smith, R. J.; Holder, K. M.; Ruiz, S.; Hahn, W.; Song, Y.; Lvov, Y. M.; Grunlan, J. C. Environmentally Benign Halloysite Nanotube Multilayer Assembly Significantly Reduces Polyurethane Flammability. *Advanced Functional Materials* **2018**, *28* (27), 1703289. https://doi.org/10.1002/adfm.201703289.

(160) Grexa, O.; Lübke, H. Flammability Parameters of Wood Tested on a Cone Calorimeter. *Polymer Degradation and Stability* **2001**, *74* (3), 427–432. https://doi.org/10.1016/S0141-3910(01)00181-1.

(161) Hagen, M.; Hereid, J.; Delichatsios, M. A.; Zhang, J.; Bakirtzis, D. Flammability Assessment of Fire-Retarded Nordic Spruce Wood Using Thermogravimetric Analyses and Cone Calorimetry. *Fire Safety Journal* **2009**, *44* (8), 1053–1066. https://doi.org/10.1016/j.firesaf.2009.07.004.

(162) Östman, B.; Boström, L. Fire Protection Ability of Wood Coverings. *Fire Technology* **2015**, *51* (6), 1475–1493. https://doi.org/10.1007/s10694-014-0452-z.

(163) Andersson, S.; Serimaa, R.; Paakkari, T.; Saranpää, P.; Pesonen, E. Crystallinity of Wood and the Size of Cellulose Crystallites in Norway Spruce (Picea Abies). *Journal of Wood Science* **2003**, *49* (6), 531–537. https://doi.org/10.1007/s10086-003-0518-x.

(164) National Fire Protection Agency. *An Overview of the U.S. Fire Problem*; Fact Sheet; 2017.

(165) Ikonomou, M. G.; Rayne, S.; Addison, R. F. Exponential Increases of the Brominated Flame Retardants, Polybrominated Diphenyl Ethers, in the Canadian Arctic from 1981 to 2000. *Environmental Science & Technology* **2002**, *36* (9), 1886–1892. https://doi.org/10.1021/es011401x.

(166) Lyche, J. L.; Rosseland, C.; Berge, G.; Polder, A. Human Health Risk Associated with Brominated Flame-Retardants (BFRs). *Environment International* **2015**, *74*, 170–180. https://doi.org/10.1016/j.envint.2014.09.006.

(167) Garba, B. Effect of Zinc Borate as Flame Retardant Formulation on Some Tropical Woods. *Polymer Degradation and Stability* **1999**, *64*, 6.

(168) Gu, J.; Zhang, G.; Dong, S.; Zhang, Q.; Kong, J. Study on Preparation and Fire-Retardant Mechanism Analysis of Intumescent Flame-Retardant Coatings. *Surface and Coatings Technology* **2007**, *201* (18), 7835–7841. https://doi.org/10.1016/j.surfcoat.2007.03.020.

(169) Zhang, H.; Zhang, W.; Jin, C.; Li, S. Inorganic Antiflaming Wood Caused by a Ti O 2 -Decorated ZnO Nanorod Arrays Coating Prepared by a Facile Hydrothermal Method. *Journal of Nanomaterials* **2016**, *2016*, 1–9. https://doi.org/10.1155/2016/2358276.

(170) Zhang, T.; Yan, H.; Wang, L.; Fang, Z. Controlled Formation of Self-Extinguishing Intumescent Coating on Ramie Fabric via Layer-by-Layer Assembly. *Industrial & Engineering Chemistry Research* **2013**, *52* (18), 6138–6146. https://doi.org/10.1021/ie3031554.

(171) Apaydin, K.; Laachachi, A.; Ball, V.; Jimenez, M.; Bourbigot, S.; Toniazzo, V.; Ruch, D. Intumescent Coating of (Polyallylamine-Polyphosphates) Deposited on Polyamide Fabrics via Layer-by-Layer Technique. *Polymer Degradation and Stability* **2014**, *106*, 158–164. https://doi.org/10.1016/j.polymdegradstab.2014.01.006.

(172) Leistner, M.; Abu-Odeh, A. A.; Rohmer, S. C.; Grunlan, J. C. Water-Based Chitosan/Melamine Polyphosphate Multilayer Nanocoating That Extinguishes Fire on Polyester-Cotton Fabric. *Carbohydrate Polymers* **2015**, *130*, 227–232. https://doi.org/10.1016/j.carbpol.2015.05.005.

(173) Narkhede, M.; Thota, S.; Mosurkal, R.; Muller, W. S.; Kumar, J. Layer-by-Layer Assembly of Halogen-Free Polymeric Materials on Nylon/Cotton Blend for Flame Retardant Applications: Layer-by-Layer Assembly of Halogen-Free Polymeric Materials. *Fire and Materials* **2016**, *40* (2), 206–218. https://doi.org/10.1002/fam.2280.

(174) Shamoun, R. F.; Reisch, A.; Schlenoff, J. B. Extruded Saloplastic Polyelectrolyte Complexes. *Advanced Functional Materials* **2012**, *22* (9), 1923–1931. https://doi.org/10.1002/adfm.201102787.

(175) Fu, J.; Fares, H. M.; Schlenoff, J. B. Ion-Pairing Strength in Polyelectrolyte Complexes. *Macromolecules* **2017**, *50* (3), 1066–1074. https://doi.org/10.1021/acs.macromol.6b02445.

(176) Smith, R. J.; Long, C. T.; Grunlan, J. C. Transparent Polyelectrolyte Complex Thin Films with Ultralow Oxygen Transmission Rate. *Langmuir* **2018**, *34* (37), 11086–11091. https://doi.org/10.1021/acs.langmuir.8b02391.

(177) Cain, A. A.; Murray, S.; Holder, K. M.; Nolen, C. R.; Grunlan, J. C. Intumescent Nanocoating Extinguishes Flame on Fabric Using Aqueous Polyelectrolyte Complex Deposited in Single Step: Intumescent Nanocoating Extinguishes Flame on Fabric. *Macromolecular Materials and Engineering* **2014**, *299* (10), 1180–1187. https://doi.org/10.1002/mame.201400022.

(178) Jimenez, M.; Guin, T.; Bellayer, S.; Dupretz, R.; Bourbigot, S.; Grunlan, J. C. Microintumescent Mechanism of Flame-Retardant Water-Based Chitosan-Ammonium Polyphosphate Multilayer Nanocoating on Cotton Fabric. *Journal of Applied Polymer Science* **2016**, *133* (32), 43783. https://doi.org/10.1002/app.43783.

(179) Spearpoint, M. J.; Quintiere, J. G. Predicting the Burning of Wood Using an Integral Model. *Combustion and Flame* **2000**, *123* (3), 308–325. https://doi.org/10.1016/S0010-2180(00)00162-0.

(180) Spearpoint, M. J.; Quintiere, J. G. Predicting the Piloted Ignition of Wood in the Cone Calorimeter Using an Integral Model - Effect of Species, Grain Orientation and Heat Flux. *Fire Safety Journal* **2001**, *36*, 391–415.

(181) Nolte, A. J.; Rubner, M. F.; Cohen, R. E. Determining the Young's Modulus of Polyelectrolyte Multilayer Films via Stress-Induced Mechanical Buckling Instabilities. *Macromolecules* **2005**, *38* (13), 5367–5370. https://doi.org/10.1021/ma0507950.

(182) Feng, X.; Pelton, R.; Leduc, M. Mechanical Properties of Polyelectrolyte Complex Films Based on Polyvinylamine and Carboxymethyl Cellulose. *Industrial & Engineering Chemistry Research* **2006**, *45* (20), 6665–6671. https://doi.org/10.1021/ie060511f.

(183) Jaber, J. A.; Schlenoff, J. B. Mechanical Properties of Reversibly Cross-Linked Ultrathin Polyelectrolyte Complexes. *Journal of the American Chemical Society* **2006**, *128* (9), 2940–2947. https://doi.org/10.1021/ja055892n.

(184) Pascual, A.; Toma, M.; Tsotra, P.; Grob, M. C. On the Stability of PEEK for Short Processing Cycles at High Temperatures and Oxygen-Containing Atmosphere. *Polymer Degradation and Stability* **2019**, *165*, 161–169. https://doi.org/10.1016/j.polymdegradstab.2019.04.025.

(185) Geoffroy, L.; Samyn, F.; Jimenez, M.; Bourbigot, S. Additive Manufacturing of Fire-retardant Ethylene-vinyl Acetate. *Polymers for Advanced Technologies* **2019**, 1–13. https://doi.org/10.1002/pat.4620.

(186) Guo, Y.; Chang, C.-C.; Halada, G.; Cuiffo, M. A.; Xue, Y.; Zuo, X.; Pack, S.; Zhang, L.; He, S.; Weil, E.; Rafailovich, M. H. Engineering Flame Retardant Biodegradable Polymer Nanocomposites and Their Application in 3D Printing. *Polymer Degradation and Stability* **2017**, *137*, 205–215. https://doi.org/10.1016/j.polymdegradstab.2017.01.019.

(187) Regazzi, A.; Pucci, M. F.; Dumazert, L.; Gallard, B.; Buonomo, S.; Ravel, R.; Lopez-Cuesta, J.-M. Controlling the Distribution of Fire Retardants in Poly(Lactic Acid) by Fused Filament Fabrication in Order to Improve Its Fire Behaviour. *Polymer Degradation and Stability* **2019**, *163*, 143–150. https://doi.org/10.1016/j.polymdegradstab.2019.03.008.

(188) Schaaf, P.; Schlenoff, J. B. Saloplastics: Processing Compact Polyelectrolyte Complexes. *Advanced Materials* **2015**, *27* (15), 2420–2432. https://doi.org/10.1002/adma.201500176.

(189) Zhu, F.; Cheng, L.; Yin, J.; Wu, Z. L.; Qian, J.; Fu, J.; Zheng, Q. 3D Printing of Ultratough Polyion Complex Hydrogels. *ACS Applied Materials & Interfaces* **2016**, *8* (45), 31304–31310. https://doi.org/10.1021/acsami.6b09881.

(190) Ng, W. L.; Yeong, W. Y.; Naing, M. W. Development of Polyelectrolyte Chitosan-Gelatin Hydrogels for Skin Bioprinting. *Procedia CIRP* **2016**, *49*, 105–112. https://doi.org/10.1016/j.procir.2015.09.002.

(191) de Silva, U. K.; Choudhuri, K.; Bryant-Friedrich, A. C.; Lapitsky, Y. Customizing Polyelectrolyte Complex Shapes through Photolithographic Directed Assembly. *Soft Matter* **2018**, *14* (4), 521–532. https://doi.org/10.1039/C7SM02022H.

(192) Zhang, T.; Yan, H.; Shen, L.; Fang, Z.; Zhang, X.; Wang, J.; Zhang, B. Chitosan/Phytic Acid Polyelectrolyte Complex: A Green and Renewable Intumescent Flame Retardant

System for Ethylene–Vinyl Acetate Copolymer. *Industrial & Engineering Chemistry Research* **2014**, *53* (49), 19199–19207. https://doi.org/10.1021/ie503421f.

(193) Maechling, C.; Ball, V. Exothermic–Endothermic Transition in the Titration of Poly(Allylamine Chloride) with Sodium Hexametaphoshate Associated with a Change in the Proton Release Regime. *The Journal of Physical Chemistry B* **2016**, *120* (20), 4732–4741. https://doi.org/10.1021/acs.jpcb.6b02709.

(194) Garlotta, D. A Literature Review of Poly(Lactic Acid). *Journal of Polymers and the Environment* **2001**, *9* (2), 63–84.

(195) Liao, F.; Ju, Y.; Dai, X.; Cao, Y.; Li, J.; Wang, X. A Novel Efficient Polymeric Flame Retardant for Poly (Lactic Acid) (PLA): Synthesis and Its Effects on Flame Retardancy and Crystallization of PLA. *Polymer Degradation and Stability* **2015**, *120*, 251–261. https://doi.org/10.1016/j.polymdegradstab.2015.07.012.

(196) Wang, L.; Jing, X.; Cheng, H.; Hu, X.; Yang, L.; Huang, Y. Rheology and Crystallization of Long-Chain Branched Poly(L-Lactide)s with Controlled Branch Length. *Industrial & Engineering Chemistry Research* **2012**, *51* (33), 10731–10741. https://doi.org/10.1021/ie300524j.

(197) Joseph, P.; Tretsiakova-McNally, S. Melt-Flow Behaviours of Thermoplastic Materials under Fire Conditions: Recent Experimental Studies and Some Theoretical Approaches. *Materials* **2015**, *8* (12), 8793–8803. https://doi.org/10.3390/ma8125492.

(198) Shieh, Y.-T.; Lin, Y.-S.; Twu, Y.-K.; Tsai, H.-B.; Lin, R.-H. Effect of Crystallinity on Enthalpy Recovery Peaks and Cold-Crystallization Peaks in PET via TMDSC and DMA Studies. *Journal of Applied Polymer Science* **2009**, NA-NA. https://doi.org/10.1002/app.31570.

(199) Naffakh, M.; Marco, C.; Ellis, G. Development of Novel Melt-Processable Biopolymer Nanocomposites Based on Poly(l-Lactic Acid) and WS2 Inorganic Nanotubes. *CrystEngComm* **2014**, *16* (23), 5062. https://doi.org/10.1039/c3ce42593b.

(200) Lv, Z.; Hu, Y.-T.; Guan, J.-P.; Tang, R.-C.; Chen, G.-Q. Preparation of a Flame Retardant, Antibacterial, and Colored Silk Fabric with Chitosan and Vitamin B2 Sodium Phosphate by Electrostatic Layer by Layer Assembly. *Materials Letters* **2019**, *241*, 136–139. https://doi.org/10.1016/j.matlet.2019.01.005.

(201) Lyon, R. E.; Walters, R. N. Pyrolysis Combustion Flow Calorimetry. *Journal of Analytical and Applied Pyrolysis* **2004**, *71* (1), 27–46. https://doi.org/10.1016/S0165-2370(03)00096-2.

(202) Chiang, H.; Kolibaba, T. J.; Eberle, B.; Grunlan, J. C. Super Gas Barrier of a Polyelectrolyte/Clay Coacervate Thin Film. *Macromol. Rapid Commun.* **2020**, 2000540. https://doi.org/10.1002/marc.202000540.

(203) Durmaz, E. N.; Baig, M. I.; Willott, J. D.; de Vos, W. M. Polyelectrolyte Complex Membranes via Salinity Change Induced Aqueous Phase Separation. *ACS Appl. Polym. Mater.* **2020**, acsapm.0c00255. https://doi.org/10.1021/acsapm.0c00255.

(204) Penchev, H.; Paneva, D.; Manolova, N.; Rashkov, I. Novel Electrospun Nanofibers Composed of Polyelectrolyte Complexes. *Macromol. Rapid Commun.* **2008**, *29* (8), 677–681. https://doi.org/10.1002/marc.200700844.

(205) Sun, J.; Perry, S. L.; Schiffman, J. D. Electrospinning Nanofibers from Chitosan/Hyaluronic Acid Complex Coacervates. *Biomacromolecules* **2019**, *20* (11), 4191–4198. https://doi.org/10.1021/acs.biomac.9b01072.

(206) de Jager, H.-J.; Heyns, A. M. Kinetics of Acid-Catalyzed Hydrolysis of a Polyphosphate in Water. *The Journal of Physical Chemistry A* **1998**, *102* (17), 2838–2841. https://doi.org/10.1021/jp9730252.

(207) Martin, C. J. Recent Progress in Development of Photoacid Generators. **2018**, 11.

(208) Havard, J. M.; Shim, S.-Y.; Frechet, J. M. J.; Lin, Q.; Medeiros, D. R.; Willson, C. G.; Byers, J. D. Design of Photoresists with Reduced Environmental Impact. 1. Water-Soluble Resists Based on Photo-Cross-Linking of Poly(Vinyl Alcohol). *Chemistry of Materials* **1999**, *11*, 719–725.

(209) Hartings, M. R.; Ahmed, Z. Chemistry from 3D Printed Objects. *Nature Reviews Chemistry* **2019**, *3*, 305–314. https://doi.org/10.1038/s41570-019-0097-z.

(210) Appuhamillage, G. A.; Chartrain, N.; Meenakshisundaram, V.; Feller, K. D.; Williams, C. B.; Long, T. E. 110th Anniversary : Vat Photopolymerization-Based Additive Manufacturing: Current Trends and Future Directions in Materials Design. *Industrial & Engineering Chemistry Research* **2019**, *55* (33), 15109–15118. https://doi.org/10.1021/acs.iecr.9b02679.

(211) Schwartz, J. J.; Boydston, A. J. Multimaterial Actinic Spatial Control 3D and 4D Printing. *Nature Communications* **2019**, *10*, 791. https://doi.org/10.1038/s41467-019-08639-7.

(212) Ober, C. K.; Wegner, G. Polyelectrolyte-Surfactant Complexes in the Solid State: Facile Building Blocks for Self-Organizing Materials. *Adv. Mater.* **1997**, *9* (1), 17–31. https://doi.org/10.1002/adma.19970090104.

(213) Kocak, G.; Tuncer, C.; Bütün, V. PH-Responsive Polymers. *Polym. Chem.* **2017**, *8* (1), 144–176. https://doi.org/10.1039/C6PY01872F.

(214) Shaikh, S. M. R.; Nasser, M. S.; Hussein, I.; Benamor, A.; Onaizi, S. A.; Qiblawey, H. Influence of Polyelectrolytes and Other Polymer Complexes on the Flocculation and Rheological Behaviors of Clay Minerals: A Comprehensive Review. *Separation and Purification Technology* **2017**, *187*, 137–161. https://doi.org/10.1016/j.seppur.2017.06.050.

(215) Wang, N.; Ji, S.; Zhang, G.; Li, J.; Wang, L. Self-Assembly of Graphene Oxide and Polyelectrolyte Complex Nanohybrid Membranes for Nanofiltration and Pervaporation. *Chemical Engineering Journal* **2012**, *213*, 318–329. https://doi.org/10.1016/j.cej.2012.09.080.

(216) Meka, V. S.; Sing, M. K. G.; Pichika, M. R.; Nali, S. R.; Kolapalli, V. R. M.; Kesharwani, P. A Comprehensive Review on Polyelectrolyte Complexes. *Drug Discovery Today* **2017**, *22* (11), 1697–1706. https://doi.org/10.1016/j.drudis.2017.06.008.

(217) Buriuli, M.; Verma, D. Polyelectrolyte Complexes (PECs) for Biomedical Applications. In *Advances in Biomaterials for Biomedical Applications*; Tripathi, A., Melo, J. S., Eds.; Springer Singapore: Singapore, 2017; Vol. 66, pp 45–93. https://doi.org/10.1007/978-981-10-3328-5_2.

(218) Luo, Y.; Wang, Q. Recent Development of Chitosan-Based Polyelectrolyte Complexes with Natural Polysaccharides for Drug Delivery. *International Journal of Biological Macromolecules* **2014**, *64*, 353–367. https://doi.org/10.1016/j.ijbiomac.2013.12.017.

(219) Priolo, M. A.; Holder, K. M.; Guin, T.; Grunlan, J. C. Recent Advances in Gas Barrier Thin Films via Layer-by-Layer Assembly of Polymers and Platelets. *Macromol. Rapid Commun.* **2015**, *36* (10), 866–879. https://doi.org/10.1002/marc.201500055.

(220) Richardson, J. J.; Cui, J.; Björnmalm, M.; Braunger, J. A.; Ejima, H.; Caruso, F. Innovation in Layer-by-Layer Assembly. *Chemical Reviews* **2016**, *116* (23), 14828–14867. https://doi.org/10.1021/acs.chemrev.6b00627.

(221) Wilts, E. M.; Pekkanen, A. M.; White, B. T.; Meenakshisundaram, V.; Aduba, D. C.; Williams, C. B.; Long, T. E. Vat Photopolymerization of Charged Monomers: 3D Printing with Supramolecular Interactions. *Polymer Chemistry* **2019**, *10* (12), 1442–1451. https://doi.org/10.1039/C8PY01792A.

(222) Bagheri, A.; Jin, J. Photopolymerization in 3D Printing. *ACS Applied Polymer Materials* **2019**, *1* (4), 593–611. https://doi.org/10.1021/acsapm.8b00165.

(223) Delgado, J. D.; Schlenoff, J. B. Static and Dynamic Solution Behavior of a Polyzwitterion Using a Hofmeister Salt Series. *Macromolecules* **2017**, *50* (11), 4454–4464. https://doi.org/10.1021/acs.macromol.7b00525.

(224) Culebras, M.; Cho, C.; Krecker, M.; Smith, R.; Song, Y.; Gómez, C. M.; Cantarero, A.; Grunlan, J. C. High Thermoelectric Power Factor Organic Thin Films through Combination of Nanotube Multilayer Assembly and Electrochemical Polymerization. *ACS Applied Materials & Interfaces* **2017**, *9* (7), 6306–6313. https://doi.org/10.1021/acsami.6b15327.

(225) Stevens, D. L.; Parra, A.; Grunlan, J. C. Thermoelectric Performance Improvement of Polymer Nanocomposites by Selective Thermal Degradation. *ACS Appl. Energy Mater.* **2019**, *2* (8), 5975–5982. https://doi.org/10.1021/acsaem.9b01079.

(226) Bédard, M. F.; Sadasivan, S.; Sukhorukov, G. B.; Skirtach, A. Assembling Polyelectrolytes and Porphyrins into Hollow Capsules with Laser-Responsive Oxidative Properties. *Journal of Materials Chemistry* **2009**, *19* (15), 2226. https://doi.org/10.1039/b818774f.

(227) Occhetta, P.; Visone, R.; Russo, L.; Cipolla, L.; Moretti, M.; Rasponi, M. VA-086 Methacrylate Gelatine Photopolymerizable Hydrogels: A Parametric Study for Highly Biocompatible 3D Cell Embedding: VA-086 GelMA Photopolymerizable Hydrogels. *Journal of Biomedical Materials Research Part A* **2015**, *103* (6), 2109–2117. https://doi.org/10.1002/jbm.a.35346.

(228) Chollakup, R.; Beck, J. B.; Dirnberger, K.; Tirrell, M.; Eisenbach, C. D. Polyelectrolyte Molecular Weight and Salt Effects on the Phase Behavior and Coacervation of Aqueous Solutions of Poly(Acrylic Acid) Sodium Salt and Poly(Allylamine) Hydrochloride. *Macromolecules* **2013**, *46* (6), 2376–2390. https://doi.org/10.1021/ma202172q.

(229) Ligon, S. C.; Husár, B.; Wutzel, H.; Holman, R.; Liska, R. Strategies to Reduce Oxygen Inhibition in Photoinduced Polymerization. *Chemical Reviews* **2014**, *114* (1), 557–589. https://doi.org/10.1021/cr3005197.

(230) Camino, G.; Costa, L.; Martinasso, G. Intumescent Fire-Retardant Systems. *Polymer Degradation and Stability* **1989**, *23* (4), 359–376. https://doi.org/10.1016/0141-3910(89)90058-X.

APPENDIX

UV-PROTECTION FROM CHITOSAN DERIVITIZED LIGNIN MULTILAYER THIN FILM*

A.1 Introduction

In an effort to gain greater independence from fossil fuels, researchers have found wood, and more specifically lignin, to have tremendous potential in both nanotechnology and as a potential chemical feedstock.[1–3] Lignin has a high natural abundance in wood, accounting for as much as 25% of some species' total mass.[4] Furthermore, as lignin is inedible, its use as a chemical feedstock does not compete with food production. Despite its potential, the functional use of lignin is inhibited by its hydrophobicity and difficulty to process both chemically and physically.[5] Lignin is an amorphous, crosslinked network of both carbon-carbon and ether linkages produced from the polymerization of three different lignol monomers.[6] Due to the randomness of lignin's polymerization (and variation in the ratios of its constituent monomers among wood species), it has a complex, yet indefinite, three-dimensional structure that is responsible for much of the strength of plant cell walls.[7] Despite the difficulty of processing lignin, a great number of uses for functionalized lignin have been developed in recent years. These applications include flame retardants,[8–10] cellular imaging aids,[11] supercapacitors,[12] environmental remediation,[13] and UV protection.[14,15]

In recent years, layer-by-layer (LbL) assembly has risen to prominence as a way of depositing functional coatings on almost any substrate.[16,17] These coatings impart highly effective

*Reprinted with permission from Kolibaba, T.J.; Stevens, D.L.; Pangburn, S.T.; Condassamy, O.; Camus, M.; Grau, E.; Grunlan, J.C., UV-protection from chitosan derivatized lignin multilayer thin film. *RSC Advances* **2020**, *10*, 32959-32965.

functionality from a coating that is often just a few hundred nanometers thick. Many of these functional coatings have incorporated biomaterials and/or renewable materials for many industrially important end-uses.[18–22] Despite its relatively high abundance of somewhat acidic protons (and therefore theoretical ease in utilizing it as an anionic ingredient in LbL films), lignin is very challenging to dissolve in an appreciable amount in water without utilizing extremely high pH.[23] This restriction allows only strong polycations, such as quaternized amines, to be used. Many polycations are weak (i.e. pH-sensitive) polyamines that will be uncharged at the high pH required to use unmodified lignin in LbL. This is why most of lignin's use in multilayer assemblies are currently very scarce, primarily using poly(diallyldimethylammonium chloride) as the polycation.[24–26] One notable exception is the work by Su and coworkers to developed a cationic quaternized lignin that forms films when grown with a polycarboxylic acid.

In the present study, lignin was chemically modified through alkaline oxidation under pressure to yield hydrosoluble lignin. This modified lignin is shown to grow layer-by-layer with biologically-sourced, cationic chitosan (CH) to yield films that have high UV absorbance. The LbL growth is hypothesized to be due to a combination of both hydrogen bonding and ionic interactions between CH and the hydrosoluble lignin. These highly absorbing films were deposited onto spin coated poly(3,4-ethylenedioxythiophene):poly(styrene sulfonate) (PEDOT:PSS) films to demonstrate their potential to protect photovoltaic materials. A 20 bilayer (BL) CH/Lignin film reduces the degradation rate of a PEDOT:PSS film by a factor of 6 over the course of 1 hour of high intensity ultraviolet light exposure.

A.2 Experimental

A.2.1 Materials and Substrates

Hydrochloric acid (ACS reagent, 37%), sodium hydroxide (ACS reagent, ≥97.0%), ammonium bisulfate (98%), methanol (ACS reagent, ≥99.5%), chloroform, 2-chloro-4,4,5,5-tetramethyl-1,3,2-dioxaphospholane (TMDP, 95%), *endo*-*N*-hydroxy-5-norbornene-2,3-dicarboxylic acid imide (97%), chromium(III) acetylacetonate, pyridine, *N*,*N*-dimethylformamide (DMF), polyethylenimine (PEI, M_n 10,000 g/mol and M_w 25,000 g/mol) and poly(diallyldimethylammonium chloride) (PDDA, M_w 400,000-500,000 g/mol, 20 wt% in water) were purchased from Sigma-Aldrich (St. Louis, MO, USA). Chitosan (CH, Item FGC-1, 95% deacetylated, 50-60 cP) was purchased from the GTC Bio Corporation (Qingdao, Shandong Province, China). Deuterated chloroform ($CDCl_3$) was purchased from Eurisotop (Saclay, France). Technical lignin was isolated from Pinus pinaster through an ammonium bisulfate cooking process, followed by an alkaline extraction to remove residual lignin from the crude pulp. The lignin used in this study was extracted from the resultant effluent by adjusting its pH to 1 with HCl. A solution of poly(3,4-ethylenedioxythiophene):polystyrene sulfonate (PEDOT:PSS, Clevios PH1000) was purchased from Heraeus Precious Metals (Hanau, Germany). All aqueous solutions were prepared in 18 MΩ deionized (DI) water. Samples for ellipsometry were prepared on single side polished (100) silicon wafers from University Wafer (South Boston, MA, USA). Samples for UV/Vis spectroscopy were prepared on quartz slides (Chemglass, Vineland, NJ, USA). Samples for UV degradation studies were deposited on 2.5 x 2.5 x 0.1 cm glass slides (Vistavision^{TM}, VWR International, Radnor, PA, USA). All substrates were rinsed sequentially with DI water, methanol, and DI water, and were then dried with a stream of filtered air. Cleaned

substrates were then exposed to an air plasma for 5 minutes in a 32G plasma cleaner (Harrick Plasma Inc. Ithaca, NY, USA).

A.2.2 Modification of Lignin

Lignin modification was performed according to previously published work.[22,23] Lignin (2 g) was dissolved in 50 mL of NaOH (0.615 M) and stirred in an autoclave at 120 °C under 10 bar of O_2 for 1 hour. After cooling and relieving pressure, the obtained solution was adjusted to pH 2 with 1 M HCl. During this process some material precipitated out of solution, and is referred to as precipitated lignin. The acidified solution was then extracted with chloroform to remove organosoluble lignin. Finally, the lignin solution was dried and washed with methanol to remove residual NaCl to yield the hydrosoluble lignin. This process yielded 58 wt% hydrosoluble lignin (the lignin utilized and referred to throughout the main text of this study) and 42 wt% precipitated lignin, with no appreciable amount of organosoluble material obtained. Lignin molar mass and dispersity were characterized by size-exclusion chromatography in a Tosoh GPC (Tosoh Bioscience GmbH, Griesheim, Germany) with three TSK columns (G3000, G4000, G3000PW) monitored by a 280 nm UV detector. Samples were referenced to a poly(styrene sulfonate) calibration curve. The sample and calibration standards were run in a pH 12 sodium hydroxide solution eluent at 1 mL/min.

The degree of functionality of the lignin was determined with a quantitative ^{31}P NMR technique that phosphorylates hydroxyl groups and references them to a phosphorylated hydroxyl-containing internal standard.[27,28] Due to the water sensitivity of this technique, all solvents were dried on 3 Å molecular sieves and all glassware was dried overnight in a 110 °C oven. A dried lignin sample (~40 mg) was dissolved in 500 μL of anhydrous pyridine/$CDCl_3$ (1.6:1 v/v) mixture,

along with an internal standard (*endo*-*N*-hydroxy-5-norbornene-2,3-dicarboximide, 2-10 mg) and chromium(III) acetylacetonate (1 mg). To ensure lignin solubility, 500 μL of DMF was added to the mixture. Next, 250 μL of the phosphorylating agent TMDP was added and the mixture was agitated for 1 hour. Finally, 400 μL of this mixture, along with 200 μL of $CDCl_3$ were transferred to an NMR tube for analysis. The ^{31}P NMR study was performed at room temperature in an AVANCE I NMR (Bruker, Billerica, MA, USA) equipped with a 5 mm direct probe (operating at 162.0 MHz). Data acquisition was made with the "reverse gate" zgOig program from the Bruker Topspin database. The spectral window was optimized at 10,000 Hz with an acquisition time of 1.6 s and a D1 delay of 5 s. The distribution of hydroxyl groups in the lignin was identified by integrating the following areas: aliphatic hydroxyl (150.0-145.5 ppm), condensed units (144.7-140 ppm), guaiacyl units (140.2-138.6 ppm), p-hydroxyphenyl units (138.4-136.4 ppm), and carboxylic acids (136-134 ppm).

A.2.3 Layer-by-Layer Deposition

Solutions of 0.1 wt% PEI and 0.1 wt% PDDA were prepared in DI water and rolled to homogeneity in polyethylene bottles. PDDA was adjusted to pH 4 with 1 M HCl. A solution of 0.1 wt% CH was prepared in pH 1.7 water and stirred overnight, after which it was adjusted to pH 4 with 1 M NaOH. A solution of 0.1 wt% hydrosoluble lignin (henceforth referred to simply as lignin) was prepared in DI water and rolled overnight, bath sonicated for 1 hour in a 5510 ultrasonic cleaning bath (Branson Ultrasonics Corporation, Danbury, CT, USA), and finally rolled one more night to ensure homogeneity. The lignin solution was adjusted to pH 2 with 1 M HCl. All multilayer films were grown via layer-by-layer (LbL) assembly with a homebuilt robotic dipping system.[29] After plasma treatment, substrates were first dipped in the PEI solution for 5 minutes,

followed by rinsing with DI water and drying with filtered air. The first bilayer (BL) was completed with a 5-minute immersion in the lignin solution, followed by rinsing and drying. After this first bilayer, all immersion times were 1 minute, and the PEI solution was replaced by either CH for CH/Lignin films, or by PDDA for PDDA/Lignin films. LbL films deposited on PEDOT:PSS films were done without additional plasma treatment of the substrate.

A.2.4 PEDOT:PSS Film Preparation

PEDOT:PSS films were prepared via a previously published spin coating method.[30] A cleaned, dried and plasma treated glass slide was spin coated (KW-4A Spin-Coater, Chemat Technology, Northridge, CA, USA) with 300 μL of PEDOT:PSS at 500 rpm for 5 seconds then accelerated to 3000 rpm for 15 seconds. The coated films were annealed in a 120 °C oven for 15 minutes. After annealing, 150 μL of methanol was deposited directly onto the substrate in the oven and allowed to further anneal for 10 minutes. The film was then removed from the oven and exposed to another 150 μL of methanol and spun on the spin coater again using the same parameters. The substrate was then annealed in the 120 °C oven for 10 minutes. After coating, the substrate was put in a UV resistant container to avoid exposure to ambient light. The coating was measured by ellipsometry to be ~80 nm thick.

A.2.5 Characterization

Thickness of films on silicon wafers was measured by ellipsometry (Alpha-SE Ellipsometer, J.A. Woollam Co., Inc., Lincoln, NE, USA). UV/Vis absorbance of the LbL films on quartz slides was measured using a Hitachi U-4100 UV–Vis–NIR spectrometer (Tokyo, Japan). Resistance of films on glass slides was measured on a Keithley 2000 Multimeter (Cleveland, OH,

USA). PEDOT:PSS coated glass slides, with and without CH/Lignin coatings, were cut in half (ca. 1 x 2 cm^2). Contact resistance was reduced by applying silver paint (Electron Microscopy Sciences, Hatfield, PA, USA) on the end of the slide fragments (on both sides), followed by annealing in a Thermofisher TF55030A-1/ Blue M Single Segment Tube Furnace (Waltham, MA, USA) under argon at 150 °C for 15 minutes. Films were exposed to ~250 nm light by being placed immediately under a pair of GERM-3000008 germicidal UV-C light bulbs (1000Bulbs, Garland, TX, USA) attached to a Black-Ray UV Bench Lamp 78 W ballast (UVP, Lipland, CA, USA).

A.3 Results and Discussion

A.3.1 Modification of Lignin

Technical lignin (i.e. the most common form of extracted lignin) was modified under basic oxidative conditions in an autoclave at 10 bar to yield hydrosoluble lignin.[23] Following the functionalization, modified lignin was characterized by size exclusion chromatography and solubility tests. Additionally, the distribution of hydroxyl functionalities (i.e. fraction of aliphatic, phenolic, and carboxylic hydroxyls groups) was determined through derivatization of these groups and analysis with ^{31}P NMR.[27,28] The properties of the technical and hydrosoluble lignin are summarized in **Table A.1**. Size exclusion chromatography revealed a considerable decrease in molar mass relative to a poly(styrene sulfonate) calibration curve. After functionalization, the hydrosoluble lignin had considerably greater solubility in water at all pH levels, while technical lignin can only dissolve above pH 12. Furthermore, this modification did not reduce the lignin's solubility in organic solvents, despite the addition of hydrophilic groups.

Table A.1. Measured properties of both technical and modified hydrosoluble lignin.

Property	*Technical Lignin*	*Hydrosoluble Lignin*
Molar mass (M_w, g/mol)	19,000	4,000
Đ	4.5	2.0
Solubility	Water (pH ≥ 12) DMF, DMSO, MeOH	Water (Any pH) DMF, DMSO, MeOH
Aliphatic –OH Groups (mmol/g)	1.41	0.75
Phenolic –OH Groups (mmol/g)	1.61	0.40
Carboxylic Acid Groups (mmol/g)	0.36	2.80

It is clear from **Table A.1** that some of the aliphatic and phenolic hydroxyl groups are oxidized into carboxylates in the hydrosoluble lignin. **Scheme A.1** shows the reaction conditions, along with hypothetical structures for both technical and hydrosoluble lignin. The improvements in solubility are likely due to the decreased molar mass (likely breaking up some of the crosslinked structure of lignin during oxidation) of the hydrosoluble lignin, which is supported by the M_w values reported in **Table A.1**. The increase in the relative proportion of carboxylic acid groups does not prevent dissolution of the modified lignin in polar organic solvents, indicating that this form of lignin could be used in solvent-based systems if needed. Further improvements in water-solubility are anticipated due to the increased prevalence of ionizable carboxylic acid groups. In an aqueous solution, these acidic groups become negatively charged, causing the hydrosoluble lignin (henceforth simply referred to as 'lignin') to behave as a polyanion. This polyanionic behavior is hypothesized to enable the growth of multilayer films containing lignin via layer-by-layer assembly.

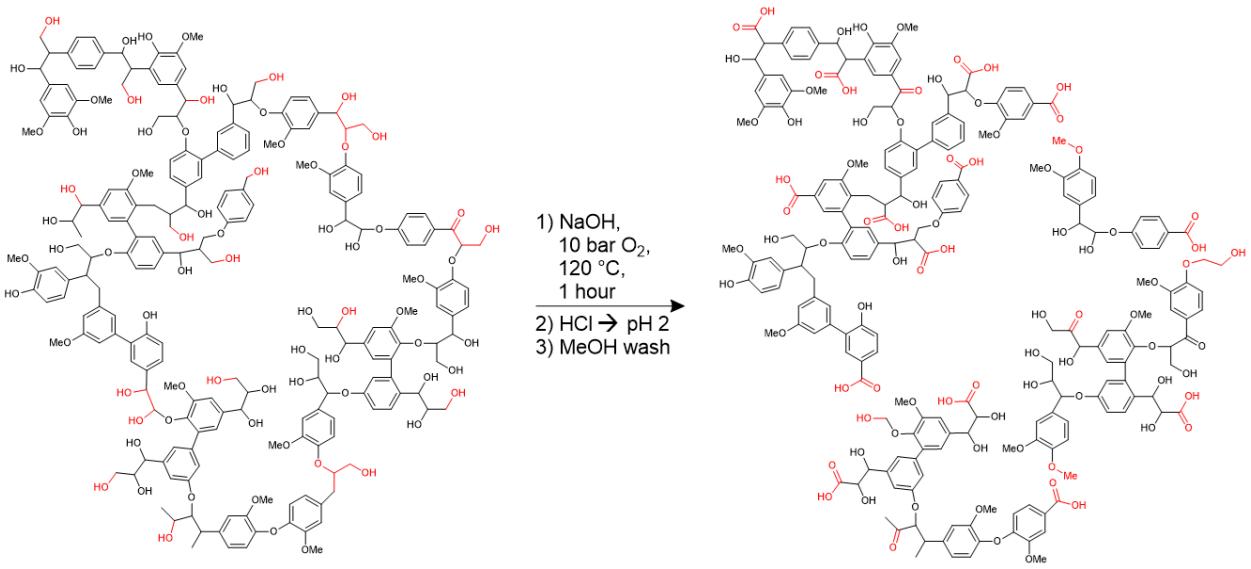

Scheme A.1. Hypothetical structure of lignin before and after modification to form hydrosoluble lignin.[7] Functional groups affected by the transformation are highlighted in red.

A.3.2 Layer-by-Layer Assembly

Lignin was paired with both chitosan (CH) and poly(diallyldimethylammonium chloride) (PDDA), two polycations used frequently in layer-by-layer assembly,[31–34] to study lignin's growth behavior. All solutions were prepared as 0.1 wt% solutions in DI water. Lignin was adjusted to pH 2 (where it would be expected to have a low charge density, as most carboxylate groups will be protonated), while the polycation solutions were both adjusted to pH 4. **Figure A.1** shows a schematic of the LbL process and the growth curves of the CH/Lignin and PDDA/Lignin films. Studying the growth curves reveals that CH/Lignin grows thicker than the analogous coating formed by pairing PDDA with lignin. Chitosan is fully charged at pH 4, so this difference in growth rate cannot be attributed to differences in the charge densities of the polycations.[35] The most likely explanation is that hydrogen bonding plays a role in film growth. Chitosan contains many hydrogen bond accepting and donating sites (i.e. hydroxyl groups), much like lignin, which can pair and cause thicker growth. Other bio-based polyphenolic compounds, such as tannic acid and

even sulfonated lignins, have demonstrated LbL growth via hydrogen bonds.[36–38] PDDA does not have either hydrogen bond donating or accepting sites, as it bears no functionality besides aliphatic carbons and quaternary ammonium groups. Since the PDDA/Lignin coating also grows layer-by-layer, it can be concluded that not all of the film deposition is a result of hydrogen bonding. Ionic bonds are a stronger form of interaction than hydrogen bonds, which suggests that CH/Lignin films may be more durable than analogous films composed of other polyphenolics.[16,39]

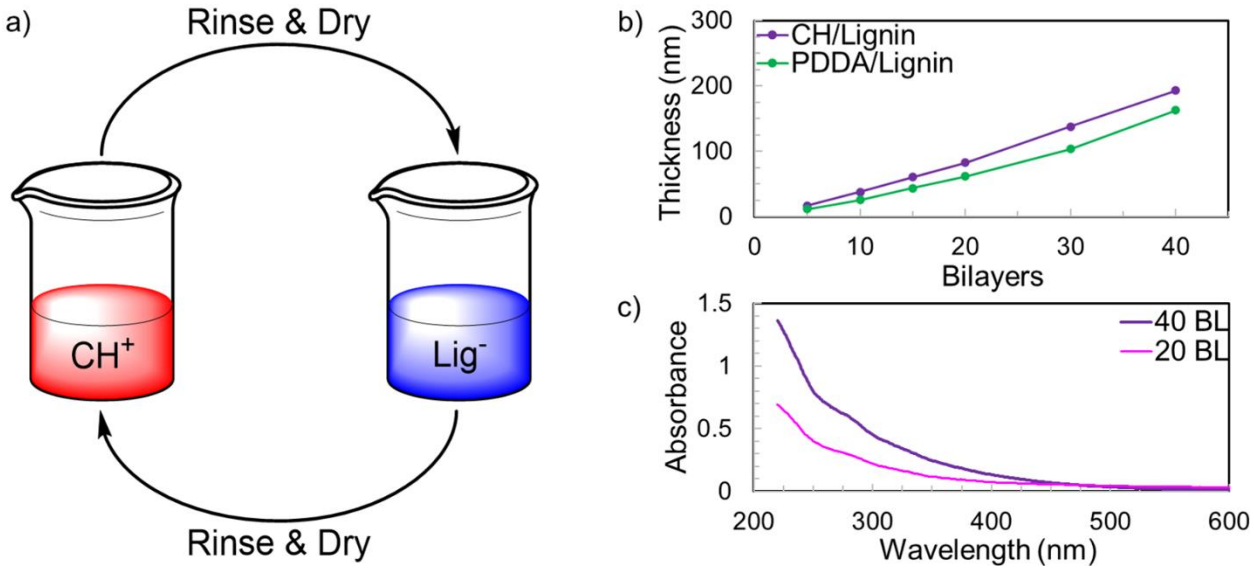

Figure A.1. (a) Schematic of the layer-by-layer process to grow CH/Lignin films. **(b)** Growth curves for Chitosan/Lignin films. **(c)** UV-Visible spectra showing absorbance of 20 and 40 BL films.

The CH/Lignin film grows linearly, depositing around 5 nm per bilayer (**Figure A.1b**). Linear growth in a LbL system typically indicates that there is little interdiffusion of adsorbed species (lignin or chitosan) during the growth process. With a low molar mass, weakly-charged polyelectrolyte like modified lignin, an exponential increase in thickness with respect to deposited bilayers would be expected.[40,41] It was reported that diffusion of ionic bonding sites that can occur through local segmental dynamics of a polyelectrolyte, play a greater role in the interdiffusion of exponentially growing polyelectrolyte systems than diffusion of the polymers themselves.[42]

Despite the relatively low molecular weight of the modified lignin, its segmental motion is limited because of its planar aromatic backbone. This limited segmental motion, which is also true for the stiff cellulosic backbone of chitosan, minimizes interdiffusion of polyelectrolytes during multilayer deposition. It was noted that changing the charge density of lignin can alter film thickness (Fig. S1), with higher pH solutions of lignin leading to thinner film growth. In all cases the growth curves remain linear, indicating little interdiffusion the of polymers regardless of growth conditions. The thinner growth is due to the increased charge density of lignin as pH rises due to deprotonation of carboxylate groups. A higher charge density requires a smaller amount of lignin to neutralize the surface charge reversal that occurs following the adsorption of chitosan onto the film during the LbL process.[16]

A.3.3 Lignin Film Properties

Deposited CH/Lignin films are transparent with a yellow hue. **Figure A.1c** shows UV-Vis absorbance curves for 20 and 40 BL films deposited on quartz slides. As would be expected for a large polyaromatic system, the films display considerable absorbance in the UV range, especially at wavelengths below 350 nm. Beyond ~350 nm, the films show very low absorbance, so they are highly visibly transparent and there is little scattering of light. The UV-Vis spectrum for the 40 BL film is approximately double the 20 BL spectrum's absorbance, which suggests a uniform film composition due to the known linear growth. This high UV absorbance, along with lignin's well documented antioxidant properties, suggest that it could have great potential as a protective coating photo-oxidatively unstable materials, like those used in photovoltaic devices.[43–47]

To demonstrate the protective capabilities of CH/Lignin nanocoatings, 10 and 20 BL were deposited coated PEDOT:PSS thin films on glass that had been methanol treated to improve

conductivity.[30] CH/Lignin was grown on top of and ~80 nm thick film of PEDOT:PSS. This system was then exposed to UV-C irradiation and the increase in the bulk resistance was used as a means of tracking the degradation of the PEDOT:PSS, as shown in the schematic in Fig. 2a.[30,48,49] All films underwent an immediate increase in resistance upon exposure to the UV light, but the unprotected PEDOT:PSS began to rapidly degrade, while the coated samples did not (**Figure A.2b**). Unprotected PEDOT:PSS resistance increases by more than 1200% with 1 hour of UV exposure, while the 10 and 20 BL films show a resistance increase of only 270% and 200%, respectively. Degradation experiments were stopped after 1 hour because the chosen wavelength leads to rapid degradation of the unprotected PEDOT:PSS films. The achieved R/R_0 values in one hour were substantially greater than previously reported degradation experiments of a similar nature.[49]

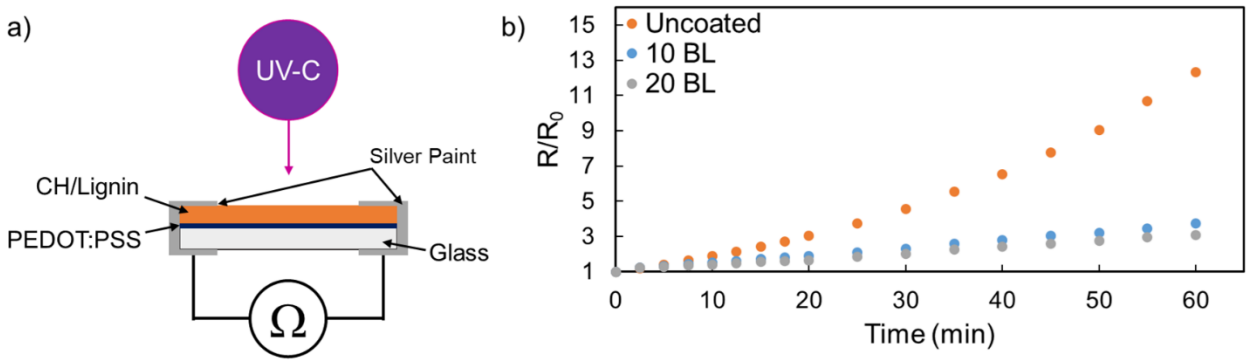

Figure A.2. (a) Schematic of the UV degradation experiment, where resistance is measured to determine film degradation rate. **(b)** Plot of normalized resistance as a function of UV exposure time for unprotected PEDOT:PSS films, as well as films coated with 10 and 20 BL of CH/Lignin.

The degradation of PEDOT:PSS is clearly trending exponentially, while the protected films appear to be degrading linearly during this exposure, indicating that protected films would likely compare even more favorably after a longer UV exposure. There are clearly diminishing returns past the initial 10 BL of CH/Lignin deposited, as the marginal improvement of the 20 BL

film is not commensurate with the increase in coating thickness or added processing steps. The combination of the change in curve shape and the minimal gain from additional coating deposition suggests that the presence of lignin is changing the decomposition mechanism of PEDOT:PSS. It is well known that the photodegradation of PEDOT and other polythiophenes proceeds through oxidation of either the sulfur or side chains which disrupts π-conjugation and ultimately reduces conductivity. Since lignin is a well-known antioxidant,[45–47] its mere presence may interrupt this process and protect underlying PEDOT. Further study would be needed to determine the true effect that the coating is having on the underlying PEDOT.

There are several other examples of lignin being used for a UV-protective purpose.[15,50,51] None of the techniques used in these studies duplicate the system described here and the present thin films achieve these results at ~80 (20 BL) and ~ 190 (40 BL) nm thickness. Most other lignin-based coatings for UV-protection typically have a thicknesses > 1 μm. While the relatively high number of processing steps can appear daunting, the scalability of LbL deposition has been demonstrated numerous times for both roll-to-roll immersion and spray-based processing.[52,53,54] As further applications for lignin-based LbL films are developed, this scalability will be critical to ensure commercial relevance of this technology.

A.4 Conclusions

In this study, an environmentally benign method of lignin functionalization is utilized to facilitate its use as a polyanion in layer-by-layer assembly. This is the first demonstration of lignin in a totally biosourced multilayer film. It was shown that the film grows linearly, despite the low apparent molar mass of the modified lignin, with the rate of growth altered by adjusting the pH of the lignin solution. Furthermore, evidence was presented to suggest that there is both hydrogen

and ionic bonding involved in the assembly of lignin with chitosan. The utility of these coatings was demonstrated through the UV-protection of PEDOT:PSS, where protected films degraded at a fraction of the rate of unprotected polymer. Due to the versatile nature of layer-by-layer assembly, there is great promise for the utilization of lignin as a component in a variety of potential renewable, multifunctional films.

APPENDIX REFERENCES

(1) Schutyser, W.; Renders, T.; Van den Bosch, S.; Koelewijn, S.-F.; Beckham, G. T.; Sels, B. F. Chemicals from Lignin: An Interplay of Lignocellulose Fractionation, Depolymerisation, and Upgrading. *Chemical Society Reviews* **2018**, *47* (3), 852–908. https://doi.org/10.1039/C7CS00566K.

(2) Ponnusamy, V. K.; Nguyen, D. D.; Dharmaraja, J.; Shobana, S.; Banu, J. R.; Saratale, R. G.; Chang, S. W.; Kumar, G. A Review on Lignin Structure, Pretreatments, Fermentation Reactions and Biorefinery Potential. *Bioresource Technology* **2019**, *271*, 462–472. https://doi.org/10.1016/j.biortech.2018.09.070.

(3) Berglund, L. A.; Burgert, I. Bioinspired Wood Nanotechnology for Functional Materials. *Advanced Materials* **2018**, *30* (19), 1704285. https://doi.org/10.1002/adma.201704285.

(4) Sun, Y.; Cheng, J. Hydrolysis of Lignocellulosic Materials for Ethanol Production: A Review. *Bioresource Technology* **2002**, 11.

(5) DeMartini, J. D.; Pattathil, S.; Miller, J. S.; Li, H.; Hahn, M. G.; Wyman, C. E. Investigating Plant Cell Wall Components That Affect Biomass Recalcitrance in Poplar and Switchgrass. *Energy & Environmental Science* **2013**, *6* (3), 898. https://doi.org/10.1039/c3ee23801f.

(6) Upton, B. M.; Kasko, A. M. Strategies for the Conversion of Lignin to High-Value Polymeric Materials: Review and Perspective. *Chemical Reviews* **2016**, *116* (4), 2275–2306. https://doi.org/10.1021/acs.chemrev.5b00345.

(7) Hill, C. A. S. *Wood Modification: Chemical, Thermal and Other Processes*; John Wiley & Sons, Ltd: Chichester, UK, 2006. https://doi.org/10.1002/0470021748.

(8) Ferry, L.; Dorez, G.; Taguet, A.; Otazaghine, B.; Lopez-Cuesta, J. M. Chemical Modification of Lignin by Phosphorus Molecules to Improve the Fire Behavior of Polybutylene Succinate. *Polymer Degradation and Stability* **2015**, *113*, 135–143. https://doi.org/10.1016/j.polymdegradstab.2014.12.015.

(9) Mendis, G. P.; Weiss, S. G.; Korey, M.; Boardman, C. R.; Dietenberger, M.; Youngblood, J. P.; Howarter, J. A. Phosphorylated Lignin as a Halogen-Free Flame Retardant Additive for Epoxy Composites. *Green Materials* **2016**, *4* (4), 150–159. https://doi.org/10.1680/jgrma.16.00008.

(10) Prieur, B.; Meub, M.; Wittemann, M.; Klein, R.; Bellayer, S.; Fontaine, G.; Bourbigot, S. Phosphorylation of Lignin to Flame Retard Acrylonitrile Butadiene Styrene (ABS). *Polymer Degradation and Stability* **2016**, *127*, 32–43. https://doi.org/10.1016/j.polymdegradstab.2016.01.015.

(11) Cauley, A. N.; Wilson, J. N. Functionalized Lignin Biomaterials for Enhancing Optical Properties and Cellular Interactions of Dyes. *Biomaterials Science* **2017**, *5* (10), 2114–2121. https://doi.org/10.1039/C7BM00518K.

(12) Zhang, L.; You, T.; Zhou, T.; Zhou, X.; Xu, F. Interconnected Hierarchical Porous Carbon from Lignin-Derived Byproducts of Bioethanol Production for Ultra-High Performance Supercapacitors. *ACS Applied Materials & Interfaces* **2016**, *8* (22), 13918–13925. https://doi.org/10.1021/acsami.6b02774.

(13) Ge, Y.; Li, Z. Application of Lignin and Its Derivatives in Adsorption of Heavy Metal Ions in Water: A Review. *ACS Sustainable Chemistry & Engineering* **2018**, *6* (5), 7181–7192. https://doi.org/10.1021/acssuschemeng.8b01345.

(14) Qian, Y.; Qiu, X.; Zhu, S. Lignin: A Nature-Inspired Sun Blocker for Broad-Spectrum Sunscreens. *Green Chem.* **2015**, *17* (1), 320–324. https://doi.org/10.1039/C4GC01333F.

(15) Farooq, M.; Zou, T.; Riviere, G.; Sipponen, M. H.; Österberg, M. Strong, Ductile, and Waterproof Cellulose Nanofibril Composite Films with Colloidal Lignin Particles. *Biomacromolecules* **2019**, *20* (2), 693–704. https://doi.org/10.1021/acs.biomac.8b01364.

(16) Decher, G.; Schlenoff, J. B. *Multilayer Thin Films: Sequential Assembly of Nanocomposite Materials, Second Edition*; John Wiley & Sons, Ltd, 2012.

(17) Richardson, J. J.; Cui, J.; Björnmalm, M.; Braunger, J. A.; Ejima, H.; Caruso, F. Innovation in Layer-by-Layer Assembly. *Chemical Reviews* **2016**, *116* (23), 14828–14867. https://doi.org/10.1021/acs.chemrev.6b00627.

(18) Laufer, G.; Kirkland, C.; Cain, A. A.; Grunlan, J. C. Clay–Chitosan Nanobrick Walls: Completely Renewable Gas Barrier and Flame-Retardant Nanocoatings. *ACS Applied Materials & Interfaces* **2012**, *4* (3), 1643–1649. https://doi.org/10.1021/am2017915.

(19) Pan, H.; Song, L.; Ma, L.; Pan, Y.; Liew, K. M.; Hu, Y. Layer-by-Layer Assembled Thin Films Based on Fully Biobased Polysaccharides: Chitosan and Phosphorylated Cellulose for Flame-Retardant Cotton Fabric. *Cellulose* **2014**, *21* (4), 2995–3006. https://doi.org/10.1007/s10570-014-0276-5.

(20) Pan, Y.; Zhan, J.; Pan, H.; Wang, W.; Tang, G.; Song, L.; Hu, Y. Effect of Fully Biobased Coatings Constructed via Layer-by-Layer Assembly of Chitosan and Lignosulfonate on the Thermal, Flame Retardant, and Mechanical Properties of Flexible Polyurethane Foam. *ACS Sustainable Chemistry & Engineering* **2016**, *4* (3), 1431–1438. https://doi.org/10.1021/acssuschemeng.5b01423.

(21) Shi, D.; Ran, M.; Zhang, L.; Huang, H.; Li, X.; Chen, M.; Akashi, M. Fabrication of Biobased Polyelectrolyte Capsules and Their Application for Glucose-Triggered Insulin Delivery. *ACS Applied Materials & Interfaces* **2016**, *8* (22), 13688–13697. https://doi.org/10.1021/acsami.6b02121.

(22) Camus, M.; Condassamy, O.; Ham-Pichavant, F.; MIchaud, C.; Mignani, G.; Mastroianni, S.; Grau, E.; Cramail, H.; Grelier, S. Oxidative Depolymerization of Alkaline Lignin from Pinus Pinaster by Oxygen and Air for Value-Added Bio-Sourced Synthons. *ChemRxiv* Preprint. https://doi.org/10.26434/chemrxiv.12459236.

(23) Kalliola, A.; Vehmas, T.; Liitiä, T.; Tamminen, T. Alkali-O2 Oxidized Lignin – A Bio-Based Concrete Plasticizer. *Industrial Crops and Products* **2015**, *74*, 150–157. https://doi.org/10.1016/j.indcrop.2015.04.056.

(24) Pillai, K.; Navarro Arzate, F.; Zhang, W.; Renneckar, S. Towards Biomimicking Wood: Fabricated Free-Standing Films of Nanocellulose, Lignin, and a Synthetic Polycation. *Journal of Visualized Experiments* **2014**, *88*, e51257. https://doi.org/10.3791/51257.

(25) Su, L.; Zhang, S.; Jiang, G.; Pang, J.; Wang, D.; Shi, J.; Fang, G. Layer-by-Layer Self-Assembly of a Lignin-Poly(Vinyl Alcohol) Based Polyelectrolyte with a Conductivity Method. *Journal of Applied Polymer Science* **2017**, *134* (9). https://doi.org/10.1002/app.44416.

(26) Mishra, P. K.; Wimmer, R. Aerosol Assisted Self-Assembly as a Route to Synthesize Solid and Hollow Spherical Lignin Colloids and Its Utilization in Layer by Layer Deposition. *Ultrasonics Sonochemistry* **2017**, *35*, 45–50. https://doi.org/10.1016/j.ultsonch.2016.09.001.

(27) Granata, A.; Argyropoulos, D. S. 2-Chloro-4,4,5,5-Tetramethyl-1,3,2-Dioxaphospholane, a Reagent for the Accurate Determination of the Uncondensed and Condensed Phenolic Moieties in Lignins. *Journal of Agricultural and Food Chemistry* **1995**, *43* (6), 1538–1544. https://doi.org/10.1021/jf00054a023.

(28) Sadeghifar, H.; Cui, C.; Argyropoulos, D. S. Toward Thermoplastic Lignin Polymers. Part 1. Selective Masking of Phenolic Hydroxyl Groups in Kraft Lignins via Methylation and Oxypropylation Chemistries. *Industrial & Engineering Chemistry Research* **2012**, *51* (51), 16713–16720. https://doi.org/10.1021/ie301848j.

(29) Jang, W.-S.; Grunlan, J. C. Robotic Dipping System for Layer-by-Layer Assembly of Multifunctional Thin Films. *Review of Scientific Instruments* **2005**, *76* (10), 103904. https://doi.org/10.1063/1.2084447.

(30) Alemu, D.; Wei, H.-Y.; Ho, K.-C.; Chu, C.-W. Highly Conductive PEDOT:PSS Electrode by Simple Film Treatment with Methanol for ITO-Free Polymer Solar Cells. *Energy & Environmental Science* **2012**, *5* (11), 9662. https://doi.org/10.1039/c2ee22595f.

(31) Li, S.; Lin, X.; Liu, Y.; Li, R.; Ren, X.; Huang, T.-S. Phosphorus-Nitrogen-Silicon-Based Assembly Multilayer Coating for the Preparation of Flame Retardant and Antimicrobial Cotton Fabric. *Cellulose* **2019**, *26* (6), 4213–4223. https://doi.org/10.1007/s10570-019-02373-5.

(32) Zhao, Y.; Gao, C.; Van der Bruggen, B. Technology-Driven Layer-by-Layer Assembly of a Membrane for Selective Separation of Monovalent Anions and Antifouling. *Nanoscale* **2019**, *11* (5), 2264–2274. https://doi.org/10.1039/C8NR09086F.

(33) Stevens, D. L.; Gamage, G. A.; Ren, Z.; Grunlan, J. C. Salt Doping to Improve Thermoelectric Power Factor of Organic Nanocomposite Thin Films. *RSC Adv.* **2020**, *10* (20), 11800–11807. https://doi.org/10.1039/D0RA00763C.

(34) Delgado, J. D.; Schlenoff, J. B. Polyelectrolyte Complex Films from Blends Versus Copolymers. *Macromolecules* **2019**, *52* (20), 7812–7820. https://doi.org/10.1021/acs.macromol.9b01834.

(35) Pelton, R. Polyvinylamine: A Tool for Engineering Interfaces. *Langmuir* **2014**, *30* (51), 15373–15382. https://doi.org/10.1021/la5017214.

(36) Erel-Unal, I.; Sukhishvili, S. A. Hydrogen-Bonded Multilayers of a Neutral Polymer and a Polyphenol. *Macromolecules* **2008**, *41* (11), 3962–3970. https://doi.org/10.1021/ma800186q.

(37) Shutava, T.; Prouty, M.; Kommireddy, D.; Lvov, Y. PH Responsive Decomposable Layer-by-Layer Nanofilms and Capsules on the Basis of Tannic Acid. *Macromolecules* **2005**, *38* (7), 2850–2858. https://doi.org/10.1021/ma047629x.

(38) Deng, Y.; Wang, T.; Guo, Y.; Qiu, X.; Qian, Y. Layer-by-Layer Self-Assembled Films of a Lignin-Based Polymer through Hydrogen Bonding. *ACS Sustainable Chem. Eng.* **2015**, *3* (6), 1215–1220. https://doi.org/10.1021/acssuschemeng.5b00178.

(39) Fu, Y.; Bai, S.; Cui, S.; Qiu, D.; Wang, Z.; Zhang, X. Hydrogen-Bonding-Directed Layer-by-Layer Multilayer Assembly: Reconformation Yielding Microporous Films. *Macromolecules* **2002**, *35* (25), 9451–9458. https://doi.org/10.1021/ma0207881.

(40) Elbert, D. L.; Herbert, C. B.; Hubbell, J. A. Thin Polymer Layers Formed by Polyelectrolyte Multilayer Techniques on Biological Surfaces. *Langmuir* **1999**, *15* (16), 5355–5362. https://doi.org/10.1021/la9815749.

(41) Shiratori, S. S.; Rubner, M. F. PH-Dependent Thickness Behavior of Sequentially Adsorbed Layers of Weak Polyelectrolytes. *Macromolecules* **2000**, *33* (11), 4213–4219. https://doi.org/10.1021/ma991645q.

(42) Fares, H. M.; Schlenoff, J. B. Diffusion of Sites versus Polymers in Polyelectrolyte Complexes and Multilayers. *Journal of the American Chemical Society* **2017**, *139* (41), 14656–14667. https://doi.org/10.1021/jacs.7b07905.

(43) Thakur, V. K.; Thakur, M. K.; Raghavan, P.; Kessler, M. R. Progress in Green Polymer Composites from Lignin for Multifunctional Applications: A Review. *ACS Sustainable Chem. Eng.* **2014**, *2* (5), 1072–1092. https://doi.org/10.1021/sc500087z.

(44) Figueiredo, P.; Lintinen, K.; Hirvonen, J. T.; Kostiainen, M. A.; Santos, H. A. Properties and Chemical Modifications of Lignin: Towards Lignin-Based Nanomaterials for Biomedical Applications. *Progress in Materials Science* **2018**, *93*, 233–269. https://doi.org/10.1016/j.pmatsci.2017.12.001.

(45) Boeriu, C. G.; Bravo, D.; Gosselink, R. J. A.; van Dam, J. E. G. Characterisation of Structure-Dependent Functional Properties of Lignin with Infrared Spectroscopy. *Industrial Crops and Products* **2004**, *20* (2), 205–218. https://doi.org/10.1016/j.indcrop.2004.04.022.

(46) Aguié-Béghin, V.; Foulon, L.; Soto, P.; Crônier, D.; Corti, E.; Legée, F.; Cézard, L.; Chabbert, B.; Maillard, M.-N.; Huijgen, W. J. J.; Baumberger, S. Use of Food and Packaging Model Matrices to Investigate the Antioxidant Properties of Biorefinery Grass Lignins. *J. Agric. Food Chem.* **2015**, *63* (45), 10022–10031. https://doi.org/10.1021/acs.jafc.5b03686.

(47) Crouvisier-Urion, K.; Bodart, P. R.; Winckler, P.; Raya, J.; Gougeon, R. D.; Cayot, P.; Domenek, S.; Debeaufort, F.; Karbowiak, T. Biobased Composite Films from Chitosan and Lignin: Antioxidant Activity Related to Structure and Moisture. *ACS Sustainable Chem. Eng.* **2016**, *4* (12), 6371–6381. https://doi.org/10.1021/acssuschemeng.6b00956.

(48) Dawidczyk, T. J.; Walton, M. D.; Jang, W.-S.; Grunlan, J. C. Layer-by-Layer Assembly of UV-Resistant Poly(3,4-Ethylenedioxythiophene) Thin Films. *Langmuir* **2008**, *24* (15), 8314–8318. https://doi.org/10.1021/la800967x.

(49) Guin, T.; Cho, J. H.; Xiang, F.; Ellison, C. J.; Grunlan, J. C. Water-Based Melanin Multilayer Thin Films with Broadband UV Absorption. *ACS Macro Lett.* **2015**, *4* (3), 335–338. https://doi.org/10.1021/acsmacrolett.5b00080.

(50) Hambardzumyan, A.; Foulon, L.; Chabbert, B.; Aguié-Béghin, V. Natural Organic UV-Absorbent Coatings Based on Cellulose and Lignin: Designed Effects on Spectroscopic Properties. *Biomacromolecules* **2012**, *13* (12), 4081–4088. https://doi.org/10.1021/bm301373b.

(51) Parit, M.; Saha, P.; Davis, V. A.; Jiang, Z. Transparent and Homogenous Cellulose Nanocrystal/Lignin UV-Protection Films. *ACS Omega* **2018**, *3* (9), 10679–10691. https://doi.org/10.1021/acsomega.8b01345.

(52) Mateos, A. J.; Cain, A. A.; Grunlan, J. C. Large-Scale Continuous Immersion System for Layer-by-Layer Deposition of Flame Retardant and Conductive Nanocoatings on Fabric. *Industrial & Engineering Chemistry Research* **2014**, *53* (15), 6409–6416. https://doi.org/10.1021/ie500122u.

(53) Xiang, F.; Givens, T. M.; Grunlan, J. C. Fast Spray Deposition of Super Gas Barrier Polyelectrolyte Multilayer Thin Films. *Industrial & Engineering Chemistry Research* **2015**, *54* (19), 5254–5260. https://doi.org/10.1021/acs.iecr.5b01367.

(54) Suarez-Martinez, P. C.; Robinson, J.; An, H.; Nahas, R. C.; Cinoman, D.; Lutkenhaus, J. L. Spray-On Polymer-Clay Multilayers as a Superior Anticorrosion Metal Pretreatment. *Macromol. Mater. Eng.* **2017**, *302* (6), 1600552. https://doi.org/10.1002/mame.201600552.